

**Investigation of chemical and physical processes on Arctic
aerosols through a combined approach of field and
laboratory studies**

By Pami Mukherjee

A Dissertation submitted to the Graduate School - Newark

Rutgers, The State University of New Jersey

in partial fulfillment of the requirements for

the degree of Doctor of Philosophy

Graduate Program in Environmental Science

Written under the direction of Dr. Yuan Gao

Newark, New Jersey

October, 2018

Copyright Page:

©[2018]

Pami Mukherjee

ALL RIGHTS RESERVED

ABSTRACT OF THE DISSERTATION

Investigation of chemical and physical processes on Arctic aerosols through a combined approach
of field and laboratory studies

By

Pami Mukherjee

Dissertation Director: Dr. Yuan Gao

Abstract.

The causes and effects of recent global warming have been studied extensively; but, the role of atmospheric aerosols in the Arctic biogeochemistry has not been widely explored yet.

The water-soluble Arctic aerosols directly impact the climate by participating in cloud formation and influencing its radiative property. Moreover, the amplified Arctic warming may significantly influence the solubility and bio-availability of aerosol iron (Fe)—which is a limiting nutrient for phytoplankton growth, an important sink for atmospheric carbon dioxide (CO₂).

This research investigates the chemical and physical processes on aerosols that were collected during the US Geotraces Arctic cruise in summer 2015 and natural snow samples from Newark, New Jersey in conjunction with laboratory experiments involving Fe minerals and organic ligands. We hypothesize that the Arctic aerosols were modified by

various natural and anthropogenic processes, affecting the concentrations and hygroscopic properties of the cloud condensation nuclei and soluble Fe input to the Arctic Ocean.

Laboratory studies with hematite and major organic ligands showed that oxalate, when present above a threshold amount, had a significant effect on the absorptive dissolution of Fe. The results from the Arctic Ocean expedition showed that coarse mode sea-salt was the major aerosol component and non-sea-salt-sulfate was significantly present in fine mode aerosol particles. Among the organic species, oxalate, acetate, and formate were the major components among the species examined at the pole. Calcium was enriched on the sea-spray aerosols, pre-dominantly in the fine mode, leading to significant modification of the aerosol hygroscopic growth factor. Analysis of the natural snow and ice-melts showed that freezing could induce compaction and clustering of particles, but had negligible effect on modulating Fe solubility.

This study provides significant insight into the water soluble component of Arctic summer aerosols regarding their concentrations, sources, and possible formation mechanisms, and their effects on the Arctic climate via cloud formation. The laboratory based experiments increase our understanding of the effects of various processes occurring in Arctic aerosols—including the accumulation and reactions of organic components in aerosols and the freeze concentration effect on iron chemistry, which could affect the biogeochemical cycles in the Arctic Ocean.

Acknowledgments.

First and foremost, I would like to thank my advisor Dr. Yuan Gao for her continued support and encouragement throughout my doctoral studies, for teaching me various aspects of field and laboratory studies, and for guiding me through every stage of my research.

I would like to thank my committee members, Dr. Alexei Khalizov, Dr. John Reinfelder, and Dr. Ashaki Rouff, for their invaluable input and continuous encouragement towards my research.

I am sincerely grateful to all my collaborators, Dr. Christopher Buck, Dr. Mihaela Glamoclija, Dr. William M. Landing, Dr. Christopher Marsay, and Mr. Shun Yu for working with me on significant research projects and for guiding me in the process. In particular, I would like to thank Dr. Miheala Glamoclija for teaching me the working mechanism of several state-of-the-art optical instruments, Dr. Christopher Marsay for collecting all the Arctic samples, and Mr. Shun Yu for providing me helpful guidance in operating the laboratory instruments and sample analysis.

I want to thank all my former and current laboratory members, Songyun Fan, Rafael Justino, Oren Rabinovich, Guojie Xu, Joan Zhan, and Tianyi Xu for their friendship and support. I am especially thankful to Joan for welcoming me in the laboratory and showing me all the laboratory procedures.

I am grateful to all professors and students in my department for always providing a friendly and welcoming environment. In particular, I want thank our former and current

graduate directors, Dr. Lee Slater, Dr. Adam Kustka, and Dr. Evert Elzinga for their helpful guidance on several occasions. I am very thankful to our department administrator Ms. Elizabeth Morrin and lecturer Ms. Sweeta Chauhan for offering me helpful guidance in many difficult situations and Mr. Mike Kalczynski for mentoring me in my teaching assignments.

I want to thank my parents, my sister, and my brother-in-law for their valuable counsel during many difficult times and for their continuous support through this journey. I am deeply grateful to all my friends, especially Avishek and Shaoli, for their love and support.

Finally, I want to thank the most integral part of my family and my support system, my husband, Sucharit and our daughter, Nirajana for always understanding me, supporting me, and encouraging me in every step of my PhD study.

Contents

1	Introduction.	1
1.1	Overview.	1
1.2	Objectives.	5
2	Efficiency of Organic Ligands in Adsorptive Dissolution and Photo Reductive Dissolution of Iron from Hematite.	7
2.1	Abstract.	7
2.2	Introduction.	8
2.3	Materials and Methods.	11
2.4	Results and Discussions.	15
2.5	Conclusion.	25
2.6	Tables.	27
2.7	Figures.	30
3	Insignificant Impact of Freezing and Compaction on Iron Solubility in Natural Snow	35
3.1	Abstract.	35
3.2	Introduction.	36
3.3	Methodology.	38
3.4	Results.	44

3.5	Discussion.	50
3.6	Conclusions.	61
3.7	Tables.	64
3.9	Figures.	69
4	Characterization of the Water-soluble Inorganic and Organic Species on Aerosols over the Arctic Ocean.	79
4.1	Abstract.	79
4.2	Introduction.	80
4.3	Materials and Methods.	83
4.4	Results.	89
4.5	Discussion.	100
4.6	Conclusion.	111
4.7	Figures.	113
5	Significant modification of sea-spray aerosols in the Arctic summer atmosphere.	121
5.1	Abstract:	121
5.2	Introduction.	122
5.3	Methods.	124
5.4	Results.	126
5.5	Discussion.	127

5.6	Environmental Significance.	131
5.7	Figures.	135
6	Conclusion.	138
7	Further studies.	140
8	References:	142

List of Tables.

Table 2.1 The Pearson correlation coefficients between the data for the repeated experiments. When an experiment is repeated thrice, the average of the three inter-correlations among the three sets of data is presented.27

Table 2.2 Range of dissolved Fe concentrations (μM) after reaching equilibrium.28

Table 2.3 Speciation of Fe-ligand complexes at varying ligand concentrations (Visual Minteq 3.1 Chemical model).29

Table 3.1 Summary of the snow events [<https://www.wunderground.com/us/nj/newark>]64

Table 3.2 Schematic of the snow sample treatment and analysis.65

Table 3.3 The concentrations (ppb) of Fesol, Fefil and Fetot (this study) and comparison with other precipitation samples.66

Table 3.4 Concentrations (ppm) of the soluble species detected at EDS.68

List of Figures.

Figure 2.1 The effect of varying oxalate concentration on the photo-reductive dissolution of Fe(II) from hematite. The inset shows the details for the first five hours. The error bars are representing the range of the triplicate experiments.30

Figure 2.2 Photo-reductive dissolution of Fe(II) from hematite in presence of varying concentrations (10, 50, 500 μ M, and 3mM) of oxalate, acetate, and formate. The error bars are representing the range of the triplicate experiments.31

Figure 2.3 The effect of instantaneous UV-irradiation on the photo-reductive dissolution of Fe(II) from hematite in presence of 50 μ M and 3mM concentrations of oxalate, acetate, and formate. The error bars are representing the range of the triplicate experiments.32

Figure 2.4 The adsorption dissolution of Fe(III) from hematite in the presence of 50 μ M and 3mM concentrations of oxalate, acetate, formate, and fluoride. The error bars are representing the range of the repeated set of experiments.33

Figure 2.5 Empirical correlation between oxalate and soluble Fe(II) concentrations when the ratio between oxalate and total Fe is at least R, plotted against the parameter R. The data is collected from [Buck et al., 2010], [Chen and Seifert, 2004], [Gao et al., 2013], [Xia and Gao, 2009, 2011], [Xu and Gao, 2014].34

Figure 3.1 (a) Soluble Fe (Fe(II)+Fe(III)) (analyzed immediately after collection) concentrations from nine snow events; (b) The fractional solubility of F_{sol}/F_{tot} and F_{sol}/F_{fil} (The error bars were calculated based on standard error, i.e., standard deviation69

Figure 3.2 The soluble Fe concentration and the variation in pH from six freezing experiment events. The bar represents the fractional solubility of initial F_{fil} with respect

to initial Fetot (The soluble Fe was analyzed after periodic storage immediately after melting. The error bars were calculated based on standard error, i.e., standard deviation divided by the square-root of the sample size, from three replicate samples).....70

Figure 3.3 Uni modal particle size distribution (using Beckman Coulter, N4Plus mode) of the snow-melt and in ice-melt counterparts from two selected events (event 6 and event 7).
.....71

Figure 3.4 The 6 days back trajectory analysis from the NOAA HYSPLIT-4 model (http://www.arl.noaa.gov/HYSPLIT_info.php).71

Figure 3.5 The representative SEM-TEM micrograph with associated EDAX spectra of amorphous carbon particle aggregate. This particular aggregate was observed from event 6 ice melt. Analytical spot 5 is indicative of the large particle predominantly carbon with some silicate composition. The smaller particles are of iron (spot 1) and aluminium silicate composition (spots 3 and 4). The analytical spots 2 and 3 have similar compositions, hence we are showing only one of the spectra.72

Figure 3.6 The representative SEM-TEM micrograph with associated EDAX spectra of over 50µm large particle observed within event 6 snow melt. This is a large particle with varying chemistry the main amorphous material is mostly silicate, however some portions of the particle has high content of carbon and phosphorous. The analytical spots 2 and 3 have similar compositions, so we are showing only one of the spectra.74

Figure 3.7 The representative images SEM-TEM micrograph with associated EDAX spectra of aluminium-silicate oxide particles (A) particle from event 7 ice melt (the analytical spots 1, 2, and 5 have similar chemical compositions and the analytical spots 3 and 4 have similar chemical compositions); (B) particle from event 7 snow melt.....76

Figure 3.8 The representative images SEM-TEM micrograph with associated EDAX spectra of carbon particles, that we categorized as smears due to their wide distribution and low thickness. We were able to see most of them and analyze only some of them as many were below detection limits of the EDAX detector. (A) the particle from event 10 snow melt as this particle was a bit thicker we were able to detect low level of aluminium (Al) and iron (Fe) in its composition; (B) (C) and (D).78

Figure 4.1 Sample runtimes along the ship's route: (a) Chemcomb and H-vol samplers, (b) 11-stage cascade impactor, C1-C15 represents Chemcomb, H1- H14 represents Hi-vol sampler and M1-M8 represents MOUDI, (c) Meteorological data along the ship's route.113

Figure 4.2 Back trajectory analysis using NOAA's HYSPLIT4 model for (a) the entire cruise (Aug 10 to Oct 9, 2015), (b) the first leg (Aug 10 to Aug 19), (c) the second leg (Aug 20 to Sep 20), and (d) the third leg (Sep 21 to Oct 9). The ship's track is shown as the black path. Back trajectories for 100 hours were calculated every six hours from the ship's locations, which were then clustered; the clustered trajectories along with the percentage of trajectories contained in each cluster is shown by red lines terminating in the red stars. Ensembled 100 hour back trajectories were also calculated from each point and their frequency is represented by the blue background; the value of the frequency equals the average amount of time spent by a 100hr back-trajectory per unit area (in hr/km²).114

Figure 4.3 Spatial distribution of the concentration of the water soluble species [the aerosols were collected by hi-vol TSP collector]. Each circle represents the mass of the total water soluble species analyzed in this study.....116

Figure 4.4 Mass-Size distribution of the inorganic species, (a) Sea-salt, (b) Nitrate, (c) NSS Sulfate, (d) Ammonium.	117
Figure 4.5 Mass-Size distribution of the organic species, (a) Acetate, (b) Formate, (c) Propionate, (d) Oxalate.	118
Figure 4.6 MSA over Arctic Ocean, (a) Mass-size distribution of MSA, (b) Spatial distribution of MSA concentration along the ship's route and its relationship with chlorophyll-a (Chlorophyll-a data obtained from https://oceancolor.gsfc.nasa.gov/cms/atbd/chlor_a), (c) MSA concentration (ng.m^{-3}) and MSA/NSS Sulfate molar ratio and their relationship with sea surface temperature ($^{\circ}\text{C}$) and air tem temperature ($^{\circ}\text{C}$).....	119
Figure 4.7 The general chemical characteristics of the Arctic aerosols: (a)The chloride depletion, (b) Cation/ Anion charge equivalence ratio, (c) Molar ratio of ammonium and NSS-sulfate in fine mode, (d) Molar ratio of the organics with NSS-sulfate in fine mode (specifically over the high Arctic Ocean).	120
Figure 5.1 The back trajectory analysis of the air-mass and the metrological conditions during the sampling period. The solid black lines represent the cruise track and the blue backgrounds show the air-mass source and frequency.	135
Figure 5.2 The enrichment factor of the major cations with respect of their bulk sea-water ratio with sodium: (a) bulk aerosol samples; (b) size-segregated aerosol samples.	136
Figure 5.3 Schematic describing the effect on atmospheric processing and multiple evaporation-condensation cycle on calcium enriched aerosols to produce fine mode dominance of calcium enrichment.	136

Figure 5.4 The percentage change in hygroscopic growth factor between calcium enriched aerosol system and the corresponding pure sodium chloride aerosol system at varying relative humidity.137

1 Introduction.

1.1 Overview.

The Arctic region has been severely impacted by the recent global warming trend. The surface temperature at Arctic has increased by 1.2°C in last two decades and the annual ice coverage has declined by 3.6% per decade (Jones et al., 2007; Breider et al., 2017). The effect of clouds on Arctic amplification is widely considered to be a major source of uncertainty in understanding the recent trend and predicting the future pattern of the Arctic climate change (Vavrus, 2004; Künzli et al., 2005; Inoue et al., 2006; Walsh et al., 2009; Kay et al., 2016), although some model studies claim that the role of clouds is minimal (Screen & Simmonds, 2010; Ghatak & Miller, 2013). Mauritsen et al. (2011) showed that since the central Arctic falls within a tenuous cloud regime, even a slight perturbation in the concentrations of cloud condensation nuclei (CCN) could impose substantial radiative warming effect—particularly during late summer and early winter. The aerosols serve as CCN upon which cloud droplets can form and the CCN directly influence the cloud's radiative property by increasing or decreasing the cloud's albedo and modifying the cloud's lifetime. Although the sizes of aerosol particles and the extent of solubility of the chemical species in aerosols are crucial factors in determining the activation of the CCN at different levels of supersaturation, the effects of Arctic aerosols and their variations on cloud dynamics and climate change have not yet been thoroughly examined in climate models so far due to limited aerosol data from the observations over the Arctic (Walsh et al., 2005; Chang et al., 2011). Therefore, it is of vital importance to collect and analyze Arctic aerosols—their chemical composition and size distributions—to study their properties.

Water soluble ionic species are important constituents of marine aerosols. Among them, sulfate, nitrate, chloride, and ammonium are the major components because of their ubiquitous presence and high affinity for water absorbance (Bates et al., 2001; Xu et al., 2013; Barbaro et al., 2017; Yan et al., 2017). These species come from both natural and anthropogenic sources and their concentrations show strong seasonal variations. Di-methyl sulfide (DMS), emitted from marine organisms, is the major source of non-sea-salt sulfate on fine marine aerosols of natural origin (Levasseur et al., 1994; Park et al., 2017). Anthropogenic sources via long-range transport from mid-latitudes and the surrounding continents can substantially contribute to the sulfate aerosol loading over the Arctic Ocean, but this process mostly occurs in winter (Quinn et al., 2009). Ammonium on aerosols predominantly originates from continental sources (Virkkula et al., 1995), reacts with the acidic species on aerosols, such as sulfate, nitrate, and chloride, and produces highly hygroscopic salts and thereby significantly influences the aerosols' ability to form clouds. The availability of ammonium determines whether the aerosols are highly acidic or completely neutral, and therefore, imposes a significant impact on the chemical processes occurring on the aerosol surface (Liu et al., 2016; Weber et al., 2016).

Among the water soluble organic species, methane sulfonic acid (MSA) and low molecular weight carboxylic acids (such as formic, acetic, and oxalic acids) are important constituents of marine aerosols (Xu et al., 2013; Hoque et al., 2015; Mungall et al., 2017). Similar to the biogenic non-sea-salt sulfate, MSA also originates from the atmospheric oxidation of DMS following the same reaction pathway. For instance, the oxidation of DMS with atmospheric oxidant hydroxyl radical generates both sulfur dioxide and MSA. Sulfur dioxide eventually transforms into sulfate aerosols through homogenous nucleation and

gas-to-particle conversion processes. Anthropogenic sources may significantly contribute towards the non-sea-salt sulfate budget, however MSA is pre-dominantly of biogenic origin. Therefore the MSA/non-sea-salt sulfate ratio is used as a tracer for the biogenic contribution to the non sea-salt sulfate in the marine atmosphere (Kerminen et al., 1997; Gondwe et al., 2003; Gondwe et al., 2004). The significant presence of water soluble, low molecular weight carboxylic acids on the Arctic aerosols has been reported in earlier studies (Talbot et al., 1992; Kerminen et al., 1999). Being water soluble, after condensation on the pre-existing particles or interaction with alkaline sea-salts, these species can participate in the processes of cloud formation (Novakov & Penner, 1993; Yu, 2000). Since the hygroscopic properties of the various salts of these carboxylic acids vary widely, these species can significantly modify the hygroscopic nature of the original aerosol particles.

Sea-spray aerosols (SSA) originate from the bursting of bubbles on the ocean surface and are the major source of natural aerosols in the marine environment (by mass concentration) (Andreae & Rosenfeld, 2008). The alkaline SSA are sites for various chemical processes to occur involving acidic gaseous components and oxidants (Chameides & Stelson, 1992; Song & Carmichael, 2001). Due to their hygroscopic nature, SSA are crucially important for marine cloud formation. Since these aerosols originate from the sea-water, it is believed that the chemical composition of SSA remain unaltered from that of the sea-water bulk composition (Savoie & Prospero, 1980). However, recent studies have shown the enrichment of several organic components and major sea-water cations in the sea-spray aerosols (Hara et al., 2012; Cochran et al., 2016; Salter et al., 2016). This deviation of sea-spray aerosols from sea-water composition may impact the hygroscopic properties of marine aerosols and thus would impact the radiative budget at marine environment.

In addition to marine biogenic aerosols, the element iron (Fe) in aerosols and snow is also important, as Fe is a limiting nutrient for phytoplankton growth, affecting the oceanic CO₂ cycle (Martin & Fitzwater, 1988; Martin, 1990; Tagliabue et al., 2017). The atmospheric Fe bioavailability—largely controlled by Fe solubility and speciation—is crucially important for the Arctic marine ecosystem under the warming conditions. Iron-solubility could be significantly affected due to long-term freezing during the Arctic winter. Moreover, the water soluble organic and inorganic species and the sea-spray aerosols might affect Fe solubility to various degrees and play a crucial role in the Arctic's radiative budget, and hence the Earth's climate, by influencing cloud formation (Tang et al., 1997; Xu & Gao, 2008; Paris et al., 2011).

Despite the abundance of Fe in the Earth's crust, only a small portion is available to the marine micro-organisms such as phytoplankton. One of the major sources of bio-available Fe in the ocean is deposition from the atmosphere (Duce & Tindale, 1991; Fung et al., 2000), which is a culmination of several physical and chemical processes that convert the highly insoluble Fe from its minerals to its bio-available soluble state. Air-borne low molecular weight carboxylic acids play a salient role in this process by promoting dissolution of the Fe-minerals in aerosols via two mechanisms, absorptive dissolution which yield soluble Fe(III) (Banwart et al., 1989; Sulzberger et al., 1989; Paris et al., 2011; Paris & Desboeufs, 2013) and photo-reductive dissolution which generates Fe(II) (Zuo & Hoigne, 1992; Pehkonen et al., 1995). The organic ligands form a surface complex with the Fe-minerals and facilitates the solubility of Fe. Under UV radiation, the ligands act as electron donors and promotes the reductive dissolution of Fe. These organics exist in

substantial amount at the Arctic atmosphere and could play significant role in modulating Fe solubility (Li & Winchester, 1993; Jaffrezo et al., 1998).

Atmospheric dry or wet deposition is the major source of external bio-available Fe in many parts of the world's ocean and is highly linked to the global CO₂ budget (Duce & Tindale, 1991; Gao et al., 2013). High latitude locations of the northern hemisphere experience significant amounts of snowfall each year. Because of the larger size and surface area of the snowflakes, the snow events efficiently scavenge the below-cloud aerosol particles (Sempère & Kawamura, 1994; Paramonov et al., 2011). Recent laboratory analyses (Kim et al., 2010; Jeong et al., 2012) found that the dissolution of Fe(II) from insoluble hematite is significantly enhanced after freezing the aqueous suspension of hematite (with organic ligands) and suggests the freezing concentration effect, a process in which the solutes cluster together during freezing thereby increasing the possibility of chemical interaction, as a possible reason. These processes are highly significant since the deposited snow would contain and store larger amount of soluble Fe which would eventually enter into the ocean after melting. Studying the freeze-induced effect on modulating Fe-solubility in stacked snow is more relevant for the Arctic region, since this region is experiencing the intense effect of warming and massive sea-ice melting.

1.2 Objectives.

This research aims to characterize marine aerosols collected during the US Geotraces Arctic cruise in summer 2015 and to explore Fe solubility in Fe-containing minerals and natural snow through the combined lab/field experiments. . We hypothesize that the enhanced Arctic warming, in conjunction with various natural and anthropogenic processes, would result in modification of water soluble aerosol components and

composition of sea-spray aerosols; this in turn would influence the Arctic climate by altering the amount of soluble Fe input to the Arctic Ocean, and by impacting the cloud dynamics—their formation, radiative properties, and lifetime. The primary goals are to (1) explore the processes affecting aerosol Fe dissolution, (2) quantify the presence of the water soluble aerosol species and sea-spray aerosols, and (3) identify their origins and possible formation mechanisms. The specific objectives are:

(Chapter 2) Studying the efficiency of organic ligands in adsorptive dissolution and photo reductive dissolution of hematite (Mukherjee & Gao, 2016).

(Chapter 3) Analyzing the event based snow collected over Newark, NJ for two consecutive winter seasons (December 2014 to February 2017) and their environmental implications (Mukherjee, Glamoclija, et al., 2018).

(Chapter 4) Characterizing water soluble organic and inorganic species over the Arctic Ocean (Xu et al., 2013).

(Chapter 5) Investigating the enrichment of certain chemical species in Arctic summer sea-spray aerosols.

2 Efficiency of Organic Ligands in Adsorptive Dissolution and Photo Reductive Dissolution of Iron from Hematite.

2.1 Abstract.

Organic ligands, especially oxalate, play an important role in iron dissolution from iron-containing minerals. To study the effects of organic acid ligands on the dissolution of iron-containing minerals, the dissolution kinetics of hematite in presence of oxalate, acetate, and formate were investigated under ultra-violet radiation with varying ligand concentrations (10 μ M to 3mM). The results indicate that for adsorption dissolution, oxalate is the dominating ligand for producing soluble iron (III) from hematite; for photo-reductive dissolution under ultra-violet radiation and in oxic conditions, the production of iron (II) is highly proportional to the concentrations of oxalate, whereas the effects of varying concentrations of formate and acetate are not significant. At low oxalate concentrations (10-500 μ M), the photo-reductive dissolution of iron (II) is substantially low, while at high oxalate concentrations (3mM), oxalate is equally effective as formate and acetate for producing photo-reduced iron (II) from hematite. Combining with field data from other works, it is likely that the ratios of oxalate to total iron need to be higher than a threshold range of ~1.2-5.5 in order for oxalate to effectively produce photo-reduced iron (II) from hematite. This study demonstrates that the iron (II) yield from photo-reduction of Fe(III)-oxalate complexes is significantly lower when the complexation of Fe(III)-ligand complexes are completely done, versus when it is exposed to ultra-violet radiation instantaneously.

2.2 Introduction.

Iron (Fe) is an essential nutrient for phytoplankton growth in the oceans' high nitrate and low chlorophyll (HNLC) regions (Martin & Fitzwater, 1988; Martin, 1990; Sunda & Huntsman, 1997), affecting the carbon cycle (Martin, 1990). Most of the dissolved Fe in the ocean, operationally defined as those that pass through a filter of 0.45 μm pore size, exist as hydroxides or in strongly chelated complexes with naturally occurring organic ligands (Sung & Morgan, 1980; Johnson et al., 1997; Wu et al., 2001; Liu & Millero, 2002). However, iron remains insoluble under oxic conditions with a pH above 4 (Jickells et al., 2005), thereby being unavailable for the phytoplanktons to consume. Phytoplanktons could easily uptake Fe in its reduced form (Shaked et al., 2005), Fe(II), however, some evidences claim that inorganic soluble Fe(III), organic ligand-Fe(III) complexes and some colloidal form of Fe(III) could also be consumed by micro-organisms, such as red tide microalgae (Naito et al., 2005). It is reported that a potential source of bioavailable iron is photoreductive dissolution of particulate iron oxides (Finden et al., 1984). Both Fe(II) and Fe(III) could be produced on aerosol particles in the atmosphere, affected by the presence of peroxide radicals (Zuo & Hoigne, 1992), organic ligands (Siefert et al., 1994), and solar radiation (Zhu et al., 1993; Zhu et al., 1997; Paris et al., 2011). Consequently, understanding Fe speciation and solubility in aerosols is crucial for estimating the atmospheric deposition of bio-available Fe to the ocean.

The oxidizing atmosphere in general favors the dissolved Fe(III) over Fe(II) in Fe-containing minerals, such as hematite, lepidocrocite, goethite, and several organic ligands play crucial roles in Fe dissolution, specially oxalate, through the complex formation with the Fe(III) and adsorption dissolution mechanism (Banwart et al., 1989; Sulzberger et al.,

1989; Siffert & Sulzberger, 1991; Xu & Gao, 2008; Paris et al., 2011). Under the exposure to sunlight, the Fe(III)-ligand complex absorbs energy from ultraviolet (UV) radiation; the ligand acts as a bridge and supplies electrons to the Fe(III) metal center, resulting in the formation of Fe(II) (Siffert & Sulzberger, 1991; Zhu et al., 1997; Chen & Grassian, 2013). Acetate and formate are also common organic ligands in the ambient air (Kawamura & Kaplan, 1983; Kawamura & Ikushima, 1993; Li & Winchester, 1993; Chebbi & Carlier, 1996; Kawamura & Sakaguchi, 1999; Johansen et al., 2000; Paris & Desboeufs, 2013). However, the ambient levels of these organic -species vary widely throughout the global atmosphere. For example, the concentrations of oxalate were observed to be <12.4–100.8 ng.m⁻³ in the North Atlantic (Johansen et al., 2000), 6.5–161 ng.m⁻³ in the Pacific (Kawamura & Usukura, 1993), (below detection limit)–48.4 ng.m⁻³ in Ny-Alesund, Svalbard in the Arctic (Hara et al., 2002) in the marine regions. In the urban regions, the concentration of oxalate were relatively high, for example, 2.1–9.7nmol.m⁻³ (which is equivalent to 184.8 – 853.6 ng.m⁻³) at Newark, NJ (Xia & Gao, 2010), 115–780 ng.m⁻³ in West Los Angeles (Kawamura & Kaplan, 1987), and 40–730 ng.m⁻³ in Tokyo, Japan (Kawamura & Ikushima, 1993).

Among these three ligands mentioned above, oxalate is the most abundant one in atmospheric aerosols (Turekian et al., 2003; Zobrist et al., 2006; Chen & Grassian, 2013) and it is also believed to be the most effective one affecting Fe dissolution from Fe-minerals through the formation of stable bi-dentate chelates with the Fe metal centers (Sulzberger et al., 1989; Siffert & Sulzberger, 1991; Paris & Desboeufs, 2013). In previous experimental studies (Banwart et al., 1989; Sulzberger et al., 1989; Xu & Gao, 2008), the concentrations of oxalate were mainly held at the levels of 50 to 600 times higher than the

atmospheric concentrations of oxalate found in rainwater (Paris & Desboeufs, 2013). However, in the atmosphere where the concentrations of oxalate are low while both the solar radiation and adequate oxygen are prevalent, the interactions of oxalate with Fe-minerals are complicated. For instance, under adequate O₂ exposure and solar radiation, the Fe(II) production from reducing Fe(III) could be substantially altered by H₂O₂ produced during reactions, resulting in less yield for Fe(II) (Zuo & Hoigne, 1992; Siefert et al., 1994). In addition, the photolysis of oxalate under UV radiation could also produce H₂O₂ that limits the Fe(II) formation (Zuo & Hoigne, 1992). Therefore, the concentrations of oxalate at different levels could significantly affect the Fe (II) production rate and then Fe speciation that still remains untested. Furthermore, despite being present in the atmosphere at levels comparable to oxalate, acetate and formate have not been studied extensively for Fe(II) production in Fe-minerals. On the other hand, these complex could undergo photo-reductive dissolution, resulting in the formation of Fe(II). It is still in question whether the incident solar radiation could produce Fe(II) from the organic ligand-Fe(III) complexes in the atmosphere. Fluoride could also form complex with Fe (III) (Dodgen & Rollefson, 1949; Soli & Byrne, 1996; Wang & Reardon, 2001; Dey et al., 2004) but the effect of fluoride in promoting dissolution of Fe(III) from Fe-minerals is yet to be explored.

To investigate the effects of Fe dissolution from Fe-containing minerals, laboratory experiments involving hematite and organic ligands (oxalate, acetate, and formate) were carried out at Rutgers University over an approximate 6-month period from November 2014 to April 2015. The specific objectives were to investigate: 1) The effects of these ligands at different concentrations; 2) The relative efficiency of these ligands on the photo-

reductive dissolution and adsorptive dissolution of Fe(III), along with a comparison to fluoride; 3) The effect of prior complexation with ligands on the generation of Fe(II) via photo-reduction. The results from this study will shed further light on current understanding of iron speciation and solubility in ambient aerosols and advance our knowledge of the effect of organic ligands, particularly oxalate, on iron dissolution. The threshold ratios of oxalate to total Fe, as an indicator of oxalate-promoted Fe(II) dissolution derived from this study could be used in future model studies.

2.3 Materials and Methods.

2.3.1 Preparation.

All materials used in this experiment were either pure or analytical grade. Standard pure hematite (α -Fe₂O₃) was purchased (Atlantic Equipment Engineers, Bergenfield, NJ) and used in this study, which has the molecular weight 159.69 and 99.9% purity and specific surface area of 2.7 m² g⁻¹ for particle sizes of 1–5 μM. All solutions were prepared using 18.2MΩcm Milli-Q water (Millipore, Bedford, MA, USA). Polyethylene 50ml test-tubes were pre-cleaned thoroughly before use. The UVLMS-38 EL series 3 UV (capacity 8watt) lamp was used as the source of UV radiation. The stock solutions for Fe(II) and Fe(III) were prepared by dissolving ammonium iron(II) sulfate 6-hydrate and ferric chloride, respectively. The stock solutions of the organic ligands were prepared from their sodium-salts. All stock solutions were kept at 4°C temperature in the refrigerator and the working standards were prepared before each analysis.

2.3.2 Experimental Procedures.

Four experiments were carried out: The first experiment was for studying the effects of varying oxalate concentrations (ranging from 10μM – 3mM) in photo reductive release of

Fe(II). The second experiment was conducted to compare the release of Fe(II) via photo reduction in presence of three different ligands (oxalate, acetate, and formate). Third experiment was to study the photo reductive dissolution of Fe(II) from hematite under two conditions: instantaneous irradiation of the Fe(III)-ligand complexes and pre-coated Fe(III)-ligand complexes. The fourth experiment focused on investigating the role of varying ligands (oxalate, acetate, formate, and an inorganic ligand fluoride) on adsorptive dissolution of Fe(III). All these experiments were conducted using hematite as the reference material for iron and were repeated 2-3 times. The figures display the means and the ranges of the repeated set of experiments. Tables 2.1 and 2.2 show the Pearson correlation coefficients of the replicate sets of experiments and the ranges of the concentrations at equilibrium, where the ranges have been calculated combining the values from all the repeated sets of experiments. The detailed procedures are outlined below.

2.3.2.1 Photo-reductive Production of Fe(II) from Fe(III)-Ligand Complex.

The dissolution experiment was conducted by placing 10mg of hematite in three series of 50 ml polyethylene test tubes containing oxalate, formate and acetate solutions separately at four different concentrations (10 μ M, 50 μ M, 500 μ M, 3mM). The mixtures were left for 24hrs to attain the adsorption equilibrium (Xu & Gao, 2008). The mixtures were then placed in an overhead rotator for 12hrs followed by centrifugation for 10 mins at a relative centrifugal force of 3000*g. The supernatants from each mixture were collected and placed under UV light source (254nm wavelength) for 24hrs. The pH of each solution was adjusted at 3.5 by adding 0.1N HCl solution, because the Fe becomes highly mobilized ~ below 3.6 pH from dust samples (Mackie et al. 2005). Periodic measurements (0.5hr, 1hr,

1.5hr, 2hr, 2.5hr, 3hr, 4hr, 5hr, 12hr, 18hr, and 24hr) of Fe(II) were taken from each solution after filtering the aliquots through a 0.45 μ m pore size PTFE filter.

2.3.2.2 Instantaneous Irradiation on Photo-reductive Production of Fe(II) from Fe(III)-Ligand Complex.

A comparative study was performed to investigate the effect of instantaneous irradiation on nascent Fe(III)-ligand complex on the photo reductive dissolution of Fe(II). The aim of this study was to compare the efficiency of the Fe(III)-ligand complexes formed from complete formation of Fe(III)-ligand complexes originated from hematite and ligand mixtures versus the in-situ produced nascent Fe(III)-ligand complexes in the photo-reductive generation of Fe(II). To accomplish this objective, three series of 50ml of test tubes were prepared by placing 10mg of hematite in each in presence of three organic ligands (oxalate, acetate and formate) at two concentration levels (50 μ M and 3mM). The test-tubes were then placed immediately under UV light (254nm) for 24hrs. The sample aliquots were withdrawn periodically (~1hr interval) for 24hrs of irradiation span using a 10ml of syringe with 0.45 μ m PTFE filter to measure the concentrations of dissolved Fe(II). In contrast with 2.2.1., in this step the Fe(III)-ligand complexes were irradiated instantaneously.

2.3.2.3 Formation of Fe(III) at Varying Concentrations of Organic and Inorganic Ligands.

Suspensions of 10mg hematite were prepared in four series of solutions containing oxalate, acetate, formate and fluoride at two concentration ranges (50 μ M and 3mM) and were left for 24hrs to attain the equilibrium. After then, the solutions were placed in an over-head rotator for 32 hours, while aliquots were withdrawn periodically (~1hr interval) followed

by 10 mins of centrifugation at 3000rcf to measure the concentration of soluble Fe(III) with time.

2.3.3 Measurement of Soluble Fe(II) and Fe(III).

The measurements of Fe(II) and Fe(III) concentrations were taken using Shimadzu UV-Vis 1700 spectrophotometer. The original ferrozine method (Stookey, 1970; Voelker & Sulzberger, 1996; Viollier et al., 2000) was followed with minor modification (Voelker & Sulzberger, 1996) and background experiment to assess the interference of Fe(III) in ferrozine-Fe(II) complex formation. In the presence of both Fe(II) and Fe(III) in the solution, Fe(III) could form complex with ferrozine thereby interfering with the Fe(II)-ferrozine complex coloration (Viollier et al., 2000). Therefore the following equation was used to calculate Fe(II) and Fe(III) concentrations to eliminate the Fe(III) interference (Viollier et al., 2000)..

$$C_{Fe(II)} = \frac{A_1 * \epsilon_{Fe(II)} * l * \alpha - A_2 * \epsilon_{Fe(III)} * l}{\epsilon_{Fe(II)} * l * \alpha (\epsilon_{Fe(II)} * l - \epsilon_{Fe(III)} * l)}; C_{Fe(III)} = \frac{A_2 - A_1 * \alpha}{\alpha * (\epsilon_{Fe(II)} * l - \epsilon_{Fe(III)} * l)} \dots\dots\dots(1)$$

Here, $C_{Fe(II)}$ and $C_{Fe(III)}$ are the calculated values of Fe(II) and Fe(III) concentrations; $\epsilon_{Fe(II)}$ and $\epsilon_{Fe(III)}$ are the molar absorption co-efficients for Fe(II) and Fe(III) respectively; l is the optical path length; α is the dilution factor; and A_1 and A_2 represent the absorption values before and after adding the reducing agent, respectively.

The values of $\epsilon_{Fe(II)} * l$ and $\epsilon_{Fe(III)} * l$ were obtained from the standard curves of Fe(II) and Fe(III), respectively. The dilution factor of 0.23 was introduced considering the addition of hydroxylamine hydrochloride (HA) as a reducing agent in the solutions.

For measuring A_1 , 1 ml of aliquot was withdrawn periodically from each test solution and 100 μ l of ammonium acetate buffer and 120 μ l of 4.9 mM ferrozine solution were added to

it. The absorbance was measured immediately at 562 nm wavelength using Shimadzu 1700 UV-Vis spectrophotometer. For measuring A_2 , the method was similar to the one for measuring A_1 except for that 1.5ml of 3ml hydroxylamine hydrochloride was added to each 0.5ml of aliquots and left the solution in dark for 15 mins before adding the buffer and ferrozine solution. The sample aliquots were withdrawn using a 10ml of syringe with 0.45 μ M PTFE filter to avoid the interference with undissolved hematite particles.

2.4 Results and Discussions.

The dissolution of iron from minerals has been a subject of intense study because of its significant role as a micro-nutrient in marine eco-system (Zinder et al., 1986; Wieland et al., 1988; Stumm & Wollast, 1990). Dissolution of iron could be non-reductive, producing Fe(III), or reductive, producing Fe(II). In either case, the dissolution follows two major pathways, proton promoted, or ligand promoted. The proton promoted dissolution from the Fe-minerals results in producing dissolved Fe(III), whereas the ligand assisted dissolution generates both Fe(II) and Fe(III), for instance, if the complex is exposed to UV light, the ligand can act as an electron donor to the Fe(III) metal center to produce photoreductive Fe(II). The detachment of the Fe metal center from minerals is the rate limiting step and is promoted by the surrounding ligands and/or protons in the solution (Siffert & Sulzberger, 1991). In general, transition metal complexes absorb radiation significantly in the UV region; however, the photo-chemistry of Fe in the ambient environment requires special emphasis because some of the Fe(III)-complexes can also absorb radiation in the near UV to some portion of visible spectrum which overlaps with the incoming solar radiation (Graedel et al., 1985).

Figure 2.1 shows the photo-reductive dissolution of Fe(II) from hematite at four different oxalate concentrations. The experiment had been conducted under 254nm UV light source. The formation of Fe(II) occurred only at sufficiently high concentration of oxalate (3mM). At lower concentrations of 10 and 50 μ M, the Fe(II) concentration started to decrease within 1.5hr of irradiation after a short period of increasing trend, while at the 500 μ M concentration range, the decreasing trend of Fe(II) started after 4hrs of irradiation. At high concentration (3mM), the Pearson correlation coefficient is 0.9, which demonstrates the consistency among the replicates and fairly stable surface interaction of oxalate with hematite.

However, for the lower concentration ranges, the complex nature of the interactions render them less consistent which is reflected in Table 2.1 and Table 2.2 These results indicate that the photo-reductive dissolution of Fe (II) from hematite is a function of oxalate concentrations, and the efficiency of Fe(II) production through this process could vary significantly in the global atmosphere, depending on the loading of this organic ligand in the ambient air.

The variation of Fe(II) formation under different concentrations of three ligands (oxalate, acetate, formate) in presence of 254 nm UV light was shown in Figure 2.2. The Fe(II) production through organic ligand induced photoreduction varied with changing concentrations for all ligands. However, the more pronounced effect was associated with the concentration variation of oxalate from lower concentrations (10, 50, 500 μ M) to a higher (3mM) concentration. At lower concentrations of oxalate (10 and 50 μ M), the Fe(II) concentrations showed a sustained substantial decreasing trend after 1hr of irradiation. Similar patterns were observed at a higher concentration (500 μ M) starting after 5hrs of

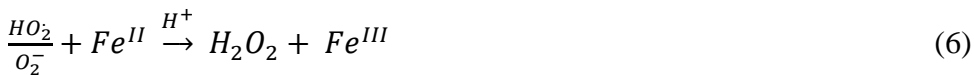
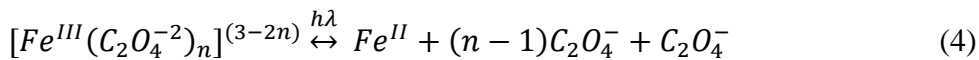
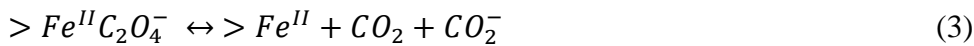
irradiation. The concentration of Fe(II) did not exhibit any increasing trend at any later point in the complete 24hrs of irradiation period. However under the high oxalate concentration (3mM), the Fe(II) concentrations showed a steady increasing trend until it reached the equilibrium (~ after 5 hours of irradiation). In the presence of formate and acetate, the Fe(II) concentrations increased for the initial 5hrs (while a comparatively steeper increasing trend occurred in the first 2hrs) of irradiation until they attained the equilibrium.

Figure 2.3 presents a comparative analysis with different organic ligands (oxalate, formate, acetate) in varying concentrations (50 μ M and 3mM), where the organic ligand and hematite mixtures had been irradiated for 24 hours under the UV light, without prior pre-coating. The varying concentration effect of oxalate is even more evident in Figure 2.3 than in Figure 2.2. For instance, in Figure 2.3, at 3mM oxalate concentration, the soluble Fe(II) concentration was ~7.5 μ M at the equilibrium, whereas in presence of 50 μ M oxalate concentration the soluble Fe(II) concentration was ~ 2.16 μ M. This indicates an almost 70% decrease in the photoreductive yield of Fe(II) when the oxalate concentration varies from 3mM to 50 μ M.

The comparison of the adsorption dissolution of Fe(III) from hematite mineral in the presence of oxalate, formate, acetate, and fluoride at two concentrations (50 μ M and 3mM) is shown in Figure 2.4. The ligand induced dissolution of Fe(III) from hematite by oxalate is substantially higher than those by formate and acetate in both concentration ranges. These three ligands were more effective in Fe(III) dissolution than fluoride; however, in the presence of fluoride, the dissolution of Fe(III) reached the equilibrium within 2hrs.

2.4.1 Effect of Varying Concentrations and Ligands

Being a d-block element, Fe shows high affinity for complex formation. The half-filled d-orbital in the Fe(III) ions creates a favorable condition for formation of a mononuclear mono-dentate or bi-dentate complex with suitable ligands. The ligands in solution bind with the surface molecules and consequently weaken the bonds closer to the surface metal atom, and this process enhances the liberation of metal Fe(III) in the solution. When exposed to solar radiation, the Fe(III)-organic ligand complex absorbs the energy from the solar radiation and enters into an excited state. At this stage, the electron donors, such as oxalate, acetate, and formate, act as a bridge and supply electron to the Fe(III) metal center, producing Fe(II) (Banwart et al., 1989; Sulzberger et al., 1989; Siefert & Sulzberger, 1991; Paris et al., 2011). In contrast with acetate and formate, the formation of a bi-dentate complex with oxalate is thermodynamically more favorable (because the process increases the entropy) and has greater stability, oxalate could be considered as a stronger ligand than acetate and formate. However, under adequate O₂ exposure, via reaction mechanisms (2-6), the oxalate radical generates H₂O₂ in the medium during the following reactions (Zuo & Hoigne, 1992; Siefert et al., 1994)..



A previous study shows that oxalate is sensitive to photolysis at approximately 320nm wavelength and forms peroxide radicals (Zuo & Hoigne, 1992). Even though, our experiment has been conducted at 254nm wavelength of UV light, the formation of H_2O_2 in the medium, either via interaction of oxalate with surrounding O_2 or by photolysis of oxalate, could lead to increased re-oxidation of Fe(II) to Fe(III), and decreases the efficiency of oxalate in producing Fe(II) from hematite. On the other hand, under similar conditions, acetate and formate have not been reported to produce H_2O_2 ; therefore, these two ligands should remain effective in photo-reduction of hematite. In this study, the production of Fe(II) via photo reduction in presence of the three organic ligands was generally fast, occurring within a few minutes of exposure to UV light. However, at low oxalate concentrations, the Fe(II) concentrations exhibited a sharp decreasing trend with time (Figures 2.1, 2.2, and 2.3), suggesting that the formation of H_2O_2 must have influenced the Fe(II) production rate. It is noteworthy that, in Figure 2.3 a slight decrease in dissolved Fe(II) concentration is observed after 6hrs in the presence of oxalate. The labile Fe(III)-oxalate bonding could facilitate Fe(III) dissolution, which might suppress the Fe(III) to Fe(II) reduction. Another plausible explanation could be the oxidation of Fe(II) to Fe(III) in the oxalate system in presence of oxygen. Since the decrease in Fe(II) concentrations after 6hr is low compared to its previous values, it would be very ambiguous to explain the possible reasons with definite claim. The varying concentrations of acetate and formate were not observed to exhibit significant effect on Fe dissolution, therefore, the dissolved Fe(II) concentrations were fairly constant after ~ 3 hours of irradiation.

When the oxalate concentration is high, the ligand effect of oxalate should pre-dominate the re-oxidization of Fe(III) to Fe(II) via in-situ production of H_2O_2 in deciding the fate of

Fe(II) production. The data analyses with the Visual Minteq 3.1 model shows that at a higher oxalate concentration (3mM), the dominant Fe-oxalate complex is $\text{Fe}-(\text{Oxalate})_3^{-3}$ (Table 2.3) which indicates the stronger ligand effect at higher concentrations. The high oxalate concentration results in increasing probability of chaos and consequently higher entropy in the system; however, binding with hematite and forming the complex should decrease the entropy (assuming the changes in enthalpy due to Fe(III)-oxalate complexation at higher oxalate concentration would be in similar order compare with oxalate at lower concentrations), thereby favoring the ligand effect of oxalate at higher concentrations. However, when the concentrations of oxalate are in lower ranges, i.e., 10 – 500 μM , the net change in the entropy due to complex formation with hematite does not favor the process enough to overcome the oxidizing effect of H_2O_2 energetically. This behavior is exhibited in Figure 2.1; to wit, oxalate is significantly less efficient than acetate and formate in low concentrations, mostly in remote marine locations, but significantly more efficient than acetate, and almost as efficient as formate in high concentrations (Figure 2.2 and Figure 2.3), especially in urban regions. A study shows that (Zhu et al., 1993), the soluble Fe(II) concentration increases significantly when an acidified 87 μM of Fe(III) solution is irradiated in presence of 0.1M $\text{Na}_2\text{C}_2\text{O}_4$ solution, whereas the soluble Fe(II) concentration decreases to almost below detection limit when the mixture is brought back to dark. In connection with our experiment, this study suggests a stronger photoreductive capacity of oxalate when it is present at sufficiently higher concentration level in the solution and the oxidizing effect of H_2O_2 pre-dominates immediately after irradiation shuts off. In this experiment, however, even at constant irradiation, the Fe(II) concentration starts to decrease after ~4 hours of irradiation in presence of 500 μM oxalate

concentration and after ~1.5 hours in presence of 10 and 50 μ M oxalate solution. It is interestingly to note that no distinct effect of varying concentrations have been observed in the case of acetate and formate. Similar trend showing the fastest photoreduction was observed when formate was used as the electron donor and hematite as the acceptor where the rate of photo reduced Fe(II) formation was 2nM/min with formate and 0.5nM/min in presence of acetate (the rate of Fe(II) production in presence of oxalate was not provided) (Pehkonen et al., 1993). This may suggest that the photoreduction process by this ligand is comparable although in the presence of oxalate, Fe(II) reacts with hydrogen peroxide and gets oxidized to Fe(III). High efficiency of formate may also be attributed to its comparatively smaller size and consequently reduced possibility of steric hindrance. Formate has been observed to be the most effective among these three ligands for photo-reduction of Fe-minerals (Zuo & Hoigne, 1992). For example, a study conducted to investigate the fog and cloud water samples at Los Angeles, California reported that, oxalate has not been observed to have an effect on Fe(II) dissolution in nature, unlike formate and acetate that showed high correlations with Fe(II) concentrations; whereas, oxalate concentrations were found to be highly positively correlated with the H₂O₂ concentrations (Erel et al., 1993). Adsorption Dissolution of Hematite in Presence of Oxalate, Acetate, Formate, and Fluoride

Although the previous photo-reductive dissolution experiment suggested that formate should be considered a stronger ligand for inducing Fe dissolution from hematite at lower concentrations, Figure 2.4 clearly demonstrates the dominance of oxalate over formate and acetate in forming Fe(III) via adsorption in both high and low concentrations. It is evident that the effect of varying concentrations is not significant with acetate and formate.

However, the Fe(III) dissolution rate increased dramatically in the presence of increased oxalate concentrations. The reason could be attributed to the fact that oxalate can form both outer-sphere and inner-sphere complexes and thereby resulting in increased dissolution of Fe(III) from hematite (Sulzberger et al., 1989)(Sulzberger et al. 1989). In addition oxalate is a bi-dentate ligand and it requires less amount umof the ligands to induce dissolution of Fe from hematite, compared to the mono-dentate ligands acetate and formate. Moreover, the ligands are the limiting reagents and once they get consumed the dissolution ceases.

A comparative analysis of fluoride from this study with the organic ligands (acetate, formate and oxalate) shows that the fluoride has no significant effect on adsorption dissolution of hematite to form Fe(III). With the fluoride concentrations at 50 μ M and 3mM, the average dissolved Fe(III) concentrations after 1hr were 5.5 μ M and 6.4 μ M, respectively, which remain almost unchanged throughout the experiment, which is evident from Table 2.2. This phenomenon strongly suggests that the organic ligand induced dissolution is highly effective in dissolved Fe(III) formation in comparison with inorganic ligand, such as fluoride, and this could be attributed to the stronger capacity of complex formation of the organic ligands with Fe-minerals.

2.4.2 Comparison between Instantaneous Irradiation on Fe(III)-Ligand Complex.

Figure 2.4 shows that 10-12 μ M Fe(III) was dissolved through adsorption-dissolution from hematite in the presence of the organic ligands used in this study. On the other hand, the comparative analysis between Figure 2.2 and Figure 2.3 indicates that substantially low amount of Fe(II) (~2 μ M) was released through photoreduction from hematite when the mixtures were irradiated after the Fe(III)-ligand complex attained the equilibrium., but if

the mixtures were allowed to be irradiated after immediate Fe(III)-ligand complex formation, as evident is Figure 2.3, the production of Fe(II) was significantly higher ($\sim 10\mu\text{M}$) and comparable to the Fe(III) production via adsorption-dissolution (Figure 2.4). Similar trends had been documented in other studies (Rijkenberg et al., 2006), where Fe(III)-ligand complexes were unable to produce Fe(II) after UV irradiation, and it was hypothesized that a different colloidal form of Fe was responsible for photo-reductive production of Fe(II) rather than Fe(III)-organic complexes. In contrast, the results of our experiment, as demonstrated in Figure 2.3, however, clearly indicate that Fe(III)-organic ligand complexes can photo-reductively produce Fe(II) via instantaneous surface complexation with organic ligands. In order for the photo-reduction to happen, the ligand has to supply the electron to the Fe(III) metal center in a higher excited energy state, which requires sufficient supply of energy from UV light source. Based on these results, we hypothesize that the photo reduction process is fast and the subsequent ligand to metal electron transfer should occur soon after the ligand-metal bond was formed. Once the ligand-Fe(III) complex reaches the equilibrium in the solution, it becomes stable and thereby difficult to induce the photo-reduction. This mechanism could be relevant for estimating the amount of dissolved Fe(II) from Fe(III)-ligand complexes via photo reduction.

The results from these laboratory experiments further infer that the photo-reduction of Fe(III)-ligand complexes and the consequent formation of Fe(II) is relevant when (1) persistent solar radiation is available for a long period of time to stimulate the Fe(III)-ligand complexes to a higher energy state so that the electron transfer process can take place, and

(2) organic ligands in the aerosols would come in contact with freshly eroded Fe-minerals in the air.

2.4.3 Comparison with Observational Data.

The results from this study are in good agreement with the data collected during field operations (Chen & Siefert, 2004; Buck et al., 2010; Xia & Gao, 2011; Gao et al., 2013; Xu et al., 2013). Results from this study suggested that the mass ratio of oxalate concentration to the total Fe concentration should be at least 1 in order to attain the steady state production of photo-reduced Fe(II). A study carried out by Xia and Gao (2011) at Newark in NJ, an urban location, where the average oxalate concentration was ~ 4 times higher than the average concentration of the total Fe, shows that the oxalate concentration was highly correlated with the dissolved Fe(II) concentration (correlation coefficient = 0.90). Whereas, in a remote Antarctic region, where the same ratio of oxalate to the total Fe was 0.16, the correlation between soluble Fe(II) and oxalate concentrations was significantly low (correlation coefficient = 0.03) (Matsumoto et al., 1997; Gao et al., 2013; Xu et al., 2013). Similar pattern was observed over the North Atlantic (Chen & Siefert, 2004), where the concentration ratio of oxalate to the total Fe was above 1, and the correlation coefficient between Fe(II) with oxalate was 0.35. A comparison of relevant data from different studies is shown in Figure 2.5 (Chen & Siefert, 2004; Buck et al., 2010; Xia & Gao, 2011; Gao et al., 2013; Xu et al., 2013). The x-axis represents the ratio (R) of the oxalate concentrations to the total Fe concentrations and the y-axis represents the correlation coefficient between soluble Fe(II) with the oxalate with all data points where the ratios of oxalate- to the total Fe were greater than R and at least 5 data points are available). In this comparison, the data set from Buck et al. (2010) was divided into two

groups: the tropical region where the data values were from south of 23.5° N, and the temperate region where the values were from north of 23.5° N. Figure 2.5 reveals that all the data sets are associated with a sharp increase (except for Antarctica) where the correlation coefficients in the Y-axis show a sudden elevation (represented by the solid vertical lines). Based on the results from these observations and from this laboratory experiment, it appears that the values of R has to be at least 1-6.5 in order for oxalate to influence the photo reduction process. When the R value is low (below 1), oxalate could be inefficient for producing soluble Fe(II) via photo-reduction, and other organic ligands such as formate may play more important role in Fe dissolution. On the other hand, when the R value is high (above 1.0), oxalate could be highly effective for photo-reductive production of soluble Fe(II).

2.5 Conclusion.

Results from this study lead to following conclusions:

- 1) Among the three ligands tested in this study, oxalate is the strongest organic ligand to induce adsorption dissolution of hematite to produce dissolved Fe(III).
- 2) In oxic environment and under UV radiation, the varying concentrations of oxalate play a crucial role in determining the Fe speciation: the production Fe(II) via photo-reduction of Fe(III) could be substantially hindered at low concentrations, and the concentration ratios of oxalate to the total Fe should be at least 1:1 or higher. However, formate and acetate were not sensitive with the concentration variation during the photo-reduction of hematite.
- 3) Pre-complexation of Fe(III)-ligand could reduce the photo-reduction of hematite. For instance, in the presence of 3mM ligand concentration, the amount of soluble Fe(II)

decreased ~ 70%- 80% when the Fe(III)-ligand complexes were irradiated after equilibrium as compared with instantaneous irradiation on the in-situ produced nascent Fe(III)-ligand complexes.

The Fe deposited from the atmosphere readily gets complexed with organic ligands in sea waters in the surface ocean, and the complexation with organic ligands substantially hinders the photo reduction of hematite. These processes also depend on the mineralogy of the Fe minerals, sources and abundance of the ligands, and thus more field experiments need to be carried out for better understanding of Fe dissolutions in dust in addition to the lab-based experiments.

2.6 Tables.

Table 2.1 The Pearson correlation coefficients between the data for the repeated experiments. When an experiment is repeated thrice, the average of the three inter-correlations among the three sets of data is presented.

		Oxalate	Acetate	Formate	Fluoride
Photo-reductive	10 μ M	0.66	0.74	0.73	N/A
dissolution of Fe(II)	50 μ M	0.56	0.59	0.65	N/A
(Figure 2.2)	500 μ M	0.61	0.61	0.53	N/A
	3 mM	0.90	0.95	0.89	N/A
Photo-reductive	50 μ M	0.54	0.50	0.53	N/A
dissolution of Fe(II)	3 mM	0.46	0.89	0.93	N/A
after instantaneous UV-					
irradiation (Figure 2.3)					
Adsorption dissolution	50 μ M	0.95	0.70	0.76	0.61
of Fe(III) (Figure 2.4)	3 mM	0.92	0.85	0.59	0.47

Table 2.2 Range of dissolved Fe concentrations (μM) after reaching equilibrium.

		Oxalate	Acetate	Formate	Fluoride
Photo-reductive dissolution of Fe(II) (Figure 2.2)	10 μM	0.04	- 0.28	- 0.72 – 1.08	N/A
		0.28	0.98		
	50 μM	0.10	- 0.35	- 0.70 – 1.23	N/A
		0.29	1.05		
	500 μM	0.34	- 0.51	- 0.74 – 1.06	N/A
		1.27	1.18		
	3 mM	1.34	- 0.96	- 1.5 – 2.52	N/A
		2.6	1.38		
Photo-reductive dissolution of Fe(II) after instantaneous UV- irradiation (Figure 2.3)	50 μM	2.32	- 2.62-	4.62-5.95	N/A
		3.71	3.47		
	3 mM	5.26-	7.34-	7.86-9.08	N/A
		9.95	7.97		
Adsorption dissolution of Fe(III) (Figure 2.4)	50 μM	8.9	- 5.32	- 6.97 – 9.36	5.14 -
		12.3	7.89		5.87
	3 mM	12.3	- 7.89	- 8.9 – 11.0	5.7 -
		14.9	8.99		6.6

Table 2.3 Speciation of Fe-ligand complexes at varying ligand concentrations (Visual Minteq 3.1 Chemical model).

Speciation	10 μ M	50 μ M	500 μ M	3mM
[Fe-(Oxalate) ₂] ⁻	6.77E-09	1.6E-07	8.98E-06	5.17E-05
[Fe-(Oxalate) ₂] ⁻²	9.45E-22	1.98E-20	6.1E-19	2.20E-18
[Fe-(Oxalate) ₃] ⁻³	5.69E-10	7.15E-08	3.39E-05	6.39E-04
[Fe-Oxalate] (aq.)	3.17E-18	1.31E-17	5.09E-17	6.62E-17
[Fe-Oxalate] ⁺	9.68E-10	4.73E-09	3.57E-08	8.77E-08
[Fe-Formate] ⁺²	2.10E-15	1.05E-14	1.08E-13	6.91E-13
[Fe-(Acetate) ₂] ⁺	1.62E-17	4.05E-16	4.06E-14	1.47E-12
[Fe-(Acetate) ₃] (aq.)	2.48E-21	3.10E-19	3.10E-16	6.67E-14
[Fe-Acetate] ⁺	3.64E-21	1.82E-20	1.80E-19	1.05E-18
[Fe-Acetate] ⁺²	5.22E-15	2.61E-14	2.64E-13	1.63E-12

2.7 Figures.

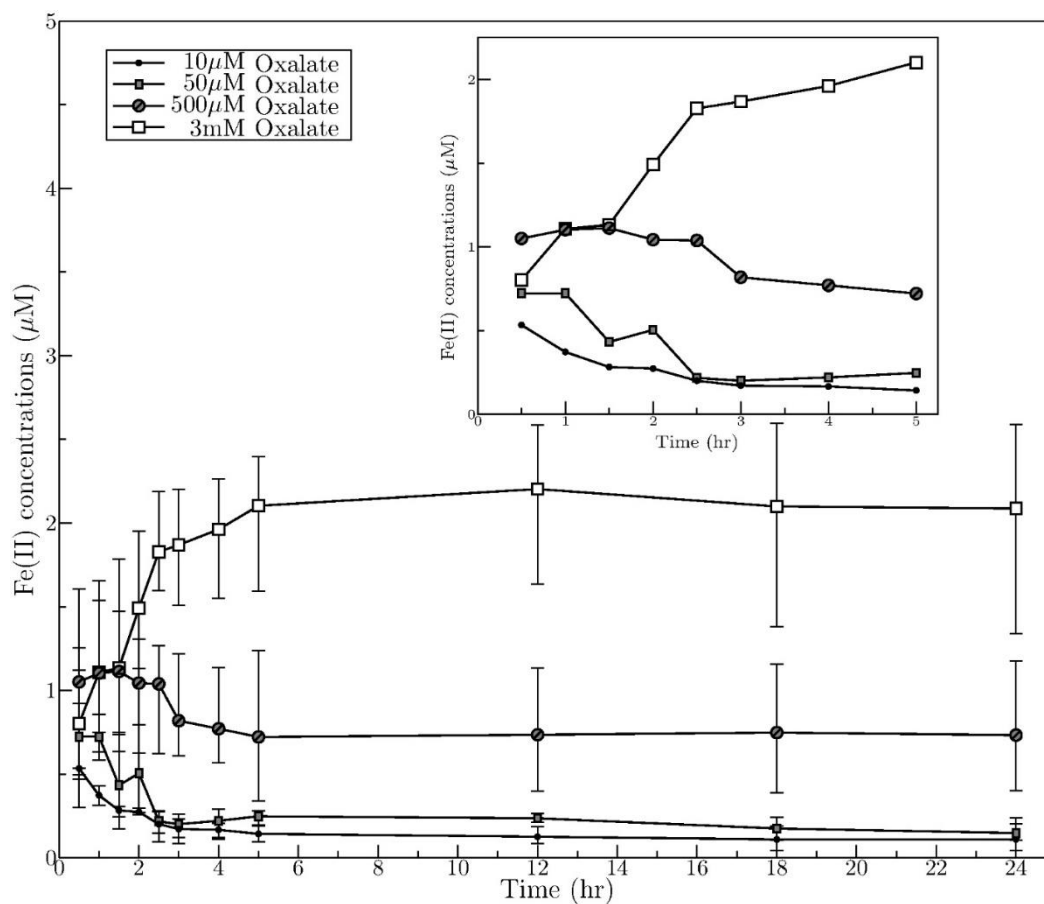


Figure 2.1 The effect of varying oxalate concentration on the photo-reductive dissolution of Fe(II) from hematite. The inset shows the details for the first five hours. The error bars are representing the range of the triplicate experiments.

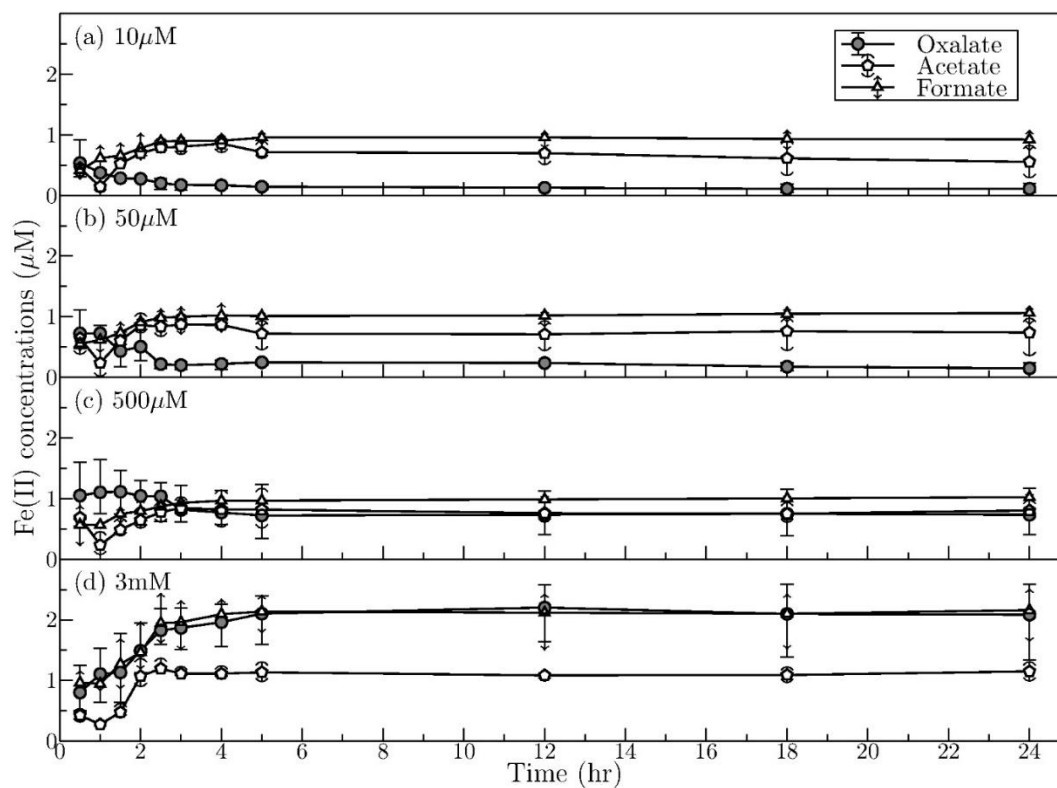


Figure 2.2 Photo-reductive dissolution of Fe(II) from hematite in presence of varying concentrations (10, 50, 500 μM , and 3mM) of oxalate, acetate, and formate. The error bars are representing the range of the triplicate experiments.

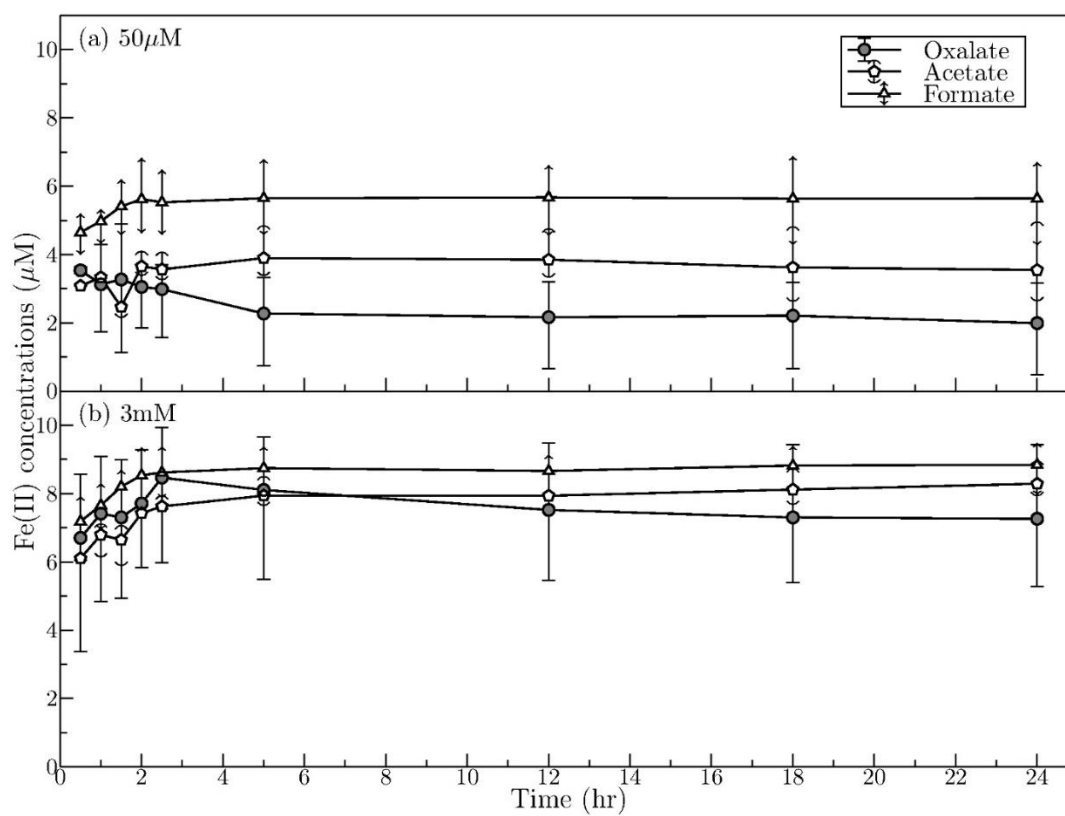


Figure 2.3 The effect of instantaneous UV-irradiation on the photo-reductive dissolution of Fe(II) from hematite in presence of 50 μM and 3mM concentrations of oxalate, acetate, and formate. The error bars are representing the range of the triplicate experiments.

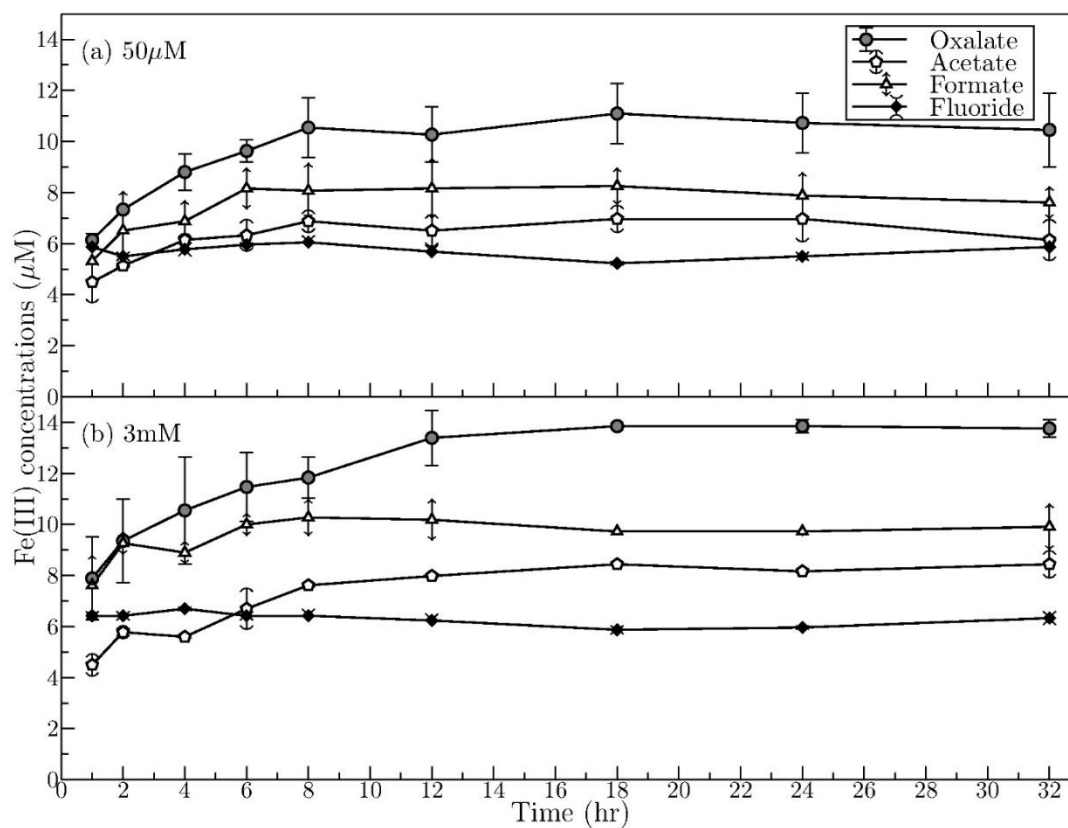


Figure 2.4 The adsorption dissolution of Fe(III) from hematite in the presence of 50 μM and 3 mM concentrations of oxalate, acetate, formate, and fluoride. The error bars are representing the range of the repeated set of experiments.

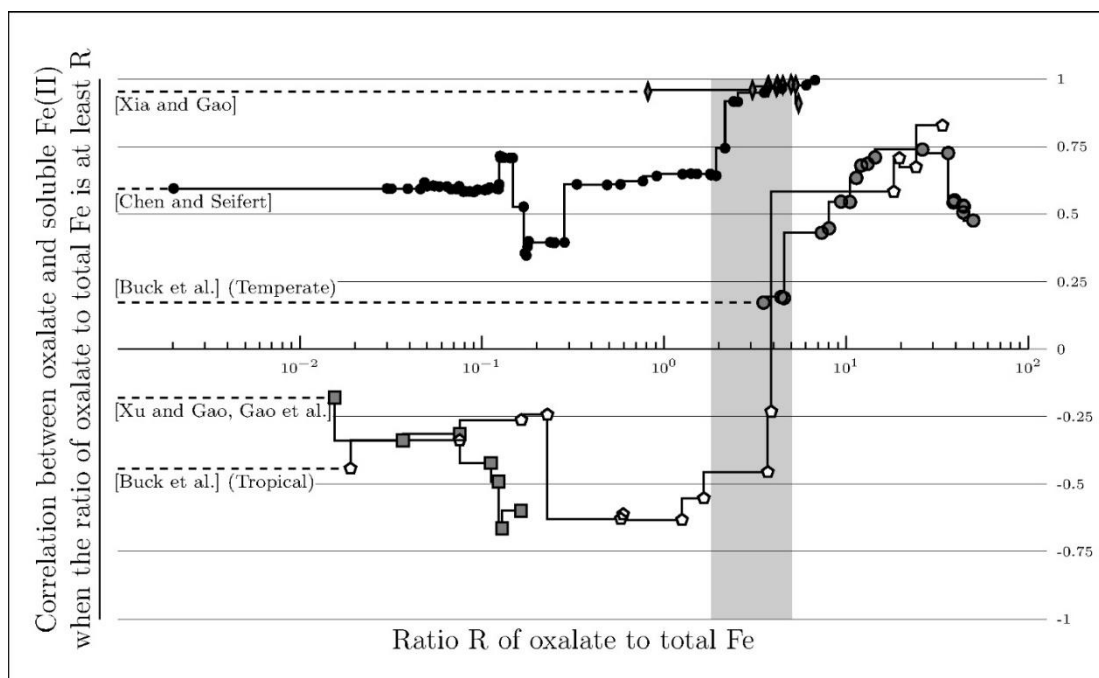


Figure 2.5 Empirical correlation between oxalate and soluble Fe(II) concentrations when the ratio between oxalate and total Fe is at least R, plotted against the parameter R. The data is collected from [Buck et al., 2010], [Chen and Seifert, 2004], [Gao et al., 2013], [Xia and Gao, 2009, 2011], [Xu and Gao, 2014].

3 Insignificant Impact of Freezing and Compaction on Iron Solubility in Natural Snow

3.1 Abstract.

To explore the freezing effect on iron (Fe) solubility in natural environments, especially in Polar regions, event based freshly fallen snow samples were collected at Newark, New Jersey on the US East Coast for two consecutive winter seasons (2014–2015 and 2015–2016). These samples were analyzed for the concentrations of soluble iron (Fe_{sol}) using UV-Vis Spectroscopy and filterable iron (Fe_{fil}) and total iron (Fe_{tot}) using Atomic Absorption Spectroscopy. The average fractional solubility of the Fe_{sol} (the portion that passes through a $0.22\mu m$ pore-size filter) with respect to the total Fe in the samples was $23.3\pm 12.2\%$, with the majority of the soluble Fe being present as Fe(III). Approximately 48.5% of the total Fe existed as Fe_{fil} (the portion that passes through $0.45\mu m$ pore size filter media). No significant correlation was found between the soluble ionic species and soluble Fe. Samples from six snow events were kept frozen for 10 days, and analyzed in periodic intervals to study the post-freezing modification in Fe solubility. Events 1 and 2 showed increasing trend in the soluble Fe concentrations; however, the events 5, 6, 7, and 8 showed no noticeable increments. The pattern shown in Events 1 and 2 is associated with high fraction of Fe_{fil} and one unit pH drop, suggesting that the freeze-induced modification in Fe solubility could be linked with the amount of Fe_{fil} and the acidity change in the samples. To further investigate the freeze-induced compaction of particles, samples from three events 6, 7, and 10 were analyzed by SEM-STEM-EDS microscopy, and the results showed that due to freezing, in general, the particles in the ice-melt counterparts tend to compact

and cluster and form larger aggregates compared to the particles in snow-melt. These results show, despite the freeze-induced compaction in snow was observed from STEM images, the snow freezing might not have significant effect in increasing Fe solubility from materials in the snow. These results further suggest that freezing process with fresh snow in high-latitude regions may not impose significant modification on Fe solubility in snow.

Key words: Iron solubility, freeze-induced compaction, urban snow events, scanning electron microscopic analysis

3.2 Introduction.

Iron (Fe) is a critical micro-nutrient affecting the marine eco-systems. Atmospheric deposition (dry and wet) is an important external source of Fe in the surface waters of several large remote oceanic basins (Duce & Tindale, 1991; Fung et al., 2000; Gao et al., 2001). The uptake of Fe by marine phytoplankton critically depends on the amount of dissolved Fe, known as bio-available Fe (Wells et al., 1995; Sunda, 2001). High latitude locations of North America experience significant amounts of snowfall each year. Field studies have shown that, compared to rainfall, snow events are more efficient for below cloud scavenging of aerosol particles (Sempère & Kawamura, 1994; Paramonov et al., 2011) because of the larger size and surface area of the snowflakes. This effect is important since the snow would scavenge and store suspended insoluble Fe-containing particles, which can further produce soluble Fe. The smaller particles (0.2–2 μm) associated with the dendritic crystals in the snowflakes are particularly important in characterizing this unique filtering effect due to the porosity of snowflakes, which allows the air to pass through while collecting the falling solids (Franz & Eisenreich, 1998).

The effect of freeze concentration on the Fe solubility from several iron minerals has been studied in laboratory set-ups (Kim et al., 2010; Jeong et al., 2012). These studies reported

that both the photo reductive dissolution of Fe(II) and non-reductive dissolution of Fe(III) in dark from insoluble iron oxides enhance significantly after freezing the aqueous suspension of the iron oxides (with organic ligands). The authors suggested that the “freeze concentration effect”, a process when the solutes cluster together during freezing thereby increasing the possibility of chemical interaction (Kim et al., 2010; Jeong et al., 2012), resulted in increased Fe solubility. Similar enhancements in chemical processes involving other metals by freeze-concentration effect were reported, such as auto-oxidation of N(III) and S(IV) in frozen solutions (Betterton & Anderson, 2001) and oxidation of nitrite by dissolved oxygen under the freezing condition (Takenaka et al., 1996; Takenaka et al., 1998). Both of these phenomena, the efficient scavenging of Fe-containing aerosols by snow and the increased Fe dissolution from Fe-minerals in frozen ice, are highly significant, especially in Polar regions, since the deposited snow would contain and store larger amount of soluble Fe which would eventually enter into the ocean after melting, providing more bio-available Fe to the surface sea waters. Evidence of enhanced (approximately 2 to 14 fold) Fe solubility in the sea-ice mixed layer was observed in Ross Sea as a result of melting sea-ice (Sedwick & DiTullio, 1997; Sedwick et al., 2000). Fe-deposition to the oceans is particularly relevant in the Polar oceans, which remain frozen for long periods of time, but recent warming in some of those regions has caused intense melting of sea-ice (Polyakov et al., 2010).

Certain organic ligands, such as oxalate and inorganic sulfate, which are ubiquitous in the ambient air, could also play a crucial role in enhancing Fe solubility in aerosols (Pehkonen et al., 1993; Siefert et al., 1994; Luo & Gao, 2010; Chen & Grassian, 2013; Paris & Desboeufs, 2013).

In the laboratory-based experiments to study Fe solubility in frozen ice by (Kim et al., 2010; Jeong et al., 2012) , the concentration of the species and the acidity of the medium were controlled at levels not always found in the natural system. In addition, the studies were performed by freezing aqueous suspensions, which might have produced higher freezing concentration effects than freezing fresh snow, which is a complex mixture of ice crystals, air, chemical species (Domine et al., 2006), and occasionally liquid water (Colbeck, 1982).

In this study, we collected event-based snow samples at Newark, New Jersey for 2 consecutive winter seasons (2014–2015 and 2015–2016) with the following goals: (1) to analyze the fractional solubility and speciation of iron in the freshly fallen snow and the changes after transformation into ice due to freezing, (2) to identify the role of organic and inorganic species (such as acetate, formate, oxalate, sulfate) in modulating Fe solubility, (3) to characterize post-freezing modifications on the particle morphology and chemistry present in snow and understand their effect on Fe solubility.

Here we present the results of the modifications of Fe solubility in freshly fallen snow, both in its original form and after freezing (compaction) to resemble the natural setting. These data from fresh snow are representative of the processes occurring in the Polar regions and will advance our current understanding about the possible sources of bio-available Fe from the global warming induced melting of the stacked ice.

3.3 Methodology.

3.3.1 Snow Sample Collection.

Acid-cleaned 250ml PTFE bottles were used for event based snow collection in Newark, New Jersey, for two consecutive winter seasons (2014–2015 and 2015–2016): five events

in 2014–2015 and four events in 2015-2016 winter seasons. Table 3.1 provides the description of the snow events and the relevant meteorological information. The samples were collected during the snowfall when the snow accumulation reached enough height to avoid ground contamination.

For each snow event, the samples were collected from four different locations of the study site to account for the spatial variation of the concentration in the study site. The snow samples were scooped from the surface using pre-cleaned Teflon spatula or the cap of the pre acid cleaned PTFE bottles. Rigorous cleaning was applied to the cleaning of the PTFE bottles. The bottles were rinsed thoroughly with 18.2 M Ω Milli-Q water followed by cleaning in 2% decon detergent to get rid of the decon detergent. After that the bottles were rinsed with Milli-Q water again and re-filled with 10% analytical grade hydrochloric acid (HCl) and leached at 60°C for 48 hours. The bottles were rinsed again and re-filled with 1% trace metal grade HCl and leached at 60°C for another 24 hours. After that the bottles were rinsed with Milli-Q water and re-filled with 0.1% trace metal grade HCl for storage until snow collection. The syringe-filter was rinsed with Milli-Q water before each use. With this procedure, the absorbance values for the bottle blanks for soluble Fe were close or often below detection levels. The average weight of the snow samples from each container was approximately 29.7 ± 0.7 g and the average density was 0.12g/ml.

Only those events were considered when the snow accumulations reached sufficient height from the ground to prevent any contamination from the ground, similar to the methods used by other investigators (Edwards & Sedwick, 2001; Sattler et al., 2001; Lalonde et al., 2002; Ferrari et al., 2008). Only nine such snow events occurred in two consecutive years which allowed us to collect sufficient amount of samples for analysis but continuous measurement

in future will be performed. After collection, the bottles were capped and triple bagged with plastic Ziploc bags immediately and brought back to the laboratory for filtration, storage, and analysis.

Sixteen sets of snow samples from event 2 and event 3 in pre-cleaned zip lock bags were prepared and placed under natural solar radiation for approximately 4 hours to study the sunlight induced modification of Fe solubility and speciation.

3.3.2 Analysis of Soluble (Fe_{sol}), Filterable (Fe_{fil}) and Total Iron (Fe_{tot}).

The snow samples were thawed at room temperature in a 100 class clean room, and divided into three portions. One portion was filtered through 0.22 μ m PTFE syringe filter for soluble Fe analysis at UV-Visible spectroscopy (UV-Vis Shimadzu-1700) using a 10cm path length cell (Starna Cells, Inc). The second portion was filtered through 0.45 μ m syringe filter acidified to pH 2 (with 0.1M nitric acid) (Özsoy & Saydam, 2001) and refrigerated immediately for Fe analysis using atomic absorption spectroscopy (iCE-3000 series, Thermo Fisher Scientific). The definition of Fe solubility is complicated due to complex Fe chemistry in aqueous solution. The traditional definition of soluble fraction of any trace metal in aqueous solution is the portion that passes through 0.4–0.45 μ m filter media and stored at pH 2. This definition would lead much uncertainty specifically because Fe exists both in both colloidal and soluble form. Therefore, the traditionally defined soluble fraction of Fe would contain both dissolved iron and the colloidal particles and it is impossible to distinguish the “truly dissolved” iron from the colloidal form of iron (Johnson et al., 1994). In this study, according to (Özsoy & Saydam, 2001), the portions of the iron in the snow samples that passed through 0.22 μ m and 0.45 μ m filters were defined as soluble fraction of iron (i.e., Fe_{sol}) and filterable fraction of iron (i.e., Fe_{fil}), respectively. The total Fe (Fe_{tot}),

which is the total of the dissolved iron (both in soluble and colloidal form) and the insoluble iron, was measured using the atomic absorption spectroscopy from the unfiltered snow samples after acidifying the samples at pH 2 with optima grade hydrochloric acid (Kieber et al., 2001). The detection level was approximately 20ppb. All the values were corrected by the respective field blank values. The concentration of Fe in the samples was approximately 33% to >100 % higher than the field blank values. The speciation of the soluble Fe was analyzed in UV-Vis spectrophotometer, following the ferrozine method described in Stookey (1970) and Xia and Gao (2010). Briefly, for the soluble Fe(II) analysis, 20ml of filtered snow samples were mixed with 8ml of ammonium acetate (~pH 5.5) and 1mM ferrozine solution and the absorbance of the samples were measured at 562 nm wavelength. For the soluble Fe(III) analysis, 5 ml of 0.1M hydroxylamine hydrochloride was added to reduce the Fe(III) to Fe(II) and then the total soluble Fe(II) was measured. Soluble Fe(III) was calculated after subtracting the initial soluble Fe(II) from the final soluble Fe(II). The method detection level for Fe analysis was 5.7 ppb.

In order to study the freezing concentration effect on modulating the solubility of iron, six snow events (events 1, 2, 5, 6, 7, and 8) were stored in the freezer at -20 °C immediately after collection and were taken out at periodic (2days, 5days, 7days, and 10days) intervals followed by melting in a 100 class laminar flow clean room at room temperature in the dark. After complete melting, aliquots were withdrawn and the concentration of Fe_{sol} was measured following previously described procedure. Table 3.2 provides the schematic of the snow sample treatments.

3.3.3 Analysis of Water-soluble Organic and Inorganic Species.

The filtered (passing through 0.22 μ m syringe filter) samples were analyzed using the Ion Chromatography (Dionex-2000) for water-soluble organic and inorganic species including acetate, formate, oxalate, methane sulfonate, and sulfate, and the major cations (sodium, potassium, and calcium). For the anion analysis, AS11 analytical column (2 X 250mm², Dionex) and KOH eluent generator cartridge (EGC II KOH, Dionex) were used, while for the cations, CS12A analytical column (2 X 250mm², Dionex) and MSA generator cartridge (EGC II MSA, Dionex) were used. A 25 μ l sample loop were employed for the analysis. The method detection level for the major anions were: 0.008 ppm for propionate, 0.007 ppm for acetate and formate, 0.018 ppm for oxalate, 0.013 ppm for sulfate, 0.015 ppm for chloride, and 0.016 ppm for MSA; and for the major cations was below 0.01 ppm. Propionate and MSA were below detection levels in the samples.

3.3.4 STEM Morphological Analysis of the Snow Particles.

The 6 days back trajectory analysis (NOAA Hysplit model) had been conducted for nine snow events. The analysis showed that the events were influenced mostly by continental air masses, except event 7 where the air mass slightly were mixed with the marine air coming from the Atlantic Ocean. Based on the air masses, three snow events (event 1, event 6, and event 7) were selected for further morphology and mineral analyses. Morphology and mineralogy of the particles present in the snow and ice were examined using Scanning Transmission Electron Microscopy (STEM) with Energy Dispersive Spectroscopy (EDS) (high-resolution Field Emission Scanning Electron Microscope, Hitachi S-4800). The thawed snow samples that were stored in the fridge and the frozen ice samples that were melted at room temperature prior to the analysis were mounted on TEM grid (silicon

dioxide, copper 97 μ m grid hole size, Ted Pella) and analyzed using 20kv voltage under standard vacuum conditions. For each sample, entire TEM grid was analyzed and particles that allowed EDS analysis were investigated for elemental composition, which produced approximately 30 different analytical spots for each sample. At least 1 replicate was performed for each sample to ensure the consistency in the samples textural and elemental composition. Random sampling of the mixed solution is the only way to do this kind of analyses and we had done all of the analyses in duplicates, and if duplicates differed we performed triplicates to observe every detail of the sample. On the first set of samples analyzed, more repeats were performed to make sure the approach was working. We also analyzed bulk samples from two events (event 6 and 7) using Beckman Coulter N4 Plus particle counter at NJIT to compare the analyses by SEM-TEM. The results from the two approaches agreed, and this ensured the applicability of the morphological and chemical analyses of the samples using SEM/TEM/EDS system.

We dipped the copper grid into the solution to collect particles; however, due to particles' impaction, there is a possibility that some particles may bypass the grids and may not get collected at all. The particle impaction may only be significant for very small particles, but in our samples we were able to observe particles in nm size ranges. However, the SEM TEM instrument has a limitation resolve very high magnifications of few nm sizes. In the future, I may apply to analyze these kind of samples at Synchrotron facilities to observe and analyze the finest particles fractions that are in the solution.

To perform a comparative study the post-freezing modification of the particle morphology in the snow, the snow-melt counterparts of frozen ice samples were analyzed for event 6 and event 7. In order to avoid freezing and formation of ice-crystals (which would be an

analogous of long term freezing in the environment), the snow-melt counterparts were stored in the refrigerator at approximately 5°C (which would be comparable to the melted snow without having stayed in sub-zero environment). As the samples from event 6 and event 7 were stored in the fridge for some time, we have performed additional set of analysis after immediate snow collection to ensure that the data collected for the first two events are indeed representative for the observed particle characteristics of the snow and ice counterparts. An extra set of snow samples was collected in 2016-2017 (event 10, Table 3.1), and its snow-melt was analyzed within 4 days of collection.

3.4 Results.

3.4.1 Total Fe, Filterable Fe and Soluble Fe Concentrations in Snow Samples.

The total Fe_{sol} (soluble Fe(III) and soluble Fe(II) wherever present) in the nine snow events varied from 4.1-21.0ppb with an average of 12.5 ppb (standard deviation 6.3ppb) (see Figure 3.1a and Table 3.3). Similar wide variation in Fe concentrations in snow samples has been observed elsewhere, for instance in snow collected from a single site in the remote south Polar region (Edwards & Sedwick, 2001). The measured soluble Fe concentration in this study is comparable with the other measurements conducted in coastal locations (Table 3.3).

However, much higher concentration of soluble Fe was observed in cloud water samples at Los Angeles, Bakersfield, California and Delaware Bay by other researchers (Erel et al., 1993) and in fog water samples (Behra & Sigg, 1990). The lower soluble Fe concentration in our study might reflect the fact that higher accumulation of water droplets might have diluted the soluble Fe level, which would be more effective during snow formation (Kieber et al., 2001).

The majority of the soluble Fe from all of seven samples from events (event 1 and events 4-6 and events 8-9) was present as Fe(III), with little or no detectable Fe(II), with the exception being samples from event 2, event 3, and event 7. In events 2, 3, and 7 the ratios of soluble Fe(II) and Fe(III) were 0.50, 0.92, and 0.05 respectively.

The average concentrations of Fe_{tot} and Fe_{fil} were 58.1 ± 17.4 ppb and 28.0 ± 15.1 ppb respectively (Table 3.3). Comparable ranges of total Fe concentrations were observed in the rainwater samples at Northern Atlantic coast (Table 3.3). Comparatively lower total Fe winter mean value (10 ppb) of precipitation samples reported by (Song & Gao, 2009), at the same study site at Newark, New Jersey, could be explained by the difference in the methodology; their samples were filtered through a $0.45 \mu m$ syringe filter before analysis, therefore the total iron reported there will be comparable to the total Fe_{fil} in this study.

The high Fe_{fil} concentrations were not associated with the maximum Fe_{tot} values. Figure 3.1b describes the fractional solubility of total Fe_{sol} with respect to Fe_{fil} and Fe_{tot} (operationally defined as Fe_{sol}/Fe_{fil} , and Fe_{sol}/Fe_{tot} , times 100). The fractional solubility of Fe_{sol}/Fe_{tot} ranges from 4.9-42.8%, comparable to the values reported from the south Polar snow samples with geometric mean 32% (Edwards & Sedwick, 2001) and the rainwater samples from Turkey with average 7.5% (Özsoy & Saydam, 2001), and both of those studies found wide ranges in the fractional solubility. High fractional solubility was observed in rain samples collected at Kerguelen Islands, southern Indian Ocean (Heimbürger et al., 2013).

Similarly, the fractional solubility of Fe_{sol}/Fe_{fil} varies from 16.5-88.5%. Approximately, 24% higher colloidal Fe (defined as the fraction that passes through $0.4 \mu m$) than the soluble Fe was reported by Kieber et al. (2001) in Willington NC rainwater samples, 13% higher

by Hofmann et al. (1991) in one rainwater sample collected in Germany, and 20% (geometric mean) higher in Turkey rainwater samples by Özsoy and Saydam (2001).

3.4.2 Freezing Concentration Effect on the Fe Solubility.

Figure 3.2a-2d shows the results from the frozen snow samples. This experiment was conducted as a laboratory analog to the natural environments where snow would compact and form ice, such as the Polar Regions. The data collected from the six freezing experiments events indicate that the total soluble Fe (Fe_{sol}) substantially increased with freezing time in events 1 and 2, with the average increment of 2.1 and 3.6 times with respect to the initial soluble Fe, respectively. However, in the other events the changes in Fe_{sol} concentrations were not significant and only occasional increments in the soluble Fe were observed. For example, in event 5 the soluble Fe concentrations increased initially (until day 5) and decreased after that.

3.4.3 Particle Morphology.

Three snow events (event 1, event 6 and event 7) were selected for morphology and mineral analyses. The back trajectory analysis (Figure 3.4) showed that all the events were influenced mostly by north American continental air masses (including selected events 1 and 6), except event 7 where the air mass was slightly mixed with the marine air coming from the Atlantic ocean (Figure 3.4 contains the representative images of the back trajectory analysis for the events 1, 6, 7, and 10). For two events (event 6 and 7) we used snow-melt and ice-melt (the frozen counterpart) to investigate the modification in the particle morphology and chemical composition due to freeze-induced compaction under STEM-EDS. The event 1 was collected in early 2015 while the protocol for STEM was established in later 2015. We did not include the STEM results from Event 1 because we

suspected that the longer storage time for samples from this event in the refrigerator might not reflect accurate morphology.

In addition to that, another set of snow (event 10) was collected and the snow-melt and the ice-melt counterpart after freezing were analyzed within four days to investigate the morphology and the elemental compositions of the particles in snow, quickly after the collection. Figures are shown in Figure 3.5-3.8.

The observed particles widely ranged in size from submicron scale to 100 μ m, and in morphology from smear-like morphology to complex corrugated aggregates. Most of the particles were aggregates, composed of a larger amorphous (corrugated) particle (that is composed of Carbon or it may be Silicate-Aluminum Oxide) that holds together smaller particles of different compositions. Very few compact and uniform in composition crystalline particles were observed and they were mostly larger in size (50 to 100 μ m). Numerous particles on TEM grid seemed very thin and were too thin to be analyzed by EDS, due to their morphology we treated these particles as smears, rather than calling them particles.

Event 6 – Snow-Melt.

Based on the morphologies observed under STEM, it seems the particles have been overly soaked and started to dissolve in the snow-melt. This sample, as its ice-melt counterpart, has three groups of particles; a large about 100 μ m in size aggregates with the main amorphous mass composed mostly of Si, O, C and Al, and the grains attached may be of very diverse chemistry including S, Cl, P and Ca; the next group of particles are smoother pieces of 1 to 10 μ m in size and they are uniformly composed of Si, O, Al and some C; the

third group of particles are nanoparticles associated with the smears. These are mostly composed of C, O with minor contribution of Si and Al, these were not found in any of the ice-melt samples from this snow event.

Event 6 – Ice-Melt.

Based on the analysis of three subsamples, we have observed that ratio of smear vs. crystalline particle is 50:50%. Some of the particles are very large, up to 100 μ m. Smears are mostly composed of Carbon (C), Silicate (Si) and Oxygen (O) with some Aluminum (Al) or in some cases they were of Al and O composition with some Si. The Al rich smears may occasionally hold Calcium (Ca). The amorphous particles have the same composition as the smears, but unlike smears they enclose grains of different composition so we call them aggregates in here. Aggregates are usually less than 1 μ m and 1 to 5 μ m in size and the grains may be of Sulfur (S), Chlorine (Cl), Fe, Ca, Sodium (Na) compositions, and less commonly may contain Potassium (K) and Phosphorus (P) compounds. Third category of particle morphology included smooth crystalline particles of Si, O, and Al composition.

Event 7 – Snow-Melt.

The particles from this sample are comparatively smaller than those from equivalent ice-Melt with majority of the grains being between 5 to 1 μ m and less than 1 μ m in size. The most common compositions are Al, Si, C, O with occasional presence of Cl, Na, K, and Ca. Unlike its frozen counterparts, the snow samples are mostly represented with smear structures, often too thin to be analyzed with EDS. Similarly to snow-melt from Event 6, the structure morphology seemed as if they were dissolving.

Event 7 – Ice-Melt.

This snow event mostly contains particles of 1–10 μm in size. Lower number of particles (approximately 10%) is of a larger size, 10–50 μm . The observed particles have mixed composition; smooth crystalline particles are mostly composed of Al, Si, O; corrugated particles of C composition along with Al, Si, and O were observed, and C-rich smears too. Similarly to ice-melt from Event 6, corrugated particle morphology is prominent in this sample. These particles are mostly composed of C and O. The definite crystalline structure is absent in this sample, while C containing structures are abundant. Similar morphological structures were detected in previously published SEM studies of snow samples and have been identified as soot originated from biomass burning and fossil fuels (Clarke & Noone, 1985; Zhiyuan et al., 2009). A few coarse and fine-grained particles composed of Cl, Na, and K, indicate the presence of salt precipitation or re-crystallization of dissolved salt amongst the observed grains. As observed from the NOAA Hysplit back trajectory analysis, the air mass for event 7 was influenced by marine air from the Atlantic Ocean; therefore, these particles could be of marine origin associated with the ocean surface evaporation

Event 1 – Ice-Melt.

Unlike the ice-Melts from Events 6 and 7, these samples contained fewer particles. The particles' morphology and composition are very much alike the other two ice-melt samples. The major compositions are Al, Si, C, and O, while occasionally Cl and K were observed. Interestingly, few particles in the ice-Melts from Events 7 and 1 contain Fluoride (F), which has strong anthropogenic sources [(Walna et al., 2013) and the references there in]. Air mass back trajectory analysis show that samples were influenced by continental air masses, and the presence of F indicates the influence of pollution-laden air. Few samples also

contain S, presence of which should be natural since fine mode sulfate particles played excellent role in forming cloud nuclei.

Event 10 – Snow-Melt.

The snow-melt samples were clean with very few particles. The morphology of the particles is similar to other snow-melt samples where smear particles of C and occasionally Si composition were dominant. The common size of the particles was 1–5 μm with very few particles about 10–20 μm .

Event 10 – Ice-Melt.

Similar to its snow-melt counterpart, the ice-melt samples were very clean with very few observed particles. Majority of the particles are thin, C and O containing smears. Unlike in the other analyzed ice-melt samples, the compacted structures were not found. At only few particles we were able to detect chemical diversity and Mg, F, and Al were recorded.

3.5 Discussion.

3.5.1 Total Fe, Filterable Fe, and Soluble Fe in Snow Samples.

Figure 3.1 presents the soluble Fe concentrations measured for nine snow events. The concentrations of soluble Fe(II) reported by our study seem unusually low compared to other studies which analyzed precipitation and fog water samples in urban locations (Behra & Sigg, 1990; Erel et al., 1993; Siefert et al., 1999; Kieber et al., 2001; Kieber et al., 2003). However, Zhu et al. (1993) suggested that in highly oxygenated systems, like precipitation samples, Fe(III) occupies the major fraction of the soluble Fe or the insoluble iron containing dust particles sometimes do not participate in the multiple in-cloud processing

cycles and sometimes the Fe(II) formed through in-cloud processes fail to persist over longer periods.

Moreover, since the majority of the snow events in this study occurred at early morning or at night, the absence of solar radiation could have prevented the photo reductive formation of Fe(II). Because of its high Henry's law constant, hydrogen peroxide (H_2O_2), could accumulate in the atmospheric aqueous phase. Therefore, the snow samples could contain certain amount of H_2O_2 (Kelly et al., 1985; Gunz & Hoffmann, 1990), and it can also reacts with soluble Fe(II) and generates Fe(III) and hydroxyl radical following the Fenton mechanisms (Graedel et al., 1986; Zepp et al., 1992). The interaction involving Fe species and H_2O_2 in the atmospheric aqueous phase might have significant influence on the soluble Fe speciation. The gas-phase hydroxyl radical, which is a strong oxidant, can also dissolve into the atmospheric aqueous layer and may affect the Fe speciation.

To explore whether the solar radiation could potentially enhance the soluble Fe(II) concentration in snow, a total of 16 sets of snow collected from event 2 and event 3 were packed in a pre-cleaned plastic ziplock bag and placed on top of the ground covered with snow facing the direct incident solar radiation for 4 hours. No increment of soluble Fe(II) concentration was noticed, even though these events had strong anthropogenic pollution influence (as seen from the HYSPLIT4 back-trajectory analysis).

No correlation was found between Fe_{tot} and Fe_{sol} , suggesting that the solubility of Fe does not depend on the amount of total Fe (insoluble + soluble) present. On the other hand, good correlation (0.6) exists between Fe_{fil} and Fe_{sol} indicating the possibility of similar processes generating the filterable and soluble fraction of Fe in the cloud water system.

Since the inorganic and organic anions present in the aerosol could solubilize the insoluble Fe, the fractional solubility of Fe_{sol} highly depends on the co-existence of these species (such as sulfate) and the organic ligands such as oxalate (Pehkonen et al., 1993; Paris et al., 2011; Chen & Grassian, 2013; Gao et al., 2013; Paris & Desboeufs, 2013). Weak correlation (0.25, $n=31$) exists between sulfate and Fe_{sol}/Fe_{tot} fractional solubility, suggesting that in-cloud acid processing by S-containing species (such as sulfur dioxide, sulfate) might have influenced the Fe solubility. Among the organic anions such as oxalate, formate, and acetate, no significant correlations were found with the Fe_{sol}/Fe_{tot} fractional solubility. These organic species were present in little quantity in all the snow samples which may result in poor correlation between these components with soluble Fe.

3.5.2 Freezing Effect on Fe Solubility.

Several studies have been conducted to investigate the metamorphism of the surface snow layer and its influence in processing chemical reactions (Hallett, 1961; Barrie et al., 1988a; Foster et al., 2001; Grannas et al., 2007). The chemical interaction among the species is enhanced in the unfrozen liquid during ice formation due to “freeze concentration effect” (Takenaka et al., 1996; Betterton & Anderson, 2001). Near the melting point temperature, water molecules present in a given volume of deposited snow are highly mobilized and cluster together to form a stronger, denser, and compact aggregate in order to decrease the total surface area of the snow crystals (Hobbs, 1968). Similarly, Grannas et al. (2007) observed that a liquid-like layer, formed on the surface of pure ice/snow, becomes highly concentrated with the solutes during crystallization of frozen water. Kuroiwa (1974) presented a step by step description of the growth of snow grains by vapor diffusion as a result of temperature gradient and the associated sintering effect (bond formation among

the ice grains) using time-lapse cine-photomicrography. These observations led us to hypothesize that a similar process might occur in the snow while it compacts due to freezing. This hypothesis is supported by the unimodal particle size distribution analysis of snow and frozen ice samples from two events, event 6 and event 7 (see Figure 3.3), which shows that, upon freezing of the snow, the particle size distribution shifted towards larger particle size compared to the snow-melts. The increased population in the larger particle size in the frozen ice samples might have happened due to clustering or aggregation of the smaller particles into larger size and thereby supporting the feasibility of “freeze concentration effect” to enhance the solubility of Fe. Moreover, the results from the particle morphology analysis present in snow and ice melt counterparts also suggest that the compaction process occurred due to freezing of the snow (detailed description in section 3.3; see Figure 3.7).

Laboratory experiments performed by Kim et al. (2010) and Jeong et al. (2012) using several iron oxides and organic acid suspensions, both under UV light and dark condition, showed that the dissolution of soluble Fe increased due to freeze concentration effect. While our freezing experiment measurements for events 1 and 2 were consistent with their results, the remaining four events are not in strong agreement. There could be possible reasons behind the discrepancy, including: 1) Kim et al. (2010) used UV radiation to initiate the photo reduction process. However, our experiments were conducted in dark condition, disallowing the possibility of photochemical dissolution of Fe(II). 2) Jeong et al. (2012) used low pH level (maximum pH was 4) to study the enhancement of proton and/or ligand promoted dissolution of Fe in the dark due to freezing concentration effect. However, our snow samples were acidic with average pH 5.4 and the lowest pH 4.8 (event

8). Similar range of pH was observed in snow samples collected at Fairbanks, Alaska (pH range 5.8–7.48), Hanover, New Hampshire (pH range 3.96–5.46) (Kumai, 1985), Kentville, Nova Scotia (average pH 5.6) (Herman & Gorham, 1957). After freezing, pH decreased approximately by 1 unit for events 1, 2, and 6, and remained unaltered for other events, 5, 7, and 8 (Figure 3.2); and this is somewhat consistent with our findings of increased Fe dissolution in only events 1 and 2. Changes in pH values depend on the un-uniform trapping of the species in ice, as well as the rate of freezing (Bronshteyn & Chernov, 1991), and consequently, the pattern of pH change due to freezing is difficult to explain without having detailed knowledge of the species present in the particular snow sample.

Although the modulation in the Fe solubility in the six events studied in this research did not follow a consistent pattern, the observations from event 1 and 2 indeed indicate that the freezing induced compaction of the natural snow promoted inter-species chemical activity. To further understand the un-uniform outcome in the soluble Fe concentrations from the six freezing experiments, the fractional solubility of the initial Fe_{fil} with respect to the initial Fe_{tot} were investigated. In the two events (events 1 and 2) that witnessed increase in soluble Fe concentrations, the initial Fe_{fil} fraction accounted for 67% and 89% of the initial Fe_{tot} , as opposed to the other four events where the average fractional solubility of Fe_{fil} with respect to Fe_{tot} was significantly less, around ~28% (Figure 3.2). These results indicate that the freeze-induced solubility of iron highly depends on the amount of Fe present within 0.45 μ m of particle size; and therefore, the fraction of Fe within 0.45 μ m diameter can be referred to as “readily soluble iron”. Moreover, the freeze induced increase of Fe solubility for event 1 and event 2 was also associated with the maximum initial soluble Fe amount.

The initial fractional solubility of Fe_{sol}/Fe_{tot} for event 1 and event 2 were 43% and 27%, respectively. The average initial fractional solubility of Fe_{sol}/Fe_{tot} for the other four events (5, 6, 7, and 8) was 16%. This result indicates that events 1 and 2 were influenced by air masses containing more soluble Fe or the materials that enhance Fe solubility. Since these two events were influenced by North American air masses, the anthropogenic combustion could have been a source of soluble Fe. Furthermore, Jeong et al. (2012) reported that the freeze induced Fe solubility depends on the type and surface area of the Fe-mineral. The authors found that ferrihydrite (compared to goethite and hematite) could produce more soluble Fe due to its larger surface area. Therefore the different patterns in freeze-induced Fe solubility could be linked with Fe minerals present in different snow samples. The incoherent pattern of the soluble Fe concentrations in the event 5, 6, 7, and 8 might also be associated with the variations in the initial concentrations (Figure 3.1a).

The growth of ice crystals present in snow during freezing is accompanied by movement of particles (Colbeck, 1983). Since only the water molecules present in the snow are mobile (Hobbs, 1968), the compaction of species in the freezing snow system would be dominant for the soluble or colloidal particles present in the snow (the Fe_{sol} and Fe_{fil} components, and soluble ionic species, in the context of the present study) and they would be the most likely candidates for further chemical interactions upon freezing. This phenomenon is evident from our observations where the steady increment in soluble Fe content was associated with the presence of high Fe_{fil} fraction. Moreover, Kieber et al. (2005) reported that in rain samples, about 25% of Fe-complexing ligands are strong and ferrozine cannot replace them. These strongly complexed Fe species might also be a source of soluble Fe due to the freezing effect.

Bronshteyn and Chernov (1991) argued that the non-uniform distribution of the dissolved ionic species exists between the unfrozen liquid and the “growing ice” which creates a freezing potential. The accumulation of mobile OH^- or H_3O^+ ions thus neutralizes the potential, changes the pH, and predominantly accelerates the chemical reactions due to freeze concentration effect (Takenaka et al., 1996). This suggests that the proton-induced dissolution, as a result of compaction due to freezing, should be the driving mechanism for the modification of Fe solubility and is consistent with our observations that the enhancement in Fe solubility in events 1 and 2 was associated with a decrease in pH after freezing.

In the natural environment, the freeze concentration effect might be even more complicated. Although snowfall usually occurs at sub-zero temperatures (for instance, in our events as listed in Table 3.1), they often contain liquid water from melting (Colbeck, 1982; Colbeck, 1983), and the freeze concentration effect would be highly dependent on the liquid water content as well as the number of freeze-thaw cycles encountered by the snow.

3.5.3 Particle Morphology in the Snow Samples.

The particles found in the analyzed samples have two major types of morphologies: smooth (Figure 3.5 and 3.7) and highly irregular (Figure 3.6 and 3.8). Both types are mostly composed of Si, O, and Al, while irregular particles may contain more C. Frequently, irregular structures will form aggregates with smaller grains that will attach onto corrugated surface (Figure 3.6), these attached particles may have diverse chemistry (S, Cl, Ca, Na, P, K). The C particles are mostly irregular which implies lack of ordered crystalline structure and points to possible disordered C composition, such as soot (Figure 3.8) (Clarke

& Noone, 1985; Zhiyuan et al., 2009). The presence of soot in these urban snow samples is not unusual and may originate from a variety of urban pollution sources; soot in this instance may act as ice nuclei in the cloud (Gorbunov et al., 2001; Crawford et al., 2011). Based on our observations, it is possible to hypothesize that snow may be an efficient scavenger of pollution generated soot particles in urban environment surrounded by industry and major highways. Moreover, the particles with corrugated structures would also be significant for providing surface to initiate active chemical interactions, such as dissolution of Fe-containing minerals, during compaction of snow. The smooth crystalline silicate and silicate-aluminum particles seemed as dust grains and may derive from terrestrial sand dust that has reached the atmosphere.

The soluble fine particles smaller than $1\mu\text{m}$ and which were composed of C, O, Al, and Si might act as Cloud Condensation Nuclei (CCN) or Ice Nuclei (IN) to initiate cloud formation (Xu et al., 2013). The particles within $0.45\mu\text{m}$ diameter size were also composed of the above species and were present as soluble smears. The “readily soluble iron” might also be associated with such smears (see the analytical point A in Figure 3.8) to accelerate the soluble Fe formation after freezing.

The particles that are larger than $10\mu\text{m}$ can have two sources: (1) scavenged through snow fall and, (2) clustered during freezing process (surface freezing compaction). The second mechanism seems more plausible since the larger particles were not present in any of the snow-melt counterparts. If these large particles were formed during snowfall, similar proportion of them would have been observed in the snow-melts. Large particles are often categorized as aggregates of multiple particles consisting of Al, Si and C, O compounds with Cl, K, Ca, Na, all of which indicates occurrence of active chemical processes.

Moreover, we measured soluble Cl, K, Ca, and Na in the filtered (passing through 0.2 μ m filter) snow-melt using ion chromatography (Table 3.4). Similarly, we detected Fe in the EDS analysis, both in ice and snow-melts (see Figure 3.5 and the analytical point (A) in Figure 3.8). In the ice melts, Fe was associated with larger particles (5-10 μ m) whereas, in snow-melt Fe was present both in form of small (approximately 1 μ m) particle and smear. These observations support the hypothesis that the soluble species migrate and form aggregates of larger particle or deposit on pre-existing particles with irregular structures. This phenomenon further suggests the possibility of similar processes for soluble and colloidal (passing through 0.45 μ m filter) Fe present in the snow, leading to enhanced soluble Fe formation during compaction of snow.

Finally, we observed that ice-melt samples were consistently through all of the snow events composed of larger particles than snow-melt samples. Snow melt samples had larger amount of smear particles and particles that are mostly amorphous.

The observed differences in the particles' size are consistent with the particle size measurements (see Figure 3.3). Further, Ice-melts contained more of the corrugated aggregates and silicate particles, which led us to conclude that the particles in the frozen form became more clustered.

3.5.4 Environmental Significance.

The amplified warming in the Polar regions has initiated record amount of ice melting each year (Bintanja et al., 2013; Liu et al., 2016). Studies show that, compared to the underlying sea-water, sea-ice can store twice as much trace metals, such as Fe, and becomes a large reservoir of a crucial micro-nutrient for the marine eco-system (Grotti et al., 2005; Lannuzel et al., 2008). The atmospheric deposition of Fe-containing particles could provide

a fresh addition to that reservoir. A study conducted by Sedwick and DiTullio (1997) at the Antarctic shelf water showed that “episodic release” of the bio-available iron from the melting sea-ice stimulated phytoplankton productivity.

The long-lasting freezing condition in the Polar environment could modulate the Fe solubility in the stacked snow. In the natural setting, Hawkings et al. (2014) estimated the amount of bioavailable Fe present in the melt water from the glacial runoff at Greenland and Antarctica, and these values were comparable to the addition of bioavailable Fe from the aeolian dust flux. Betterton and Anderson (2001) mentioned that the freezing induced enhancement of the chemical reactivity would be significantly relevant in natural environment associated with freeze-thaw cycles, such as snow packs and glaciers. Therefore, the global warming induced melting of the Polar ice caps could be a new source of bio-available iron to the Polar ocean surface water which eventually would impact the global carbon dioxide budget. Field studies also show that the addition of Fe in the ocean affects the cycles of other nutrient, such as nitrogen and phosphate (Falkowski, 1997; Chen et al., 2011). The results from this study clearly show that the freezing-induced increment in Fe solubility is highly linked with the amount of “readily soluble iron” present in the snow and this amount would vary widely depending on the source of the air. Furthermore, the in-cloud chemical interactions among the insoluble Fe particles with the organic ligands or inorganic anionic species could significantly enhance the amount of “readily soluble iron” in freshly fallen snow. Moreover, in the natural setting, the surface snow might be exposed to multiple freeze-thaw cycles, which would certainly modify the compaction induced “freeze concentration effect” substantially. Hence, the findings from this study suggest that each snow event is unique in its variability regarding the amount of “readily

soluble iron” and the extent of “freeze concentration effect”, and therefore, not all of them could produce significant freeze induced increase in Fe solubility and increase in bio-available Fe output to the ocean.

In addition, observational studies show that many photochemical processes occur at the Arctic surface snow at the onset of Arctic Polar sunrise (Barrie et al., 1988b; Zhou et al., 2001). Of them, the production of the oxidant, OH radical may be particularly important in influencing the Fe oxidation state in the snow (Zhou et al., 2001). Although the reaction rate of OH with soluble Fe is slow it may have impact on the Fe chemistry. The photochemical formation of organic species, such as oxalate may also influence the Fe solubility and speciation. Moreover, the sunlight induced modification in Fe chemistry in snow is also a plausible pathway to influence Fe solubility and speciation. Since we collected the freshly fallen snow samples from an urban location, the influence of photochemical processes on Fe solubility at the snow surface cannot be estimated from this study. Detailed analysis with snow samples in Polar Regions is a major scope of future research.

In addition, the results from the particle morphology analysis show the high abundance of C- containing soot like particles (Liu et al., 2017) (Figure 3.8). This is highly significant since soot particles can act as IN (Gorbunov et al., 2001; Crawford et al., 2011) and thereby modify the cloud’s radiative properties to a greater extent (Christopher et al., 2000). The presence of such particles in the freshly fallen snow also indicates that the pollution generated soot particles can be effectively removed from the atmosphere through snowfall. Finally, the soot particles present in the surface snow could also modify the radiative

property of the surface snow and thereby modulating the extent of melting; however, a more detailed study is required to systematically estimate these processes.

3.6 Conclusions.

1. The average fractional solubility of the soluble Fe with respect to the total Fe present in the freshly fallen snow samples was 23.3%. Majority of the soluble Fe was present as Fe(III), and approximately 48.5% of total Fe existed as Fe_{fil} (the portion that passes through 0.45 μ m syringe filter).

2. Results from the freezing experiments through measuring the soluble Fe periodically in conjunction with the particle morphology study show that upon freezing, the compaction of the ice grains and the movement of the liquid water could stimulate chemical transformation of species present in the snow; this is more effective for the fraction of the species that exist in soluble form (the fraction that smaller than 0.22 μ m filter) or in readily soluble colloidal form (the fraction that smaller than 0.45 μ m filter).

3. The elemental and morphological analysis shows that due to freezing the particles present in snow tend to cluster together as a result of compaction. This process would be favored in the high abundance of particles with corrugated structures to provide surface for particle clustering. As a result of this process, active chemical interactions among the species could occur.

The results from this study address the effect of freezing-induced compaction of particles on the Fe solubility in surface fresh snow. Despite the freeze-induced compaction in snow as observed in the STEM analysis, freeze-induced increment of soluble Fe (particle size < 0.22 μ m) occurred only in those events (events 1 and 2) where majority of the total Fe

existed in readily soluble or colloidal form (particle size $< 0.45\mu\text{m}$), and not in the other four events (events 5, 6, 7, and 8) when majority of the Fe existed in insoluble form. Although it varies widely, the fraction of Fe in aerosols that exist in insoluble form could be high (Zhuang et al., 1990; Gao et al., 2001; Boyle et al., 2005; Sedwick et al., 2007; Sholkovitz et al., 2012; Gao et al., 2013) and consequently, freezing-induced enhancement in Fe solubility might not be significant in the environment. From this study, it is logical to conclude that freezing and compaction of natural snow may only have negligible effect on enhancing Fe solubility.

However, in the natural environment, the effect of freezing on Fe solubility will depend on a variety of complex chemical processes and a host of new parameters, such as the extent of freeze-thaw cycle, the amount of liquid water content, the effect of solar radiation, and the different air-masses containing varying proportion of soluble and readily insoluble Fe. In addition, the mineralogy of dust in the snow play important role in Fe solubility (Journet et al., 2008). These processes were not addressed in the current research. Therefore, further thorough investigation is highly required to study the effects of these parameters and to quantitatively assess the role of freezing on modulating Fe solubility in snow and its potential as a source of bio-available Fe to the ocean.

Acknowledgement: This research was supported by NSF OCE Award 1435871 and Rutgers TA-GA development grant. The authors are grateful to Alexei Khalizov and Evert Elzinga for helpful discussions. The authors are grateful to the anonymous reviewers for constructive comments that helped substantially improve this manuscript. The authors are

also thankful to Tinayi Xu, Guojie Xu, Lasita Bhattacharya, and Songyun Fan for help with sample collection and analysis.

3.7 Tables.

Table 3.1 Summary of the snow events [<https://www.wunderground.com/us/nj/newark>]

Event	Date	Avg. Temp (°C)	Humidity (%)	Avg. Snow fall (cm)	Wind speed (Km/h)	Snow depth (cm)	Sea level pressure (cm)	Description
1	1/24/15	3.3	82	0.8	14.5	12.7	75.2	Heavy Snow
2	1/27/15	-4.4	74	0.8	20.9	20.3	75.4	Heavy/med snow
3	1/27/15	-4.4	74	0.8	20.9	20.3	75.4	Heavy/med snow
4	2/2/15	-4.4	81	1.0	24.1	20.3	75.2	Heavy/med Snow
5	3/1/15	-5.0	62	0.5	4.8	7.6	77.3	Med snow
6	1/17/16	2.2	70	0.8	14.5	1.5	76.2	Light snow
7	1/23/16	-3.9	91	0.5	37.0	3.8	75.6	Heavy snow/blizzard
8	1/24/16	-7.8	64	0.8	14.5	50.8	76.0	Med snow
9	2/5/16	2.7	68	0.8	20.9	2.54	78.3	Mild snow – occasionally heavy snow
10	2/9/17	-0.6	70	0.8	33.8	5.1	75.3	Heavy snow

Table 3.2 Schematic of the snow sample treatment and analysis.

1. Event 1-9	→	Analysis of Fe_{sol} by UV-vis spectroscopy, Fe_{fil} and Fe_{tot} by AA spectroscopy, and analysis of water soluble major anions and cations by IC.
2. Event 1, 2, 5, 6, 7, and 8	→	Analysis of Fe_{sol} of the frozen counterparts at the intervals of after 2, 5, 7, and 10 days.
3. Event 1, 6, 7 and 10	→	Morphological analysis by STEM.
4. Event 6 and 7	→	Particle size distribution analysis by Beckman Coulter, N4 plus mode.

Table 3.3 The concentrations (ppb) of Fe_{sol} , Fe_{fil} and Fe_{tot} (this study) and comparison with other precipitation samples.

	Fe_{sol}	Fe_{tot}	Fe_{fil}	Location	Type of precipitation	Reference
Max	21.0	83.1	55.4	Newark, NJ	Snow	this study
Min	4.1	28.4	8.0	Newark, NJ	Snow	this study
Std. Dev	6.3	17.4	15.1	Newark, NJ	Snow	this study
Mean	12.5	58.1	28.0	Newark, NJ	Snow	this study
VWM	12.5	58.3	28.1	Newark, NJ	Snow	this study
VWM	3.8	14.4		(coastal North Carolina, USA	rain	(Kieber et al., 2001)
VWM	3.8	12.3		North Carolina, USA	rain	(Willey et al., 2000)

Range	*5.6- 297	**101 -1512	California	fog water	(Erel et al., 1993)
Range	*1.3- 3.7		Massachusett s Bay	snow	(Zhuang et al., 1995)
Mean		65	Lenox, MA	rain	(Dasch & Wolff, 1989)
VWM		69	Rhode Island	rain	(Heaton et al., 1990)
Mean		23	New Castle, NH	rain	(Pike & Moran, 2001)
Range		1.7- 63.5	North Atlantic	Rain	(Helmers & Schrems, 1995)

*Only soluble Fe(II) was measured

** Unfiltered aliquots were acidified at pH 1

^The VWM (volume weighted mean) was calculated from snow-melt volume.

Table 3.4 Concentrations (ppm) of the soluble species detected at EDS.

	Sodium		Potassium		Calcium		Chloride	
	Std.		Std.		Std.		Std.	
	Mean	Dev	Mean	Dev	Mean	Dev	Mean	Dev
vent 1	1.17	0.15	0.06	0.04	0.16	0.1	1.24	0.01
Event 6	1.01	1.01	0.1	0.08	0.15	0.07	2.89	0.32
Event 7	0.61	0.17	0.18	0.01	0.21	0.04	1.23	0.72

3.9 Figures.

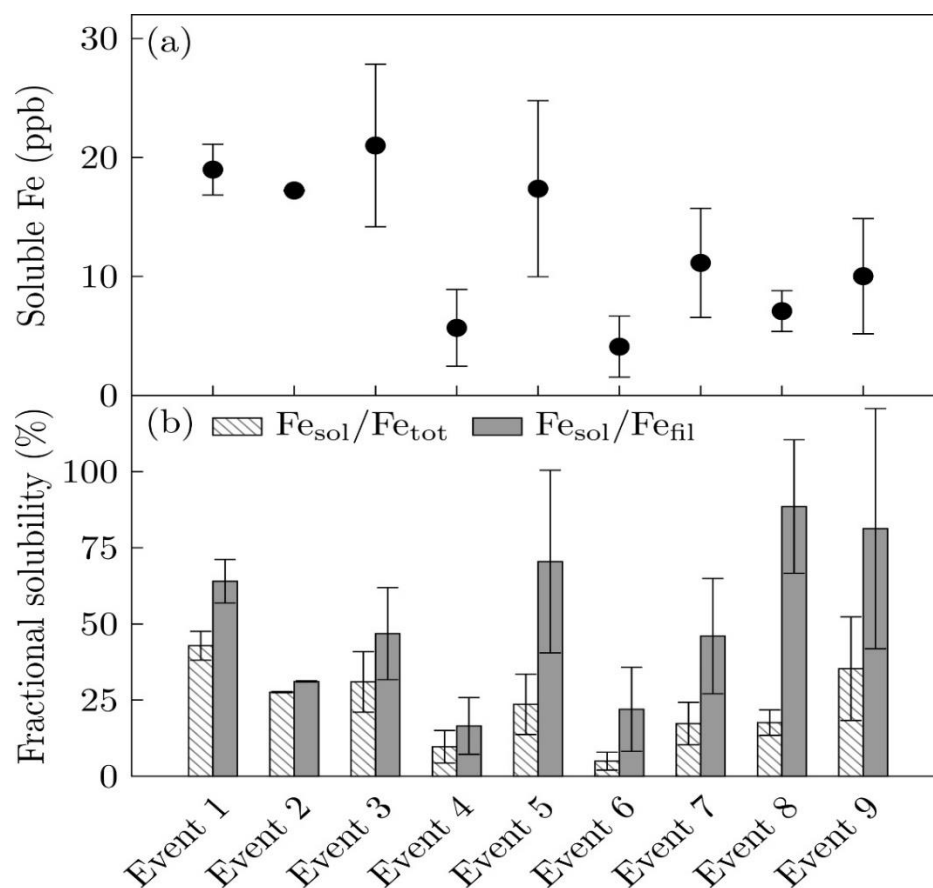


Figure 3.1 (a) Soluble Fe (Fe(II)+Fe(III)) (analyzed immediately after collection) concentrations from nine snow events; (b) The fractional solubility of Fe_{sol}/Fe_{tot} and Fe_{sol}/Fe_{fil} (The error bars were calculated based on standard error, i.e., standard deviation)

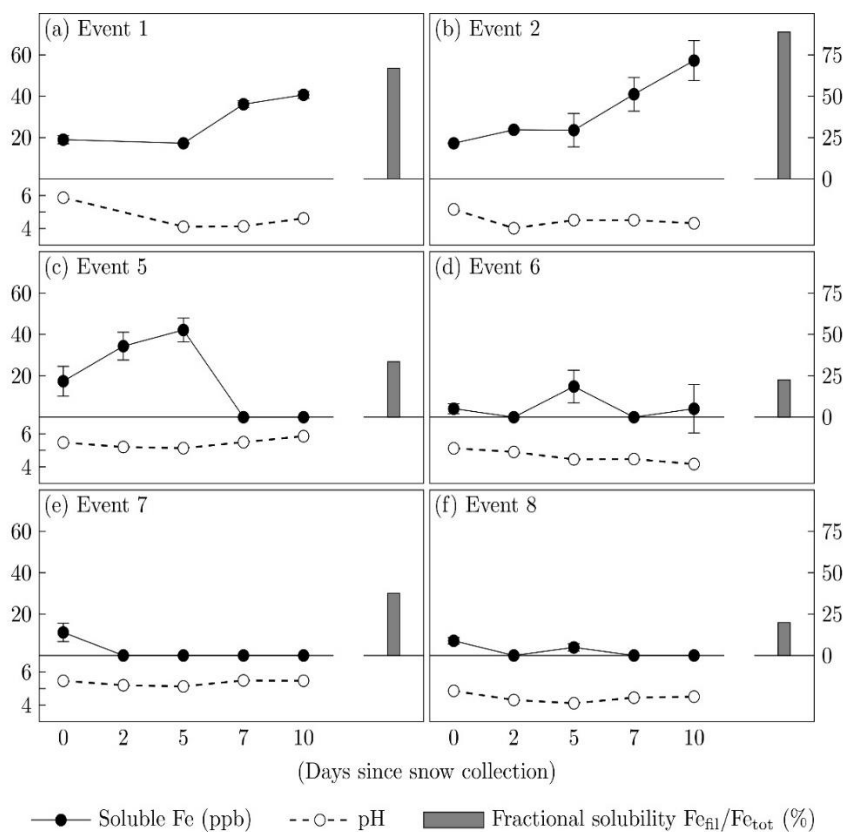


Figure 3.2 The soluble Fe concentration and the variation in pH from six freezing experiment events. The bar represents the fractional solubility of initial $F_{c_{fil}}$ with respect to initial $F_{c_{tot}}$ (The soluble Fe was analyzed after periodic storage immediately after melting. The error bars were calculated based on standard error, i.e., standard deviation divided by the square-root of the sample size, from three replicate samples).

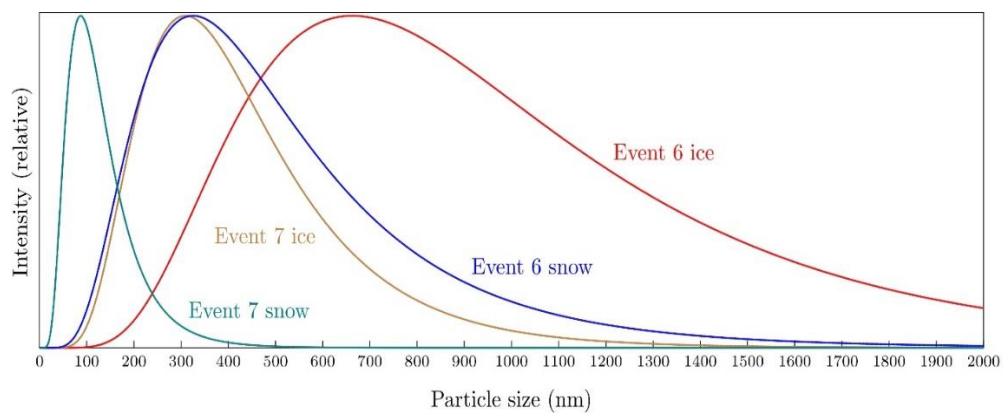


Figure 3.3 Uni modal particle size distribution (using Beckman Coulter, N4Plus mode)

of the snow-melt and in ice-melt counterparts from two selected events

(event 6 and event 7).

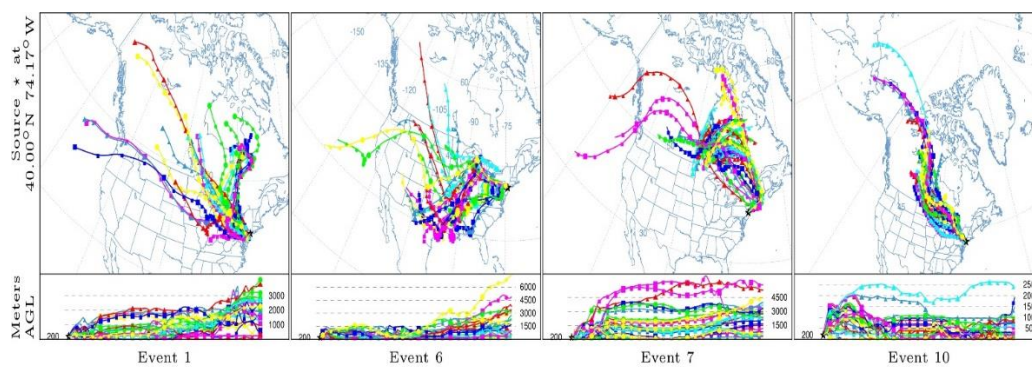


Figure 3.4 The 6 days back trajectory analysis from the NOAA HYSPLIT-4

model (http://www.arl.noaa.gov/HYSPLIT_info.php).

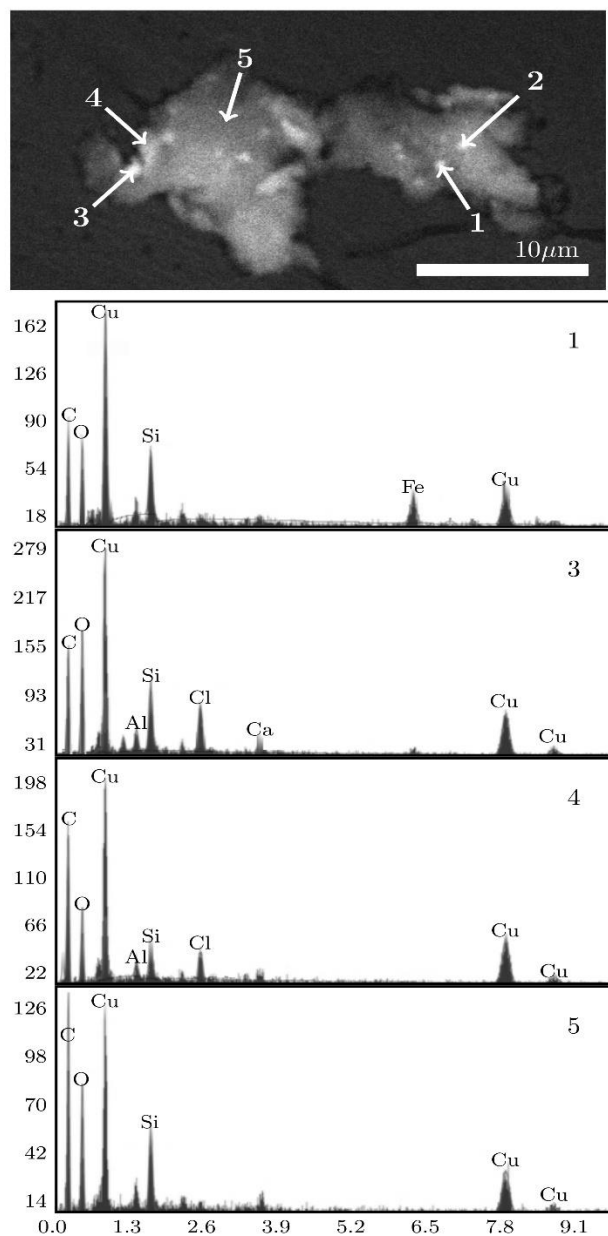


Figure 3.5 The representative SEM-TEM micrograph with associated EDAX spectra of amorphous carbon particle aggregate. This particular aggregate was observed from event 6 ice melt. Analytical spot 5 is indicative of the large particle predominantly carbon with some silicate

composition. The smaller particles are of iron (spot 1) and aluminium silicate composition (spots 3 and 4). The analytical spots 2 and 3 have similar compositions, hence we are showing only one of the spectra.

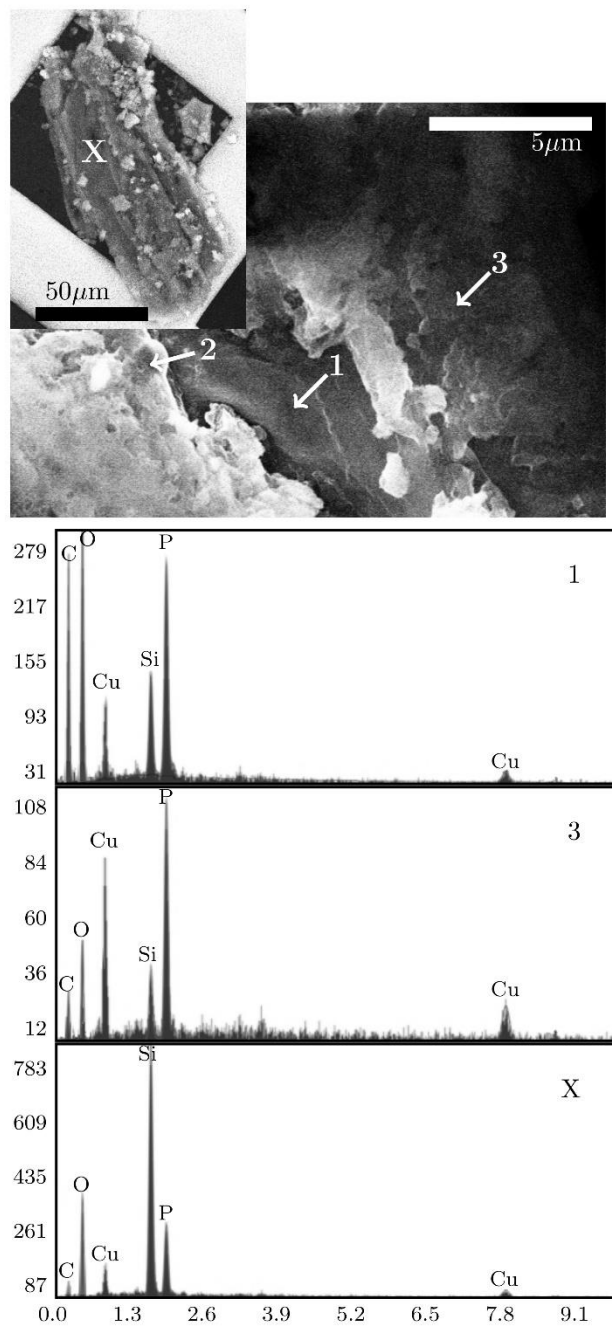


Figure 3.6 The representative SEM-TEM micrograph with associated

EDAX spectra of over 50 μm large particle observed within event 6 snow melt.

This is a large particle with varying chemistry the main amorphous material is

mostly silicate, however some portions of the particle has high content of

carbon and phosphorous. The analytical spots 2 and 3 have similar compositions, so we are showing only one of the spectra.

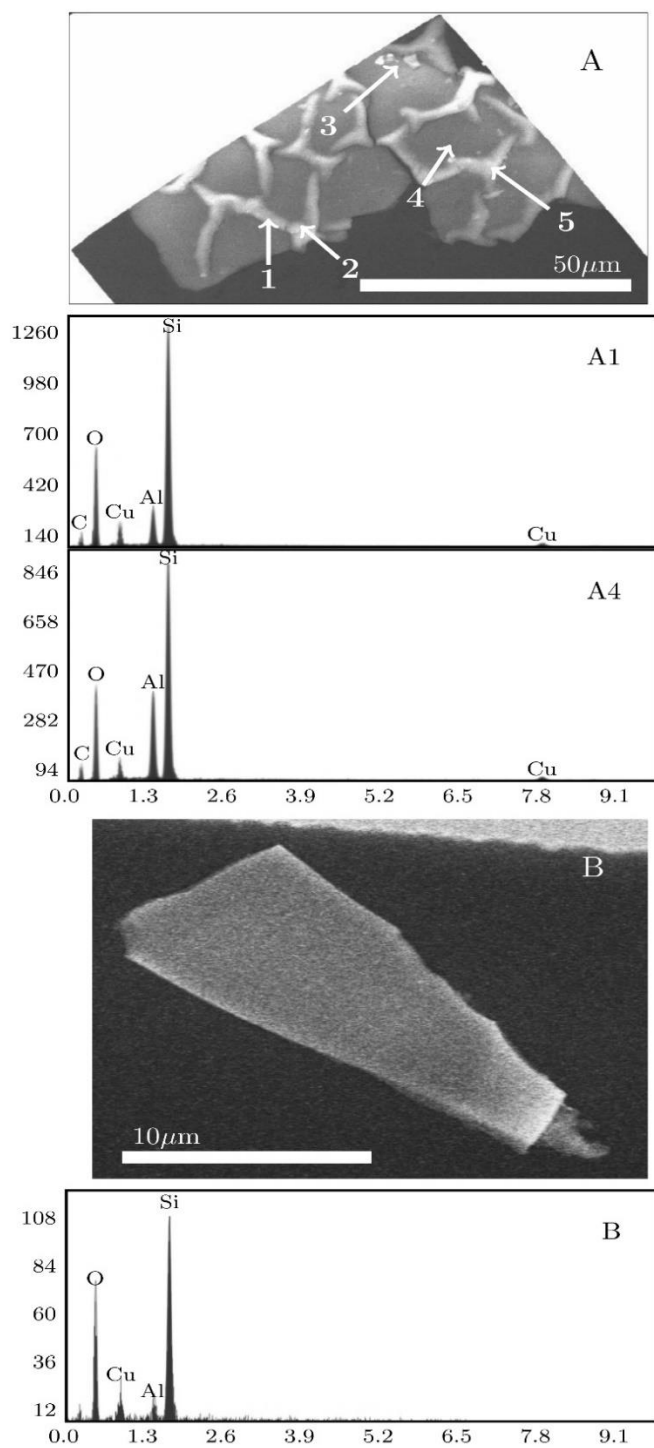


Figure 3.7 The representative images SEM-TEM micrograph with associated EDAX spectra of aluminium-silicate oxide particles (A) particle from event 7

ice melt (the analytical spots 1, 2, and 5 have similar chemical compositions and the analytical spots 3 and 4 have similar chemical compositions);

(B) particle from event 7 snow melt.

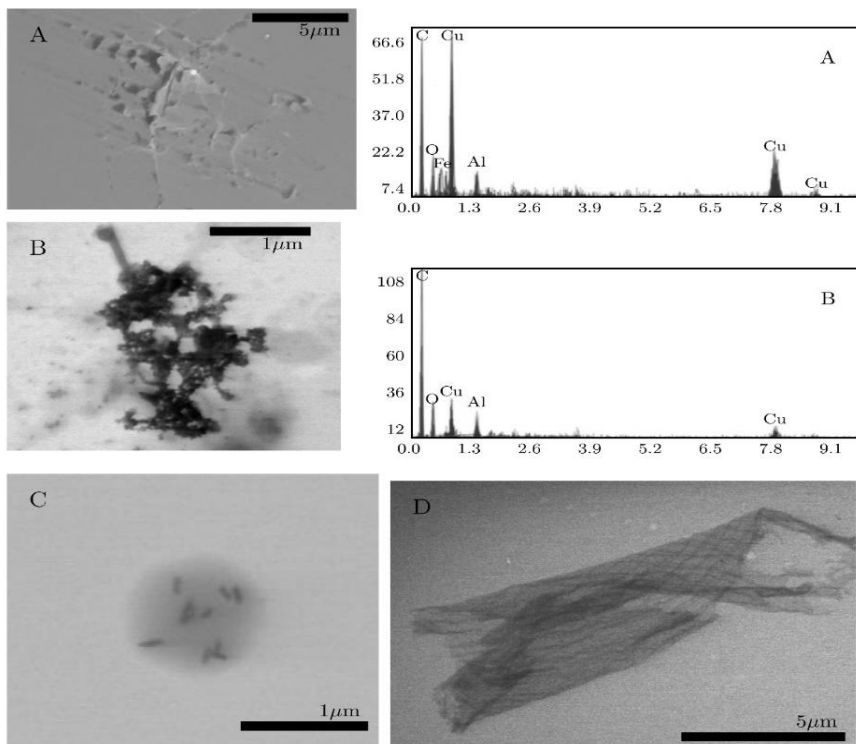


Figure 3.8 The representative images SEM-TEM micrograph with associated EDAX spectra of carbon particles, that we categorized as smears due to their wide distribution and low thickness. We were able to see most of them and analyze only some of them as many were were bellow detection limits of the EDAX detector. (A) the particle from event 10 snow melt as this particle was a bit thicker we were able to detect low level of aluminium (Al) and iron (Fe) in its composition; (B) (C) and (D).

4 Characterization of the Water-soluble Inorganic and Organic Species on Aerosols over the Arctic Ocean.

4.1 Abstract.

Atmospheric aerosols affect the Earth's climate, directly by absorbing or scattering the sunlight, and indirectly as CCN (cloud condensation nuclei) influencing the clouds' radiative property and lifetime. We present the results from 8 sets of size-segregated and 14 sets of bulk aerosol samples that were collected during a cruise over the Arctic Ocean from 2nd August to 10th October, 2015. The samples were analyzed for the concentrations and mass-size distributions of the major water-soluble species, including acetate, formate, MSA (methane sulfonate), oxalate, sea-salt, and NSS (non-sea-salt)-sulfate. NOAA Hysplit back-trajectory analysis was performed to categorize the wind patterns into three types: type-1 originating from the North Pacific and the Bering Sea, type-2 entirely consisting of polar Arctic air, and type-3 consisting of the marine Arctic air with mixing of the continental air masses of northern Russia and northern Canada. The results showed that sea-salt was the major component dominating in the coarse mode, 1.8–5.6 μm . NSSsulfate was predominantly present in the fine mode, 0.18–0.32 μm . MSA was found in type-1 and type-2 air masses, namely regions with strong oceanic influence; the average MSA concentrations varied widely from below detection level to 104 $\text{ng}\cdot\text{m}^{-3}$ and predominantly existed in the fine mode peaking at 0.18–0.32 μm . Among the organic species, oxalate, acetate, and formate were the major components, and propionate was found in trace amounts. This study aims to provide the needed information on the origins

and chemical interactions of these species over the summertime Arctic to elucidate the importance of the different sources as the contributor for CCN formation.

4.2 Introduction.

The Arctic region has witnessed intense warming—at a rate almost twice the global average rate—over the past decade (Serreze & Barry, 2011). As a direct consequence of this warming, the average annual sea-ice cover has decreased by 3.6% per decade between 1976 and 2007 (Meier et al., 2007). Recent results from satellite observation reveal ~ 77% decrease in the Arctic planetary albedo over the past 40 years (Pistone et al., 2014). The prominent reasons for warming in the Arctic are (1) decreased surface albedo as a result of sea-ice retreat (Screen & Simmonds, 2010), (2) increase in the atmospheric water vapor content that can trap infra-red solar radiation (Graversen, 2006; Graversen & Wang, 2009; Lu & Cai, 2009) (3) modification in poleward transport of atmospheric heat and moisture (Graversen et al., 2008).

Although model studies claim that the effect of cloudiness on the amplification of Arctic warming is minimal (Screen & Simmonds, 2010; Ghatak & Miller, 2013), it is a major source of uncertainty in understanding the recent trend and predicting the future pattern of the Arctic climate change (Vavrus, 2004; Künzli et al., 2005; Inoue et al., 2006; Walsh et al., 2009; Kay et al., 2016). Mauritsen et al. (2011) showed that since the central Arctic falls within a tenuous cloud regime, even a slight perturbation in the concentration of cloud condensation nuclei (CCN) could impose substantial radiative warming effect—particularly during late summer and early winter. The aerosols can serve as CCN upon which cloud droplets can form and the CCN directly influence cloud's radiative property by increasing or decreasing the cloud's albedo and modifying the cloud's lifetime. The

aerosol particle size and the extent of solubility of the chemical species determine the activation of the CCN at different levels of supersaturation, but the effects of aerosols and their variations on cloud dynamics and climate change have not yet been thoroughly examined in climate models so far due to limited aerosol data from observations over the Arctic (Walsh et al., 2005; Chang et al., 2011). Therefore, it is of vital importance to collect and analyze Arctic aerosols and to study their properties.

Over the open ocean, sulfate and ammonium aerosols play important roles as CCN (Galloway et al., 1982; Quinn et al., 1987; Vong et al., 1988). Sulfuric acid is highly probable component for nucleation in the ambient air because of its low vapor pressure and large mixing enthalpy in presence of water (Ayers et al., 1980; Zhang et al., 1993; Marti et al., 1997). Non sea-salt sulfate particles primarily exist in fine mode (Murphy et al., 1998) and originate from natural and anthropogenic processes. Dimethyl Sulfide (DMS) produced by phytoplankton through the enzymatic cleavage of DMSP (dimethyl sulfoniopropionate) is a major oceanic source of sulfur into the atmosphere (Prospero & Savoie, 1991; Bates et al., 1992). Similar to the summer time source of NSS-sulfate, MSA (methane-sulfonic acid) also originates from the oxidation of DMS emitted by the phytoplankton and ratio of MSA/NSS-sulfate is used as a tracer for determining the marine biogenic fraction of nss-sulfate aerosol (Savoie & Prospero, 1989; S. M. Li et al., 1993; Gondwe et al., 2003).

Several marine sources, such as zooplankton metabolism and decay of organic materials, could contribute to the gas phase ammonia (Quinn et al., 1988; Galloway et al., 1995; Bouwman et al., 1997; Adams et al., 1999). In general, gas to particle conversion processes lead to formation of fine mode aerosol phase ammonium (Du et al., 2010). In addition, water soluble organic species on aerosols have also been recognized for their potential to be activated as CCN (Novakov & Penner, 1993; Yu, 2000; Sun & Ariya, 2006). They could account for a large fraction of the total organic mass on aerosols (Cadle & Groblicki, 1982), and this fraction could be dominated by particles in fine modes ($< 1.5 \mu\text{m}$ aerodynamic diameter size) (Zappoli et al., 1999).

Previous results from both polar regions show that the water soluble low molecular weight carboxylic acids (such as acetic, formic, and oxalic acids) constitute a significant fraction of the total organic carbon in aerosols (Kawamura et al., 1995; Kawamura, Kasukabe, et al., 1996; Kawamura, Seméré, et al., 1996; Xu et al., 2013). Several primary sources—vegetation, biomass burning—directly emit organics into the air (Kawamura et al., 1985), whereas oxidation of biogenic olefins, hydrocarbons, and isoprene can act as potential secondary sources (Chebbi & Carlier, 1996).

A vast majority of the previous studies on Arctic aerosols have measured the concentrations of the inorganic species (Barrie & Hoff, 1985; S. M. Li et al., 1993; Suzuki et al., 1995; Norman et al., 1999; Quinn et al., 2009). In contrast, comparatively few articles (Kawamura et al., 1995; Narukawa et al., 2003; Kawamura et al., 2010) exist on the Arctic

water soluble organic components. Moreover, unlike the winter and early spring seasons, the summer Arctic air is isolated from pollutants from the surrounding continental landmasses and hence provide a favorable period for studying the chemistry of aerosols originating from local marine sources (Leck & Persson, 1996; Quinn et al., 2007). Therefore, it is important to characterize the water soluble inorganic and organic components simultaneously to assess their role as CCN, particularly in summer Arctic aerosols.

As part of the US GEOTRACES Arctic Ocean experiment, ship-board aerosol sampling was carried out over the Arctic Ocean during August–October, 2015. This paper highlights the results of the water soluble inorganic and organic species and the mass-size distributions of these species on aerosols collected during that cruise, which include sea-salt, NSS-sulfate, ammonium, nitrate, MSA, and low molecular weight carboxylic acids. Such information would add new knowledge of their chemical and physical properties, contributing towards the improvement of the current knowledge of the Arctic marine atmospheric boundary layer chemistry.

4.3 Materials and Methods.

4.3.1 Sampling.

Aerosol sampling was carried out on board the US Coast Guard icebreaker, the USCGC Healy, from August 9 to October 12, 2015 as a part of US GEOTRACES Western Arctic section (GN01). The ship started its northward journey from Dutch Harbor in Alaska (53.89°N, 166.53°W), crossing the Bering Sea and Makarov Basin, before reaching the North Pole on September 5. The return leg mostly followed the 150°W meridian, before crossing the Chukchi Sea and returning back across the Bering Sea to Dutch Harbor.

On the route, eight sets of size segregated aerosol samples (M1 - M8) were collected using a 11-stage MOUDI (Micro Orifice Uniform Deposit Impactor, MSP Corp.) and fourteen sets of bulk aerosol using a Hi-Volume sampler (H1-H14) (Tisch Environmental Inc.), as described in Figure 4.1a-b). The meteorological information, including ambient temperature, sea surface temperature, wind speed etc. is in Figure 4.1c.

During this cruise, the MOUDI samples were collected with a sampling flowrate of 30 L/min. Teflon filters (Pall corp. 47mm diameter and 1.0 μ m pore size) were used as the sampling media. The 50% cut-offs of the MOUDI stages were 0.056, 0.10, 0.18, 0.32, 0.56, 1.0, 1.8, 3.2, 5.6, 10, and 18 μ m in aerodynamic diameter. The particle size 1.8 μ m was used as a cutoff size to separate the fine and coarse fractions for MOUDI samples (Xu et al., 2013).

Both the MOUDI and its pump were housed in enclosures to protect them from rain and sea-spray, with an extension connected to the MOUDI inlet and extending from the enclosure. A rain shield was installed above the inlet.

In addition, fourteen sets of total suspended particles (TSP) bulk aerosol samples (H1–H14) were collected at Hi-Volume (Tisch 5170V-BL) using a flow rate of $\sim 1\text{m}^3/\text{min}$ with 47mm Whatman- 41 filter substrates. For each deployment, 12 replicate Whatman 41 filters were loaded on a open-face holders (Advantec MFC). For the hi-vol TSP sampling, the filters were loaded on in-line polypropylene filter holders (Sterlitech PPO-47).

Modified PVC adapters were used so that twelve of these filter holders could be loaded on each sampler (Shelley et al., 2015) (See Figure 4.1).

Fourteen sets (C1-C8, C10-C15) of low-volume TSP samples were also collected using Chemcomb (ThermoScientific) simultaneously with the Hi-volume TSP sampler (Figure 4.1). The flow rate for Chemcomb sampling was 20 L/min and the filter media for the sample collection was Zefluor PTFE filter (47mm diameter and 1.0 μ m pore size). Since MSA and NSS-sulfate were observed in only a very few events, results from the Chemcomb sampler have been included to add in interpreting the chemistry involving these two components

All the aerosol samplers were installed at the front of ship's flying bridge, ~23 m above sea level, to minimize the influence of sea spray on samples, and forward of the ship's stack. To minimize the potential for contamination from the stack exhaust, sampling was controlled by wind speed and direction, through a Campbell Scientific CR800 data-logger interfaced with an anemometer and wind vane set up in close proximity to the samplers. Using this setup, aerosol sampling was restricted to periods when in-sector conditions (defined as a relative wind direction from within $\pm 60^\circ$ of the ship's bow and a relative wind speed of $>0.5 \text{ m s}^{-1}$) persisted for at least five continuous minutes.

Clean polyethylene gloves were worn for loading and unloading of filters for the samplers, which were carried out underneath a high-efficiency particulate air (HEPA) filter blower within a plastic "bubble" clean area constructed in the ship's main laboratory. Filters were loaded onto the samplers from labeled petri-dishes using pre-cleaned Teflon tweezers and were transferred back to the same petri-dishes after sample recovery. Filter holders were double-bagged for transfer between the ship's laboratory and the samplers. Deployment

blanks were carried out using the same protocols, but with the pumps turned off. All filters from the samplers were subsequently double-bagged and stored frozen.

4.3.2 Air Mass origin.

To explore the impact of air masses of different origins on aerosol samples collected during this cruise, the ship's journey was divided into three legs: (i) the first leg from August 10 to August 19, consisting of M1 and H1; (ii) the second leg from August 20 to September 20, consisting of M2–M5, and H2–H9; (iii) the third leg from September 21 to October 9, consisting of M6–M8 and H10–H14.

This division into three legs was made based on the different origins and transport routes of the air masses during the journey. For each of the ship's locations at six hours intervals, air mass back-trajectories, both normal and ensembled, were calculated for 100 hours, using NOAA HYSPLIT 4 model (Stein et al., 2015; Rolph et al., 2017). A total of 244 normal trajectories ($4 \text{ trajectories/day} \times 61 \text{ days}$) were then clustered (Figure 4.2a), along with the percentage of trajectories in each cluster. The normal trajectories were calculated considering the altitude of the sampling platform and the ensemble trajectories were calculated from a 3×3 grids where the height of the trajectories originated from three elevations (elevation of the sampling platforms and $\pm 250\text{ft}$). A total of 6588 ensembled trajectories ($27 \text{ trajectories/location} \times 4 \text{ locations/day} \times 61 \text{ days}$) were combined to create the blue frequency background (Figure 4.2a); the color density represents the average amount of time spent by these 6588 back-trajectories per unit area (in hour/km^2). The same analysis was repeated for the three individual legs in Figure 4.2 b-d. As evident from 4.2, the wind patterns during the sampling period can be characterized into the following three types, (i) type 1 originating from the North Pacific and the Bering Sea (Figure 4.2b), (ii)

type 2 consisting of marine Arctic air entirely from the Polar region (Figure 4.2c) and (iii) type 3 consisting of the marine Arctic air that has spent time over the continental land bodies of northern Russia and northern Canada (Figure 4.2 d). The three legs mostly were associated with these three types of air masses. Specifically, during the first leg, 68% of the air mass was type 1, 18% was type 2, and 15% was type 3; during the second leg, the entire air mass was type 2; during the third leg, 35% was type 2, and the rest was type 3.

4.3.3 Chemical Analysis.

Ion chromatography (Dionex IC-2000) was applied to measure the concentrations of the water soluble anionic and cationic species (chloride, nitrate, sulfate, acetate, formate, oxalate, MSA and sodium, potassium, ammonium, calcium, magnesium) at the Rutgers University, Atmospheric

Chemistry Laboratory. For the anion analysis, AS11 analytical column ($2 \times 250\text{mm}^2$, Dionex, particle size $13\mu\text{m}$), KOH eluent generator cartridge (EGC II KOH, Dionex) and $25\mu\text{l}$ sample loop were employed, while for cations, a CS12A analytical column ($2 \times 250\text{mm}^2$, Dionex, particle size $8.5\mu\text{m}$) and MSA generator cartridge (EGC II MSA, Dionex) were used, similar to Zhao and Gao (2008). Briefly, 5ml of $18.2\text{ M}\Omega$ di-ionized water was added to a quarter of the Chemcomb and MOUDI filter substrates. The solutions were ultra-sonicated for 40mins and leached overnight and then filtered through $0.22\mu\text{m}$ PTFE syringe filter. For the hi-vol TSP filters, an ultrahigh purity (UHP) water leach was carried out following the instantaneous leach protocol of Buck et al. (2006), using an acrylic vacuum chamber. Each hi-vol filter was loaded onto a Teflon filter holder (Savillex), mounted on top of the acrylic cylinder, which contained an acid-washed 100ml polyethylene bottle and was connected to a vacuum. An acid-cleaned polycarbonate

(0.4 μ m, Nuclepore) backing filter was used to prevent small particles washing through the sample filter. The leach procedure involves 100ml of UHP water being poured slowly over the filter under vacuum, with the leachate collected in the bottle inside the chamber. Triplicate filters were subjected to this leach for each deployment. Subsamples (~5ml) for major ion analysis were taken from each leachate sample. All the MOUDI, low-vol TSP, and hi-vol TSP samples were analyzed by IC with an AS40 auto-sampler and a 25 μ l injection loop.

The method detection limits (calculated as 3.143 \times standard deviation of 7 replicates of the lowest standard solution) were 0.007ppm for propionate, 0.008ppm for acetate and formate, 0.018ppm for oxalate, 0.013ppm for sulfate, 0.007ppm for nitrate, 0.015ppm for chloride and 0.016ppm for MSA, and below 0.01ppm for major cations. The precision at low concentration standard (i.e., 0.05ppm and presented as relative standard deviation) were within 8% for all the species analyzed.

The MOUDI and HV samples were 76% – >100% higher for the organics and approximately >1000% higher for the inorganic species than their corresponding field blank values. Final concentrations have been reported after corresponding field blank correction.

4.3.4 Data Analysis

In this study, the sea-salt aerosol concentrations were calculated using the following equation: Sea salt = $\text{Cl}^- + 1.47 \times \text{Na}^+$, where 1.47 is the mass ratio of ($\text{Na}^+ + \text{K}^+ + \text{Mg}^{2+} +$

$\text{Ca}^{2+} + \text{SO}_4^{-2} + \text{HCO}_3^-$) to Na^+ in seawater (Bates et al., 2001).] NSS-SO_4^{-2} was calculated based on the equation of $\text{NSS-SO}_4^{-2} = [\text{SO}_4^{-2}]_{\text{Total}} - [\text{Na}^+] \times 0.25$, where 0.25 is the weight ratio of $\text{SO}_4^{-2} / \text{Na}^+$ in seawater (Millero & Sohn, 1992). Chloride depletion was calculated with the following equation: % Chloride depletion = $(1.81 \times [\text{Na}^+] - [\text{Cl}^-]) / (1.81 \times [\text{Na}^+]) \times 100$, assuming all Na^+ in aerosol was from seawater in which the average weight ratio of Cl^- to Na^+ equals to 1.81 (Finlayson-Pitts & Pitts Jr, 1999; Zhao & Gao, 2008). The cation to anion charge equivalence ratio was calculated based on the following equation (here $[X]$ = molar weight of each species):

$$[\text{Na}^+] + [\text{NH}_4^+] + [\text{K}^+] + 2[\text{Ca}^{++}] + 2[\text{Mg}^{++}] / [\text{C}_3\text{H}_5\text{O}_2^{-1}] + [\text{CH}_3\text{COO}^{-1}] + [\text{CHOO}^{-1}] + [\text{NO}_3^{-1}] + [\text{Cl}^{-1}] + 2[\text{SO}_4^{-2}] + 2[\text{C}_2\text{O}_4^{-2}].$$

4.4 Results.

4.4.1 Spatial Distribution of the Aerosol Species from the Bulk Measurement.

4.4.1.1 General Distribution.

The spatial distributions of the water soluble ionic species over the Arctic Ocean are shown in Figure 4.3. The center of each circle represents the average location of the sampling sites and the area is proportional to the total concentration of the water soluble aerosol species analyzed in this study. Each circle is a pie chart where the organic fraction is shown as brown, while the inorganics are shown in cyan/blue, with blue representing sulfate (of which, deep blue is the non-sea-salt fraction). The bar graphs associated with each circle displays the concentrations of selected species with organic species on top and inorganic

species son bottom (sea-salt, being present in much larger quantities, is shown in a different scale).

It is evident that the total mass varied significantly as the ship traveled from North Pacific/Bering Sea towards the North Pole. The total mass concentrations of the soluble species decreased by a factor of 4–8 near the high Arctic regions. This feature indicates the presence of clean and pristine air mass near the pole with significantly less impact from the continental and marine air masses. However, the concentrations of the water soluble organic anions (propionate, acetate, formate, MSA, and oxalate) were considerably higher near the pole compared to other locations. The following is a more detailed discussions of the major species.

4.4.1.2 Sea-salt.

The sea-salt concentrations were substantially higher for both type 1 and type 3 air-masses, corresponding to 3609.1 ng.m^{-3} and 6382.6 ng.m^{-3} , respectively, than for the type 2 air mass. Over the central to high Arctic Ocean, where the air source was dominated by polar air (type 2), the average sea-salt concentration was approximately 371.3 ng.m^{-3} , suggesting the sea-ice covered ocean surface reduced the formation of sea-salt aerosols. Moreover, over the high Arctic Ocean, a majority of the sampling events had average wind speed $\sim 5 \text{ m.s}^{-1}$, ~ 2 times lower than wind speeds in the North Pacific/Bering Sea, and the film drop mode dominated (Nilsson et al., 2001), resulting in low production of sea-salt. This phenomenon is in agreement with a prior study conducted over the high Arctic region (Leck et al.,

2002). However, for a few events when the wind speed rose to $10\text{m}\cdot\text{s}^{-1}$, high Na^+ and Cl^- concentrations were observed, corresponding to high yields of sea-salt aerosols.

4.4.1.3 Nitrate.

Nitrate concentration for type 1 air-mass was $119.5\text{ng}\cdot\text{m}^{-3}$. This value is comparable to the value ($\sim 260\text{ng}\cdot\text{m}^{-3}$) observed over Shemya Island (52.72°N , 174.24°E) in the north-eastern North Pacific Ocean, but is higher than the summer time nitrate concentration measured ($77\text{ng}\cdot\text{m}^{-3}$) at Finnish Lapland near northern Arctic circle (Ricard et al., 2002). The average nitrate concentrations were low throughout for type 2 and type 3 air masses, corresponding to $2.9\pm 7.8\text{ng}\cdot\text{m}^{-3}$ and $22.3\pm 19\text{ng}\cdot\text{m}^{-3}$, respectively. Particularly near the pole, the concentrations were below detection level for a few events. Previous studies (Talbot et al., 1992; Hillamo et al., 2001) conducted near the high Arctic region in summer have also reported low nitrate concentrations. For instance, Talbot et al. (1992) observed nitrate concentration of $10\pm 6\text{pptv}$ (equivalent to $28\pm 17\text{ng}\cdot\text{m}^{-3}$ at 273K) from a weekly ground based measurement at Alert, Canada in July–August, 1986 and $11\pm 9\text{pptv}$ (equivalent to $30\pm 25\text{ng}\cdot\text{m}^{-3}$ at 273K) in the high Arctic boundary layer from aircraft measurements in summer 1988.

4.4.1.4 Ammonium.

Ammonium concentrations varied widely during the study period, ranging from below detection level to $202\text{ng}\cdot\text{m}^{-3}$. The average ammonium concentrations for the three types of air-masses were $53.1\text{ng}\cdot\text{m}^{-3}$ (type 1), $36.1\pm 53.7\text{ng}\cdot\text{m}^{-3}$ (type 2), and $45.2\pm 88.1\text{ng}\cdot\text{m}^{-3}$ (type 3). In Arctic summer 1986, Talbot et al. (1992) observed average ammonium concentration ($55\pm 24\text{ng}\cdot\text{m}^{-3}$) comparable to our study and suggested that dead marine organisms confined in the ice pack could be a potential source of particle phase ammonium.

In addition, emission of gas phase ammonia from sea-bird guano could also be a significant source of ammonium in summer (Wentworth et al., 2016). Previous studies over the Arctic region have also reported wide range of ammonium concentrations (Fenn et al., 1963; Martin, 1990; Leck & Persson, 1996). Matsumoto et al. (1998) obtained similar results over North Pacific Ocean and suggested that the source of air mass—continental or marine—might account for such large variations. In our study, occasional mixing of marine air with the continental air mass, especially for type 3, might have resulted in the observed variation in the ammonium concentrations.

4.4.1.5 Non-sea-salt-(NSS)-sulfate.

The average NSS-sulfate concentrations for type 1 and type 2 air-masses were 193.4ng.m^{-3} (2.01nmol.m^{-3}) and 20.9ng.m^{-3} (0.22nmol.m^{-3}), respectively. For type 3 air-mass, NSS-sulfate was detected in a single event (35.4ng.m^{-3} (0.37nmol.m^{-3})) —the last one—when the ship's location was similar to the location for type 1. This phenomenon suggests that the formation of NSS-sulfate was associated with the local oceanic source and the role of different air-masses impacting NSS-sulfate concentration was not significant. In the Arctic summer the major source of NSS-sulfate is the oxidation product of DMS which is emitted by the phytoplankton (Leck & Persson, 1996) in the ocean, followed by sea to air exchange. Heintzenberg and Leck (1994) reported that in Arctic summer at Zeppelin station (75°N , 12°E) about 22% of the sulfate aerosol was of regional marine biogenic origin. NSS-sulfate was detected in all the samples at North Pole. This may be a result of ice-trapped DMS being released as sea-ice cover melts during the Arctic summer (Ferek et al., 1995), with subsequent NSS-sulfate production.

The high NSS-sulfate concentration observed over Bering Sea and Chukchi Sea was ~ 3 times lower to the values measured at Shemya (680ng.m^{-3}) and Midway Islands (310ng.m^{-3}) during the “clean” period however, the concentrations at these islands were ~2 times higher during the “dusty” period (Prospero et al., 1985). The lower values obtained near the pole were in agreement with the results obtained from previous International Arctic Ocean Expedition (IAOE-91) (Leck & Persson, 1996). In the same study, Leck and Persson (1996) observed that the concentration (0.31nmol.m^{-3}) decreased over the pack ice regions compared to the open ocean—similar to our observations for type 2. Substantially higher summer time NSS-sulfate concentrations than those observed in the present study were reported at Svalbard station (78.92° N , 11.93° E) in 2012 (Zhan et al., 2014), which could have originated from the ship emissions at the study site.

NSS-sulfate concentrations were negative for seven events, four of which contained high sea-salt concentrations. Similar negative values for NSS-sulfate have been obtained in previous studies (Aristarain et al., 1982; Wagenbach et al., 1998). Sea-salt fractionation during sea-ice formation and subsequent over-estimation of the sea-salt sulfate component is likely the cause of the observed negative values.

4.4.1.6 MSA.

The spatial variation of MSA for the three types of air-masses over the Arctic Ocean was similar to the distribution of NSS-sulfate. High MSA (72.3ng.m^{-3}) was detected in type 1. For type 2, among the eight sampling events, MSA was detected in four events with an average concentration was $3.62\pm 2.53\text{ng.m}^{-3}$. For type 3, MSA was detected in a single event (concentration was 1.44ng.m^{-3}) when the ship’s average location was $\sim 80^\circ\text{N}$,

149°W—which probably reflected the influence of type 2 polar marine air. These values are comparable to the previous results obtained over the Arctic Ocean (S. M. Li et al., 1993; Sharma et al., 2012; Ye et al., 2015)s. Ye et al. (2015) found similar wide variation in the MSA spatial distribution: the higher average MSA concentrations were associated with Chukchi Sea (67°N–71°N, 167°W–176°W; average concentration $12 \pm 16 \text{ ng.m}^{-3}$) and Norwegian Sea (69°N–75°N, 2°E–34°E; average concentration $60 \pm 80 \text{ ng.m}^{-3}$), decreasing substantially near the central Arctic Ocean (80°N–87°N, 170°W–138°E; average concentration $1.2 \pm 2 \text{ ng.m}^{-3}$).

4.4.1.7 Oxalate.

The highest oxalate concentration was associated with type 1 (18.9 ng.m^{-3}), followed by type 3 ($18.4 \pm 24.2 \text{ ng.m}^{-3}$). Near the pole (type 2), the average oxalate concentration was $2.5 \pm 4.2 \text{ ng.m}^{-3}$. The low values obtained near the pole (type 2) could be attributed to the aqueous phase photo-dissociation of the Fe(III)-oxalate complexes in the Arctic summer (Kawamura et al., 2012). These values were comparable to the earlier studies conducted at different locations of Arctic region. For instance, Talbot et al. (1992) measured 8pptv ($\sim 46 \text{ ng.m}^{-3}$ at 0°C and 1atm) of average oxalate over the sub-arctic, Li and Winchester (1993) measured 27 ng.m^{-3} of average oxalate over Barrow, Alaska, and Kawamura, Kasukabe, et al. (1996) measured $14 \pm 12 \text{ ng.m}^{-3}$ of average oxalate at Alert, Canada.

4.4.1.8 Formate, Acetate, and Propionate.

Formate concentration was very low over the Bering Sea (0.04 ng.m^{-3}) compared to average concentrations during types 2 and 3 of $15.3 \pm 24.1 \text{ ng.m}^{-3}$ and $25.7 \pm 50.8 \text{ ng.m}^{-3}$, respectively. Acetate followed a similar trend, with a considerably lower concentration (1.2 ng.m^{-3}) in the first sample, and increased concentrations over the Arctic Ocean. For type 2 and type

3 the average concentrations were $23.4 \pm 39.5 \text{ ng.m}^{-3}$ and $80.8 \pm 180.2 \text{ ng.m}^{-3}$. Similar amounts of acetate and formate have been reported previously for the polar environment (Xu et al., 2013).

The concentration of propionate was consistently below detection level in all three types of air-masses, with a trace amount ($\sim 4 \text{ ng.m}^{-3}$) of propionate detected in a single event associated with type 2 polar air. There are comparatively few studies available with propionate measurement in aerosol over the Arctic Ocean (Toom-Saunty & Barrie, 2002). Weekly snow samples collected at the Alert, Canada revealed a peak in propionate and acetate concentration peaked after polar sunrise, suggesting strong photochemical processes responsible for the production of these species (Toom-Saunty & Barrie, 2002).

4.4.2 Mass-size Distribution.

4.4.2.1 General Distribution.

In this section we discuss the mass-size distribution of the major water soluble inorganic and organic species analyzed in this study; the samples were collected by the 11-stage size segregated sampler, MOUDI (detailed description in section 2.1). Figure 4.4 presents the distribution for four inorganic components, sea-salt, NSS-sulfate, nitrate, and ammonium, and Figure 4.5 presents the distribution for the four organic compounds, propionate, acetate, formate, and oxalate. The mass-size distribution of MSA is shown in Figure 4.6a.

Similar to the spatial distribution, depending on the source of air mass, for each component, the mass-size spectrum was divided into three types. For each type, the dashed lines present the data obtained from individual MOUDI, whereas the solid line shows the composite

distribution. The composite distribution for each species and for each air-mass type was obtained by fitting the data by a sum of one, two, or three lognormal distributions using maximum likelihood estimation; of the three such fitted curves for each type, the simplest one that fitted the data well was chosen. (When going from a simple model, such as a single lognormal distribution, to a more complicated model, such as a sum of two lognormal distributions, if the normalized log-likelihood value increased by at least 0.05, the latter was preferred; otherwise, the former simpler model was used.) In general, the inorganic components were present in uni-modal distribution, and the organics show bi or tri-modal distribution. The detailed discussion for individual species is presented in this section.

4.4.2.2 Sea-salt.

Figure 4.4a presents the mass-size distribution of the sea-salt particles. In type 1 and type 3 air masses, the sea-salt distribution dominated at coarse mode, peaking at 1.8–5.6 μm and the corresponding concentrations were 1137.3 $\text{ng}\cdot\text{m}^{-3}$ and 1178 $\text{ng}\cdot\text{m}^{-3}$, respectively. The presence of coarse mode sea-salts is a common feature over the open oceans (O'Dowd et al., 1997). The super micron mode enrichment of sea-salt particles is consistent with previous studies over Polar regions (Quinn et al., 2002; Xu et al., 2013). However, for the type-2 air mass, in general, the sea-salt concentration was significantly low but in a single event (M3; sampling time 8/27/15-9/24/15) the mass-size distribution peaked at fine mode (0.1–0.32 μm). High wind speed ($>10\text{m}\cdot\text{s}^{-1}$) was observed in our study for that particular event which might have contributed to fine mode sea-salt production.

4.4.2.3 Nitrate.

Atmospheric nitrogen is an important source of nutrients to the marine eco-system over the open ocean. Mass distribution of the nitrate species in the atmosphere determines their

efficiency of deposition into the ocean surface. The mass-size distribution of nitrate was dominated at the lower end of the coarse mode, peaking at 1.8–5.6 μm size range in all three types of air-masses corresponding to concentration $\sim 38\text{ng.m}^{-3}$ (type 1), $\sim 10\text{ng.m}^{-3}$ (type 2) and $\sim 9\text{ng.m}^{-3}$ (type 3) (Figure 4.4b). However, in type 3, during the sampling period 09/26/15–10/03/15 (M7), nitrate was also present at fine particle mode peaking at 0.18–0.32 μm indicating a possible source of continental air-mass (Xiu et al., 2004). Similar coarse mode dominance of nitrate in Arctic aerosols was found in other studies (Barrie & Hoff, 1985; Ricard et al., 2002).

4.4.2.4 Ammonium.

The mass-size distribution of the ammonium particles in the aerosol was dominated in the fine mode, peaking at 0.18–0.32 μm , irrespective of the types of air-masses Figure 4.4c). The occurrence of fine mode ammonium in this study is consistent with the previous observations conducted over north Pacific ocean (Matsumoto et al., 1998) and over the high Arctic Ocean (Leck & Persson, 1996).

Coarse mode ammonium was found on one sample (M7; type3) peaking at 3.2 μm with the concentration of 14ng.m^{-3} . This sampling time coincided with the air mass type 3 which had mixed source of continental air and polar air. Similar coarse mode ammonium aerosols was observed by Yeatman et al. (2001) at the coastal sites of UK and northern Europe.

4.4.2.5 Non-sea salt sulfate.

NSS-sulfate (Figure 4.4d) existed in fine mode for all three types of air masses, peaking at 0.1–0.32 μm , corresponded to 44ng.m^{-3} for type 1, 10ng.m^{-3} for type 2 and 12ng.m^{-3} for type 3 air masses. For type 1 air mass, however $\sim 20\%$ of the total NSS-sulfate was present in particle size higher than 1 μm , predominantly concentrated at 1.0–1.8 μm with

concentration of $\sim 28 \text{ ng.m}^{-3}$. The fine mode sulfate particles are highly important in the clean marine environment because of their active participation in cloud formation and their scattering efficiency of solar radiation. The fine mode accumulation of NSS-sulfate in our study is in agreement with previous results (Leck & Persson, 1996; Matsumoto et al., 1997; Leck et al., 2002; Ghahremaninezhad et al., 2016).

4.4.2.6 Acetate, Formate, and Propionate.

The mass size distributions of acetate, formate, and propionates (Figure 4.5a-c) did not exhibit any sharp feature. They existed in all size range—a common characteristics of the marine environment (Matsumoto et al., 1998). The adsorption of these species in gas phase onto the particles collected at the filter substrate or volatile loss from the upper stages may have occurred as sampling artefact (Turpin et al., 1994). However, the temperature during sampling was low and the concentration of the major coarse mode particle—sea-salt particles—was not high, suggesting the negligible effect of these sampling artefacts on the observed trend of these low molecular weight carboxylic acids.

Comparatively few studies have been conducted over the Arctic polar region to show the size distribution of these compounds. Matsumoto et al. (1998) reported similar mass-size distribution for acetate and formate over the northwest Pacific Ocean. Propionate concentration was substantially low throughout, while acetate was found in relatively high concentrations consistently. Analysis of the organic acids from the snowfall data over the high Arctic region reported the enrichment of propionate concentration after the polar sunrise due to photochemical activities. A similar process might be significant for acetate formation in the air (Toom-Saunty & Barrie, 2002). Due to their high vapor pressure, these species (acetate, formate, and propionate) pre-dominantly exist in the gas phase and a small

amount might have been incorporated into the prevailing salt particles to form coarse mode aerosols, which explains their dominance at coarse mode.

4.4.2.7 Oxalate.

The mass-size distribution of oxalate (Figure 4.5 d) for type 1 air mass showed a bi-modal pattern, peaking at 0.18–0.32 μm and 1.0–3.2 μm , with corresponding concentrations 6.1 $\text{ng}\cdot\text{m}^{-3}$ (~1.6pptv at 273K) and 6.6 $\text{ng}\cdot\text{m}^{-3}$ (~1.7pptv at 273K), respectively (Figure 4.5d).

The concentration of oxalate was equally distributed in all size ranges for type 2 and type 3 air masses and the average concentrations (summed over all the stages) for type 2 and type 3 air masses were 106.7 \pm 64.5 $\text{ng}\cdot\text{m}^{-3}$ (~27.2 \pm 16.4pptv at 273K) and 137.8 \pm 30.9 $\text{ng}\cdot\text{m}^{-3}$ (~35.1 \pm 7.9pptv at 273K), respectively.

The existence of aerosol phase oxalate in both fine and coarse modes had been reported previously for remote marine environments (Kerminen et al., 1999; Baboukas et al., 2000; Mochida et al., 2003). These observation indicate that the gas to particle conversion and condensation on the coarse mode sea-salt particles could be the possible formation processes for oxalate. These values are substantially lower compared with those observed over continental region.

4.4.2.8 MSA.

MSA concentration increased with decreasing particle size and predominantly existed in the fine mode for all three types of air masses. For type 1 air-mass approximately 0.2% of MSA was present in coarse mode (peaking at 1.0–1.8 μm), associated with the concentration of 10.3 $\text{ng}\cdot\text{m}^{-3}$ (Figure 4.6a), suggesting condensation on the pre-existing particles. Similar to the fine mode NSS-sulfate formation, the particulate phase MSA is formed through the gas-to-particle conversion of the oxidative product of DMS. Similar

pattern of fine mode enrichment of MSA was observed in other studies over remote marine locations, such as at the northwest Pacific ocean (Matsumoto et al., 1998) and over the central Arctic ocean (Leck & Persson, 1996; Kerminen et al., 1997; Kerminen & Leck, 2001).

4.5 Discussion.

Several features of the Arctic marine environment can be gleaned from the chemical composition, mass size distribution, and the spatial distribution of the analyzed water soluble species of the Arctic aerosols. The chemical characteristics of the aerosols varied widely depending on the air masses influencing the sampling time; for instance, type 1 and 3 air masses exhibited similar features with respect to aerosols' alkalinity and chloride depletion, but type 2 air masses were different. On the other hand, the water soluble organic acids occupied a major fraction for the type 2 air mass and may play a significant role as CCN near the pole. Here we discuss three such major aspects of the Arctic aerosols in detail to understand their chemical characteristics, possible sources, formation mechanisms, and their potential to participate in cloud formation.

4.5.1 MSA and its Ratio with NSS-sulfate.

At Bering Sea (type 1), substantially high MSA concentration (~15 times higher than that for type 2 and 3) was observed (Figure 4.6b). Several reasons such as, (1) the variation in the biological productivity and abundance of different phytoplankton species, (2) availability of the atmospheric oxidants, (3) influx of oceanic DMS into the air, and (4) the variation in air temperature, solar intensity, and sea-ice extent could all result in the observed pattern of MSA in this study. For instance, Sharma et al. (2012) observed elevated MSA concentrations during the summer months at Barrow and Alert and suggested that

the decrease in sea-ice cover and the presence of OH radical together had caused this amount. Bubble bursting also increases the sea-air exchange of DMS; the higher concentrations of MSA over the Bering Sea compared to the other two regions can be attributed to the stronger winds and higher bubble bursting over the Bering Sea. In addition the sea-ice covered surface water in some places over the high Arctic ocean might have prevented the sea-to-air transport of DMS, resulting in significantly lower MSA concentrations over those locations (Ye et al., 2015).

Since MSA has marine biogenic origin and chlorophyll-a concentration can be an indicator of the biological productivity in the remote ocean (Liss et al., 1997), the chlorophyll-a concentration profile along with MSA concentration has been plotted in Figure 4.6b. Near the Bering Sea, the chlorophyll-a concentration was $\sim 1\text{mg}\cdot\text{m}^{-3}$, suggesting a region of high biological productivity resulting in high MSA concentration.

Near the pole, no chlorophyll-a was detected, presumably due to the sea-ice coverage not detected by the satellite from space, although trace level of MSA was found in every sampling events. The spatial variation of chlorophyll-a, however, is not enough to accurately represent the spatial variation for MSA, since the rate of MSA production highly depends on the distribution of different species of phytoplankton over the Arctic ocean. For example, at the central Arctic Ocean, the diatom, *Nitzschia frigida*, is the major phytoplankton species, which produces only limited amount of DMS—the major precursor of MSA (Levasseur et al., 1994; McMinn & Hegseth, 2004; Vogt & Liss, 2009) and varies significantly in space and time (Gondwe et al., 2003). In addition, the sea-ice covered central Arctic Ocean might have reduced the rate of sea-to-air DMS exchange and decreased the rate of MSA production.

Oxidation of DMS, the process that generates MSA in marine regions, also produces sulfate—defined as biogenic NSS-sulfate. Therefore the molar ratio of MSA/NSS-sulfate is considered to be a measure of biogenic contribution to the aerosol production over the remote marine environment. Since only a few samples contained detectable amount of MSA and NSS-sulfate, the combined values from the hi-volume TSP sampler, aggregate of the 11 stages of MOUDI, and the low-volume TSP samplers (Chemcomb) were used to obtain the statistically relevant results. On three occasions (H3, H4, and H10) no NSS-sulfate was found, but trace amounts of MSA existed. For H10, sulfate/sodium ratio was 0.25 which is the exact ratio for the sea salt sulfate. Significant amounts of NSS-sulfate was measured during the sampling of H2, which ended on the same day the sampling of H3 started, suggesting the MSA at H3 and NSS-sulfate at H2 were perhaps formed during same period.

For the samples where both MSA and NSS-sulfate were present, their ratio varied between 0.03–0.56. The average ratio obtained in this study (0.26, n=10) is within range of the values observed at Finnish Arctic (Kerminen et al., 1997) in summer, 1995 and at Canadian Alert from 1980-1990 (Li & Barrie, 1993). The high molar ratio (~0.32) was obtained from the Bering Sea (type 1) region. Similar high MSA/NSS-sulfate ratio was observed in an aircraft observation (1.09) over the Bering Sea in summer, 1988 (S.-M. Li et al., 1993) reflecting the reduced effect of anthropogenic impact.

The high ratio obtained in this study is comparable with the ratios obtained in previous studies with less anthropogenic influence. Since the summer Arctic is generally isolated from the pollutant laden air from the surrounding continents, the concentration of the anthropogenic NSS-sulfate is low, thereby leading to a higher MSA/NSS-sulfate ratio. The

molar ratio was well correlated with the MSA concentration ($R^2=0.32$, $n=10$) during the summer Arctic.

A high MSA/NSS-sulfate ratio might also result from a time lag between the accumulation of MSA and sulfate, since oxidation of DMS produces MSA and SO_2 as the primary products, and the latter further oxidizes to produce sulfate as a secondary product. In addition, the dry deposition of SO_2 could also cause high MSA/NSS-sulfate ratio (S.-M. Li et al., 1993). Moreover, laboratory study indicates that NSS-sulfate nucleates to form new particles, whereas MSA prefers to condense on pre-existing particles (Hoppel, 1987), and the relative rate of these two processes would also modulate the MSA/NSS-sulfate ratio.

The role of temperature affecting the MSA/NSS-sulfate ratio is a matter of much debate. In a laboratory based experiment, Yin et al. (1990) claimed that MSA formation is preferred over SO_2 production at low temperatures, and Bates et al. (1992) observed an inverse relation of the ambient temperature with MSA/NSS-sulfate molar ratio. On the contrary, higher ratio was observed in the warmer summer months on several occasions (Ayers et al., 1991; Prospero & Savoie, 1991). To understand the role of temperature on MSA concentration and the MSA/NSS-sulfate ratio, these two parameters were plotted as a function of air temperature (AT) and sea surface temperature (SST) (Figure 4.6 c). Strong positive correlation existed between the AT or SST with the MSA concentration. This high positive correlation might be biased because significantly high MSA concentrations ($n=3$) were found over the Bering Sea when the ambient temperature was $\sim 9^\circ\text{C}$, but the high MSA over this location could be the indication of high biological productivity (as evidenced from Figure 4.6b) rather than solely the temperature dependence. After discarding those three samples, the correlation decreased between the AT and the MSA

concentration ($R^2 = 0.004$, $n=10$) with negative slope and between the AT and the MSA/NSS-sulfate ratio ($R^2=0.03$, $n=7$) for the samples collected over the high Arctic Ocean. This may suggest that at low temperature the MSA formation was favored compared to the NSS-sulfate.

4.5.2 Cation/Anion ratio, Chloride Depletion.

Sea-salt particles constitute an important component of lower tropospheric marine aerosols, influence the scattering of solar radiation, and is a source of reactive halogens (Hara et al., 2004; Simpson et al., 2007). Due to their large surface area and basic nature, they react with the acidic gaseous species such as sulfuric acid, nitric acid, and certain organic acids. As a result, chloride is depleted in form of volatile HCl gas, and the reactive chloride species released from the sea-salt particles can then initiate photochemical reactions. The chloride depletion on the sea-salt particles can be calculated by comparing the observed chloride concentrations with the expected chloride concentration in sea-salts. In a majority of the events associated with air mass types 1 and 3, the mass ratios (average 1.3) of chloride to sodium were below the mass ratio of bulk sea water (1.8) suggesting the occurrence of chloride depletion from the sea-salt particles. Since little amount of sea-salt was present in type 2 air mass, nearly 60% samples showed no depletion of chloride and those events were not included in the calculation of the chloride depletion. The average chloride depletion for three types of air masses were as follows: ~ 36% for type 1, 53% for type 2 and 33% for type 3. These values are consistent with the chloride loss observed at various marine locations (Suzuki et al., 1995; Johansen et al., 2000; Kerminen et al., 2000).

The chloride loss significantly varied with varying particle size, with maximum depletion associated with decreasing particle size in fine mode (Figure 4.7a). For type 1 and type 3

air masses, the majority of chloride depletion (~60–100%) was associated with the particle size $<0.56\mu\text{m}$. The chloride depletion for the above two air masses decreased at particle size larger than $1.8\mu\text{m}$ where the average depletion was ~19%. On the other hand, for type 2 air mass the chloride loss occurred over a broad range of particles, occurring both for fine and coarse particles, and peaking at $0.56\text{--}1.8\mu\text{m}$. Similar pattern of fine mode enrichment of chloride depletion was observed in previous studies over the Arctic Ocean (Kerminen et al., 1998; Narukawa et al., 2003) as well as other marine locations (Yao et al., 2003; Hsu et al., 2007). Consistent with type 2, over the Arctic Ocean, Kerminen et al. (1998) also observed 65% and 43% of chloride depletions associated with particle sizes $1.8\text{--}3.5\mu\text{m}$ and $3.5\text{--}7.5\mu\text{m}$, respectively.

The larger surface to volume ratio of fine mode sea-salt favored sulfuric acid condensation and had probably caused more chloride depletion. Kerminen et al. (1998) proposed that the activation of sea-salt particles into cloud droplets, the consequent formation of sulfate, and the eventual release of gas phase HCl and ammonia during cloud evaporation resulted in the observed fine mode chloride depletion. For all three types of air masses, a majority of the NSS-sulfate (80–100%) was present in fine mode coinciding with the aerosol diameter most associated with chloride depletion; this suggests that NSS-sulfate played a significant role in fine mode chloride depletion. Among the organic species, MSA—having ~60–100% of its total concentration comprised of fine particles—could have also contributed to the chloride depletion (Kerminen et al., 1998). Since nitrate had significantly low concentrations in type 3 and existed in coarse mode for type 1 air mass, it might have had negligible effect on the overall chloride depletion for these two air-masses.

Although, nitrate was present in very low amount in type 2, it might have been important for the coarse mode chloride loss. The average mole equivalent ratio of coarse mode nitrate and sodium for type 2 air mass was 0.6, indicating the contribution of nitrate on chloride depletion in coarse mode. The other anions such as organic anions, mostly oxalate, might react with sea-salts during condensation or in-cloud phases (Kerminen et al., 1998). Almost 50% of the organic anions were present in coarse mode for type 2 air mass, suggesting their contribution for chloride depletion.

To further investigate the aerosol acidity, the molar charge equivalence ratio of the water soluble major cations and anions were calculated for the fine and coarse particles (Figure 4.7b). The average fine mode cation-to-anion ratio for type 1 and type 3 air masses were 0.74 and 0.65 respectively. Increased cation-to-anion ratio was observed for coarse mode particles for type 1 (0.91) and type 3 (0.99) air masses, suggesting the coarse mode particles are nearly neutralized. On the other hand, for type 2 air mass, both the coarse and fine mode ratios were 0.42 and 0.60 respectively, indicating that the aerosols in Arctic polar air were acidic in both size ranges. Similar feature of dominance of acidic particles in accumulation mode and neutralized particles in coarse mode were observed in other studies (Winkler, 1986; Kerminen et al., 2001). Accumulation of acidic species upon the fine particles and in-cloud processing of sulfate aerosols might have contributed to the higher acidity in fine mode (Kerminen et al., 2001).

Completely or close to neutralized coarse particles in type 1 and type 3 air masses suggest the interactions between alkaline sea-salt particles with acidic species in gas phase or those produced in the aerosols (Fridlind & Jacobson, 2000); and similarly, the lower concentration of sea-salt in type 2 polar air might have resulted in highly acidic aerosols.

Moreover, the concentrations of NSS-sulfate and nitrate were significantly lower near the pole, indicating that carboxylic acid anions controlled the aerosol acidity. These acidic particles in the high Arctic region might favor the formation of secondary organic aerosols via heterogeneous polymerization and hydration of several atmospheric precursors, such as isoprene, aldehydes, and carbonyls (Duncan et al., 1998; Jang & Kamens, 2001; Jang et al., 2002; Limbeck et al., 2003).

The fine mode ammonium and NSS-sulfate molar ratio was calculated since both the species accumulated in the fine mode; the results are shown in Figure 4.7c. The average ratio for type 1 was 1.8, but this value increased for type 2 and type 3 (2.8 and 3.6, respectively) which were primarily influenced by the Arctic polar air. The ratios obtained in our study are consistent with other measurements conducted over the northeast Pacific Ocean (Quinn et al., 1990) and high Arctic Ocean (Leck et al., 2002). The molar ratios indicated that the partly neutralized sulfate particles existed over the Bering Sea but completely neutralized sulfate particles were present over the polar region. For type 2 and type 3 air masses, the excess ammonium might have reacted with nitrate to form ammonium nitrate. However, both in type 2 and type 3 air masses, nitrate dominated in coarse mode. In addition, ammonium nitrate is highly volatile in nature, therefore the occurrence of ammonium nitrate particles in the Arctic aerosols was highly unlikely. This further suggests that the organic anions largely contributed to the aerosol acidity observed in type 2 and type 3 air masses.

4.5.3 Water soluble Organic Species (WSOS) and their Relevance as CCN.

Despite being present in low concentrations, the water soluble carboxylic acid anions (such as formate, acetate, propionate, and oxalate measured in this study), despite being present

in low concentrations, constituted a significant fraction (approximately 10% of the total water soluble fraction in each sample) of the type 2 polar air. For type 1 and type 3 air masses, this fraction decreased to only 2%.

More precisely, for the samples collected over the Arctic polar region, the average NSS-sulfate concentrations (bulk measurement) were $13.9 \text{ ng} \cdot \text{m}^{-3}$ (hi-vol)—accounting for only 3% of total water soluble aerosol concentration. The fine mode molar ratios for individual organic anions with the NSS-sulfate over the polar region has been plotted in Figure 4.7d. Overall, a significantly high molar ratio of ~ 8.07 was observed in the fine mode between the total WSOS and the NSS-sulfate. Matsumoto et al. (1997) found strong correlation between CCN concentration and the total soluble organic (formate, acetate, oxalate, and MSA) concentration at supersaturation levels of 1% and 0.5%. Therefore near the pole in the summer, with both sea-salt and NSS-sulfate present in low concentrations, the soluble organics assume a more significant role in the CCN formation.

Unlike oxalate, the availability of formate, acetate, and propionate in the aerosol phase is generally low, and they mostly exist in the gas phase due to their very high vapor pressures (Binran, 1984). Formic acid can be formed via aqueous phase oxidation of formaldehyde, which is an oxidation product of DMS emitted by the phytoplankton, followed by evaporation (Chameides & Davis, 1983) into the air. This mechanism might not be significant for acetic acid formation since the process is very slow and acetaldehyde has a very low solubility. The oxidation of the precursor alkene compounds by atmospheric ozone can also be a potential source of these acids in the atmosphere. Thereafter these acids can be associated with basic sea-salt particles which are abundant in the marine environment. This phenomenon can be supported by the size distribution and the good

correlation of formate with sea-salt at fine mode (0.38). Andreae et al. (1988) reported that formic and acetic acids have strong solubility and surface activity, therefore they can be associated with pre-existing aerosol particles through absorption on the particle surfaces. Moreover, in a controlled laboratory study Russell and Heist (1978) showed that homogenous nucleation of formic acid is possible at the supersaturation level of 4 to 6% at the ambient temperature range -13°C to 32°C and for acetic acid with a supersaturation of 2.5 to 5.2 at the temperature range from -13°C to 67°C (Heist et al., 1976). Although the situation in the atmosphere is quite different compared with the controlled laboratory set-up, Shao-Meng and Winchester (1989); (Li & Winchester, 1993) and Li and Winchester (1993) found high aerosol concentration of formate and acetate in the winter time Arctic environment when the temperature was very low.

The WSOS can be directly emitted from their primary sources, such as 1) biomass burning (Talbot et al., 1988), 2) automobile exhaust (Kawamura et al., 1985), 3) soil and vegetation (Keene & Galloway, 1988; Talbot et al., 1990). These sources might not be significant during the Arctic summer since the long range transport of air mass from the surrounding continents is limited. A series of low molecular weight carboxylic acids were found in Canadian aerosols with a 5–20 fold increase in their concentrations after polar sunrise (Kawamura, Kasukabe, et al., 1996; Kawamura et al., 2010). It has been suggested that direct addition from the ocean surface in form of bubble bursting through the open leads could be the potential source of several organic aerosols over the Arctic Ocean (Bigg et al., 2004; Bigg & Leck, 2008; Leck & Bigg, 2010). Fu et al. (2009) observed the formation of secondary organic aerosols from oxidation of isoprene and Ziemba et al. (2010) observed significant aerosol growth at Greenland; both of these phenomena have been

suggested to be associated with the marine organisms. It can be hypothesized that with the onset of Arctic warming and consequent melting of sea-ice, the influx of these organics would increase in the summer Arctic boundary layer.

The secondary sources of WSOC are the in-situ photochemical oxidation of the low molecular weight olefins and non-methane hydrocarbons directly emitted from the sea-surface. The major low molecular weight olefins in marine environments are ethene, propene, butenes, 1-pentene and hexene (Bonsang et al., 1988; Chebbi & Carlier, 1996). These alkenes could generate carboxylic acids such as formic, acetic, and propionic acids through gas phase reaction with ozone, with the rate constants of $11.7\text{--}1.7 \times 10^{18} \text{ cm}^3 \text{ molecule}^{-1} \text{ s}^{-1}$ at 298K (Atkinson & Carter, 1984; Atkinson, 1990; Chebbi & Carlier, 1996). Swanson et al. (2002) has detected the presence of ethene and propene in the firn layer and ambient air over the Greenland surface snow. Laurila and Hakola (1996) also measured ethene, propene, and isoprene in the ambient air over the Baltic Sea and Northern Finland. Moreover, in the clean environments, such as the summer Arctic, where the anthropogenically produced NO_x concentration is low, the reactions involving peroxy acyl radicals (mostly originating from photolysis of partly oxygenated volatile organic compounds) with HO_2 and with other peroxy radicals would be a significant source of carboxylic acids. For instance, in the cleaner air, the interaction of $\text{CH}_3(\text{CO}(\text{OO}\cdot))$ with HO_2 and with $\text{CH}_3\text{COO}\cdot$ would produce significant amount of acetic acid (Lightfoot et al., 1992; Chebbi & Carlier, 1996) (for instance please see the reactions 1-2 below).





Past measurements near the Arctic polar circle had detected isoprene, a major precursor for oxalate (Laurila & Hakola, 1996), as well as its tracer (Hu et al., 2013). The other biological processes that might have produced the WSOC, particularly oxalic acid, over remote seawater are, 1) photorespiration of the phytoplankton (Steinberg & Bada, 1984), 2) photochemical reactions of the dissolved organic matter (Kirk, 1994), and 3) diffusion from surface sediments (Peltzer & Bada, 1981). In addition, oxalic acid could be produced from its pre-cursors -glyoxal and methyl-glyoxal, both of which have been detected near the Arctic polar circle at Alert, Canada (Kawamura, Kasukabe, et al., 1996).

4.6 Conclusion.

The results from this study indicate that during GN01, the marine boundary layer in the central Arctic Ocean was dominated by pristine marine air and was barely influenced by continental air. Although high accumulations of sea-salt and nitrate were observed over the Bering Sea and Chukchi Sea (type 1) and southern Canadian Basin (type 3), they existed primarily in coarse mode and are unlikely to have participated in cloud formation. Active biological productivity resulted in accumulation of fine mode NSS-sulfate and MSA over the Bering and Chukchi Seas, but their concentrations were significantly lower samples collected further north. This suggests that NSS-sulfate and MSA play a prominent role as CCN over the Bering Sea and Chukchi Sea.

Near the pole, a significant fraction of the water soluble organic anions were present in fine mode aerosols which would be highly important in cloud formation. This feature was also true for type 3 air mass which contained a substantial amount of oxalate in all samples, and acetate and formate in one sample. Therefore, at the less polluted marine locations where

anthropogenic NSS-sulfate concentrations are low, the locally produced organic anions are the primary candidates for CCN. The nm-size growth of the aerosol particles in the ambient air cannot be explained by the sulfate condensation alone (Kulmala et al., 2000), underlining the importance of the secondary organic aerosols—produced from organic precursors via heterogeneous processes—as a source of potential CCN, especially in the summer Arctic (Yu, 2000; Limbeck et al., 2003). However, it is not yet established whether the WSOS are capable of homogeneous nucleation without any assistance from sulfate particles and further research is needed, in laboratory and field studies, to quantify their role as CCN at different super-saturation levels, and to investigate possible reaction pathways for their formation from the various pre-cursors available in the ambient air.

Acknowledgments.

The research was supported by NSF grant 1435871 (YG) and 1438047 (CB). The authors are grateful to Mr. Shun Yu for many helpful discussions. The authors also want to thank Goujie Xu and Tianyi Xu for their assistance during the preparation of the expedition. The authors are extremely grateful to the crew members of the Healy cruise for their help during the entire sampling period.

4.7 Figures.

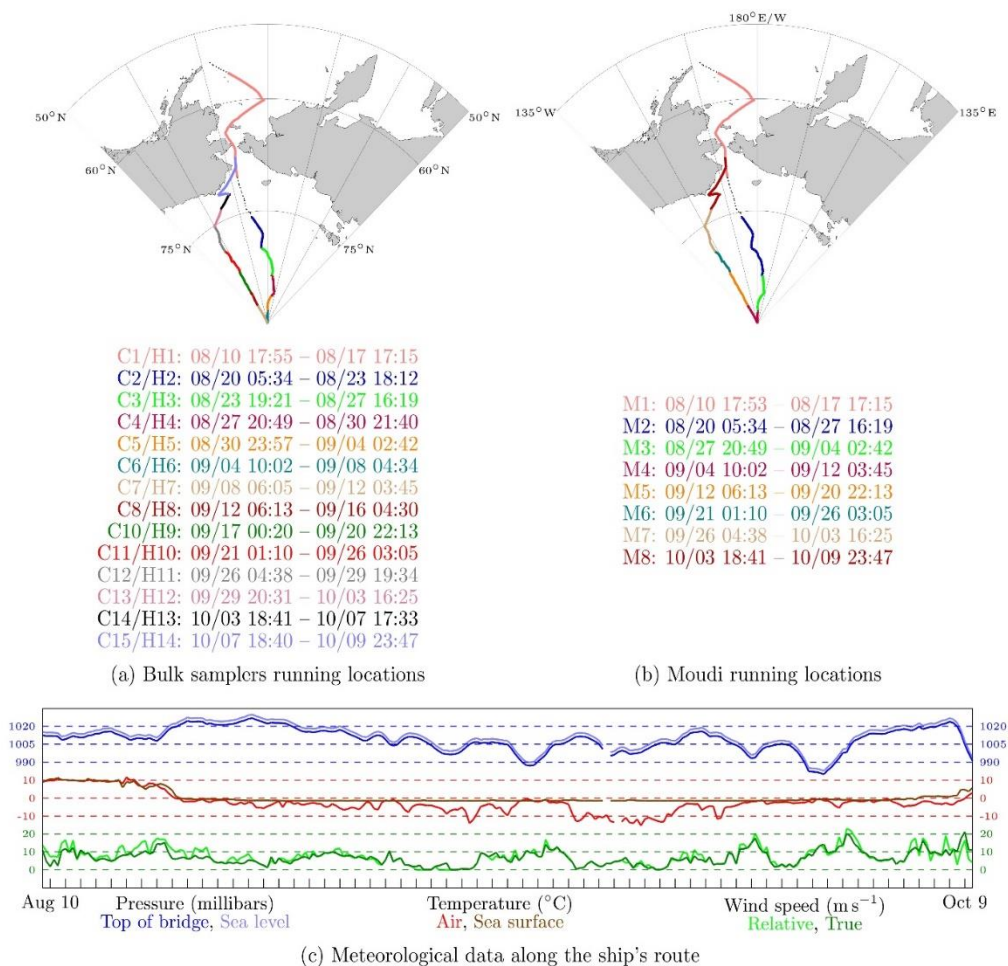


Figure 4.1 Sample runtimes along the ship's route: (a) Chemcomb and H-vol samplers, (b) 11-stage cascade impactor, C1-C15 represents Chemcomb, H1- H14 represents Hi-vol sampler and M1-M8 represents MOUDI, (c) Meteorological data along the ship's route.

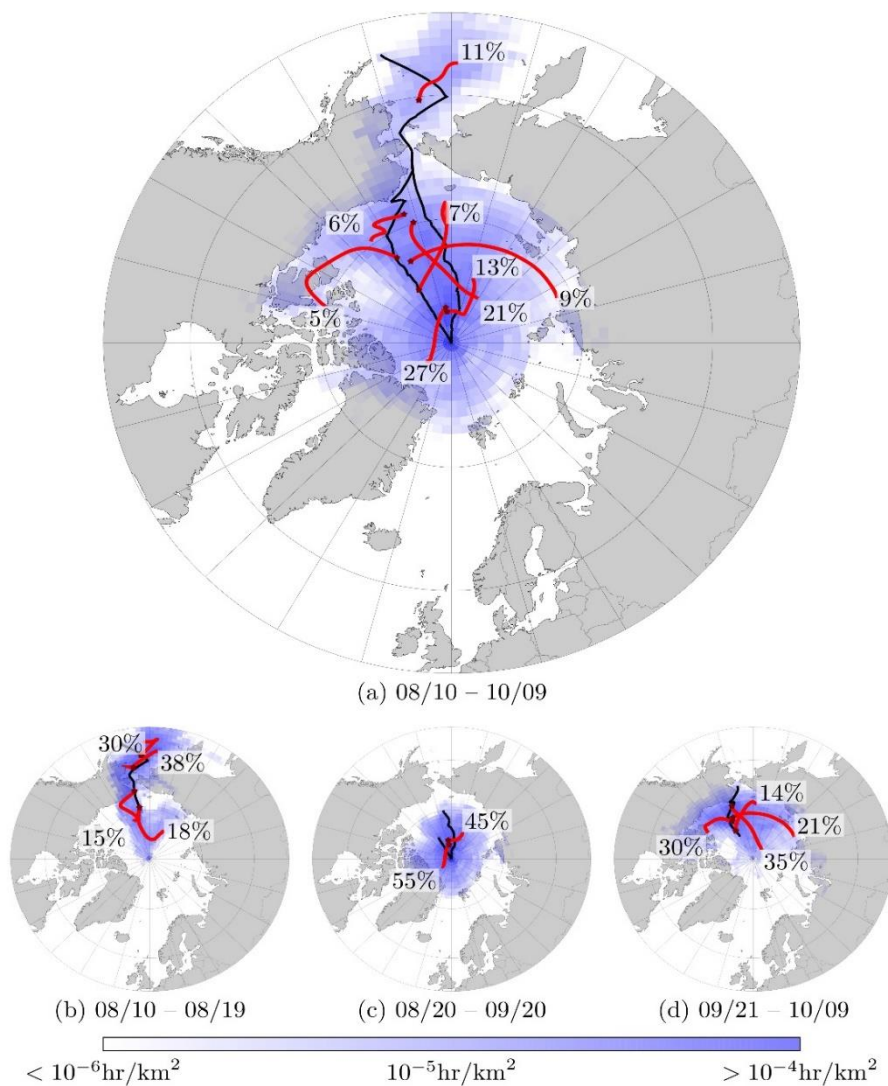


Figure 4.2 Back trajectory analysis using NOAA's HYSPLIT4 model for (a) the entire cruise (Aug 10 to Oct 9, 2015), (b) the first leg (Aug 10 to Aug 19), (c) the second leg (Aug 20 to Sep 20), and (c) the third leg (Sep 21 to Oct 9). The ship's track is shown as the black path. Back trajectories for 100 hours were calculated every six hours from the ship's locations, which were then clustered; the clustered trajectories along with the percentage of trajectories contained in each cluster is shown by red lines terminating in the red stars. Ensembled 100 hour back trajectories were also calculated from each point and their

frequency is represented by the blue background; the value of the frequency equals the average amount of time spent by a 100hr back-trajectory per unit area (in hr/km²).

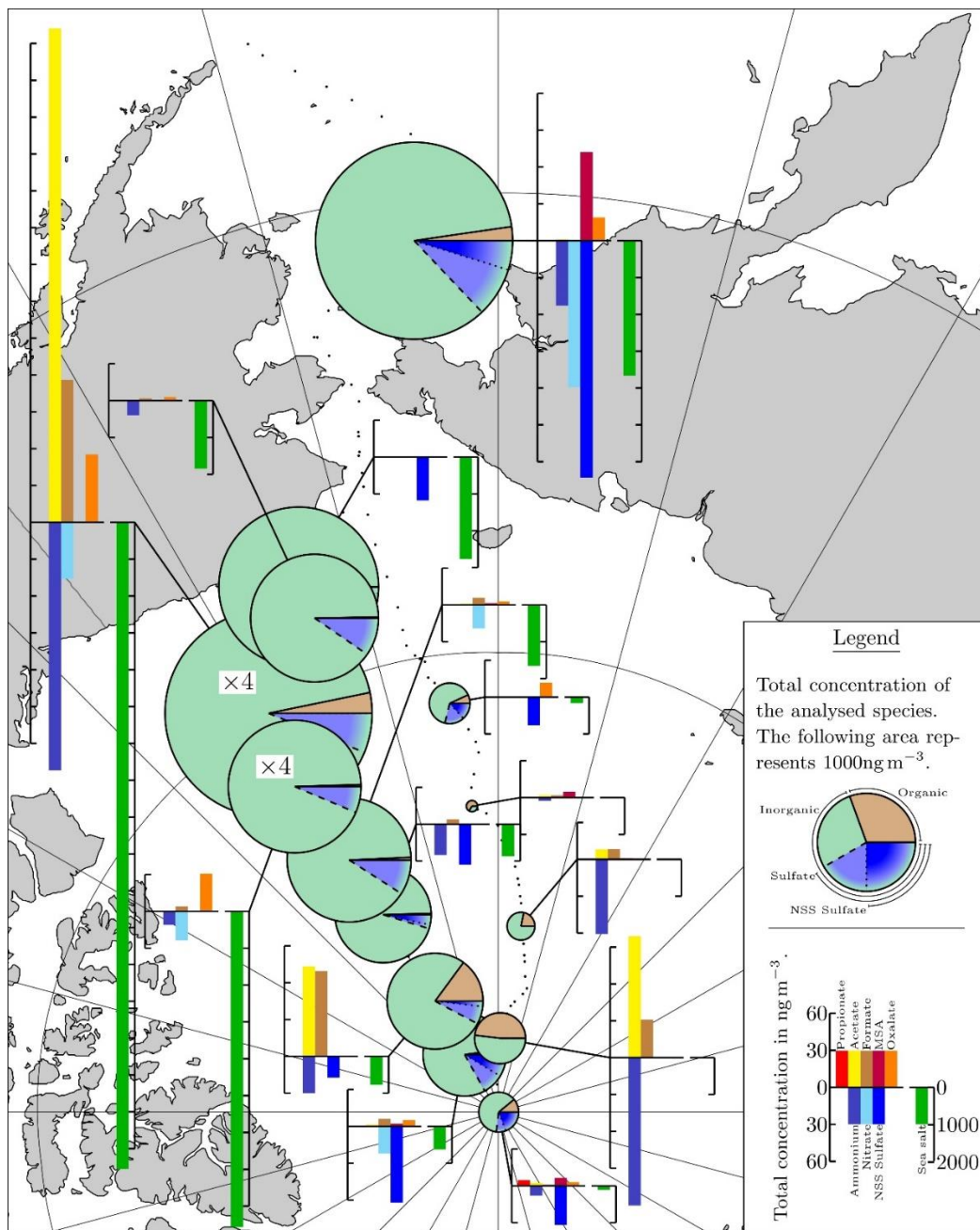


Figure 4.3 Spatial distribution of the concentration of the water soluble species [the aerosols were collected by hi-vol TSP collector]. Each circle represents the mass of the total water soluble species analyzed in this study.

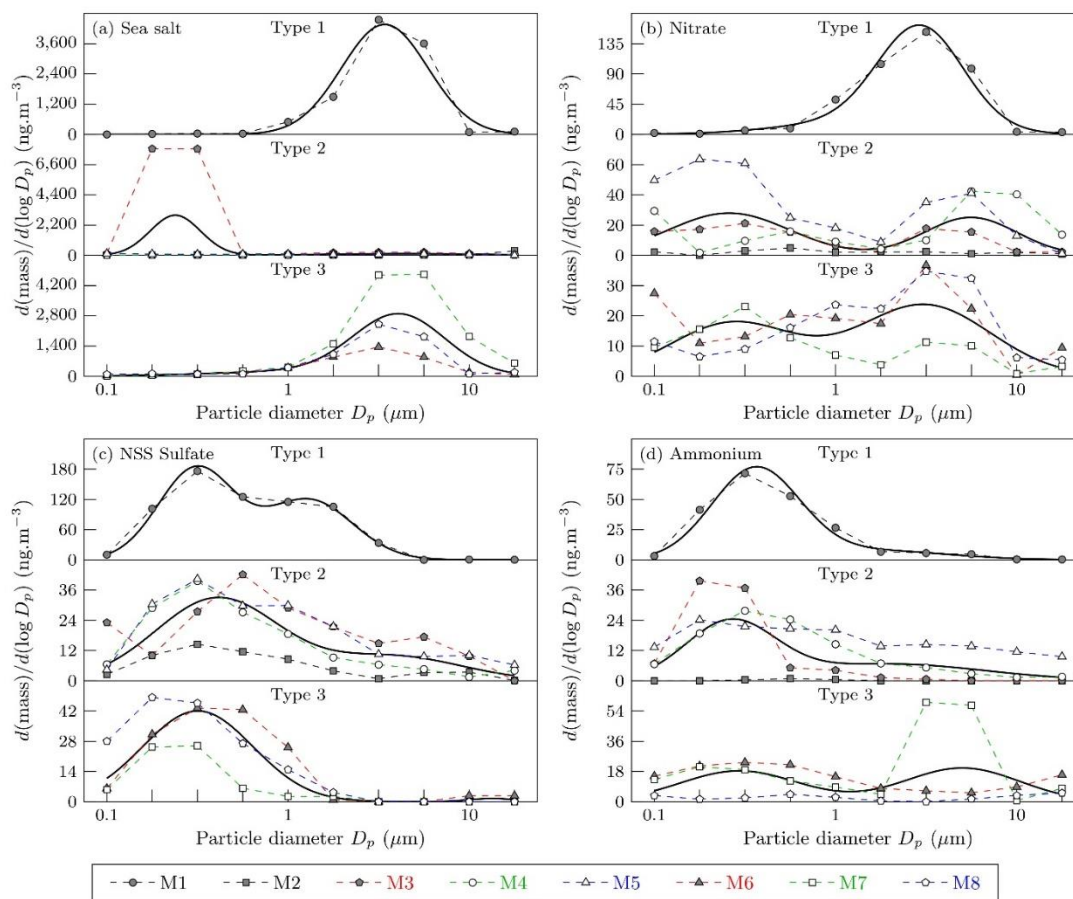


Figure 4.4 Mass-Size distribution of the inorganic species, (a) Sea-salt, (b) Nitrate, (c) NSS Sulfate, (d) Ammonium.

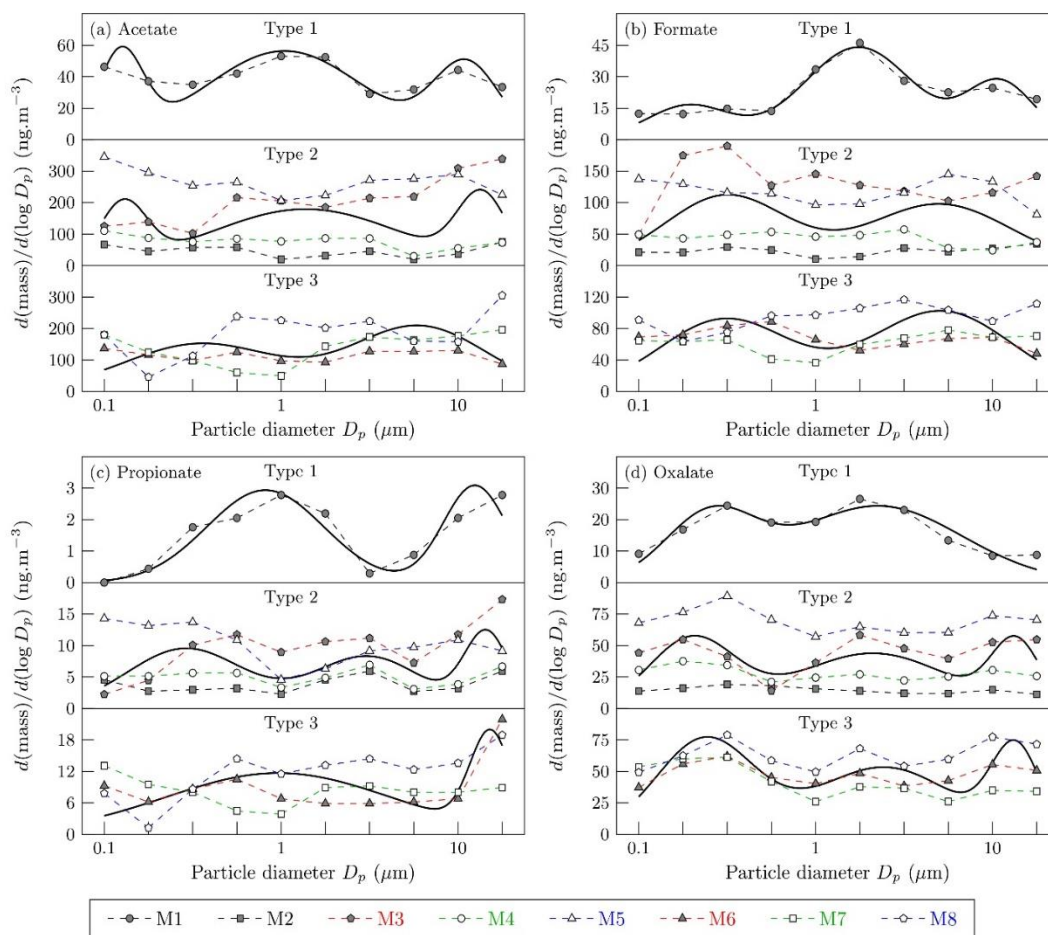


Figure 4.5 Mass-Size distribution of the organic species, (a) Acetate, (b) Formate, (c) Propionate, (d) Oxalate.

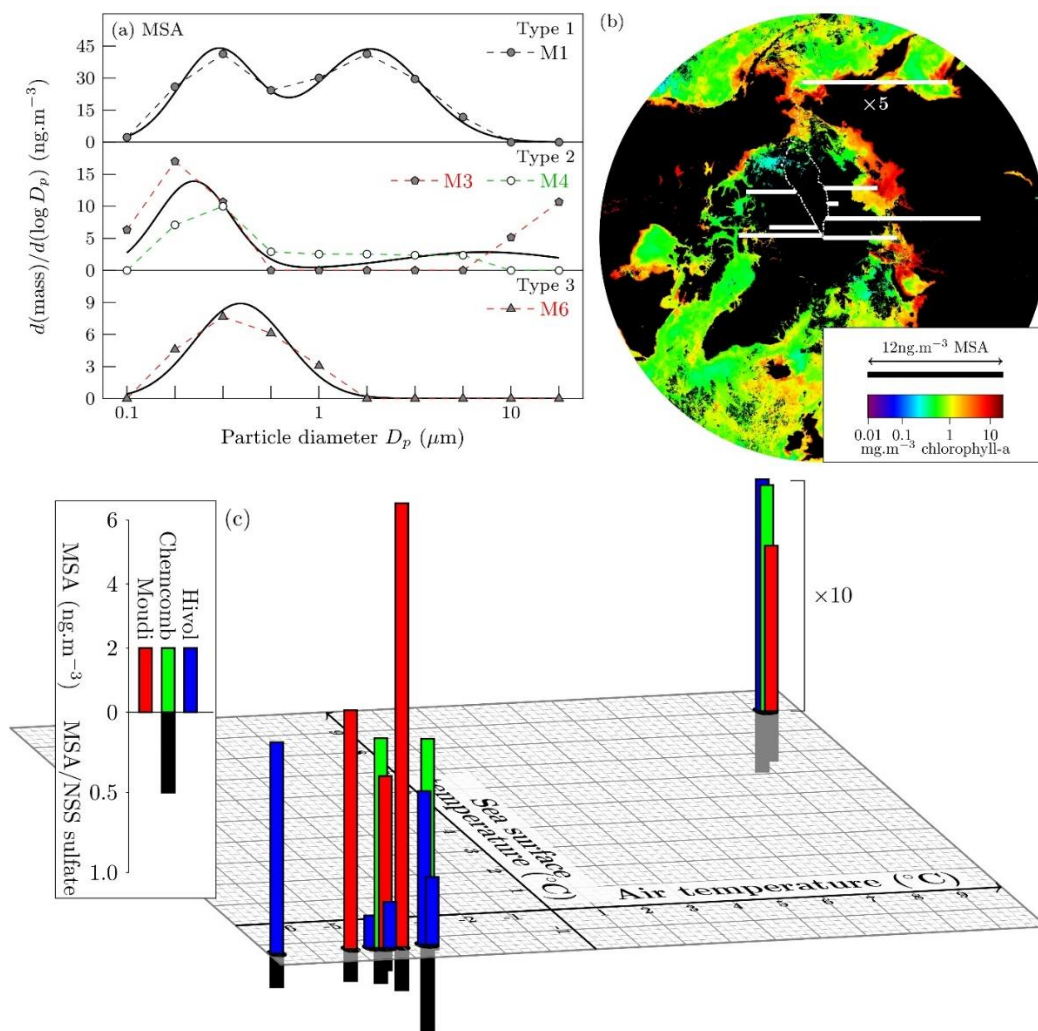


Figure 4.6 MSA over Arctic Ocean, (a) Mass-size distribution of MSA, (b) Spatial distribution of MSA concentration along the ship's route and its relationship with chlorophyll-a (Chlorophyll-a data obtained from https://oceancolor.gsfc.nasa.gov/cms/atbd/chlor_a), (c) MSA concentration ($\text{ng}\cdot\text{m}^{-3}$) and MSA/NSS Sulfate molar ratio and their relationship with sea surface temperature ($^{\circ}\text{C}$) and air temperature ($^{\circ}\text{C}$).

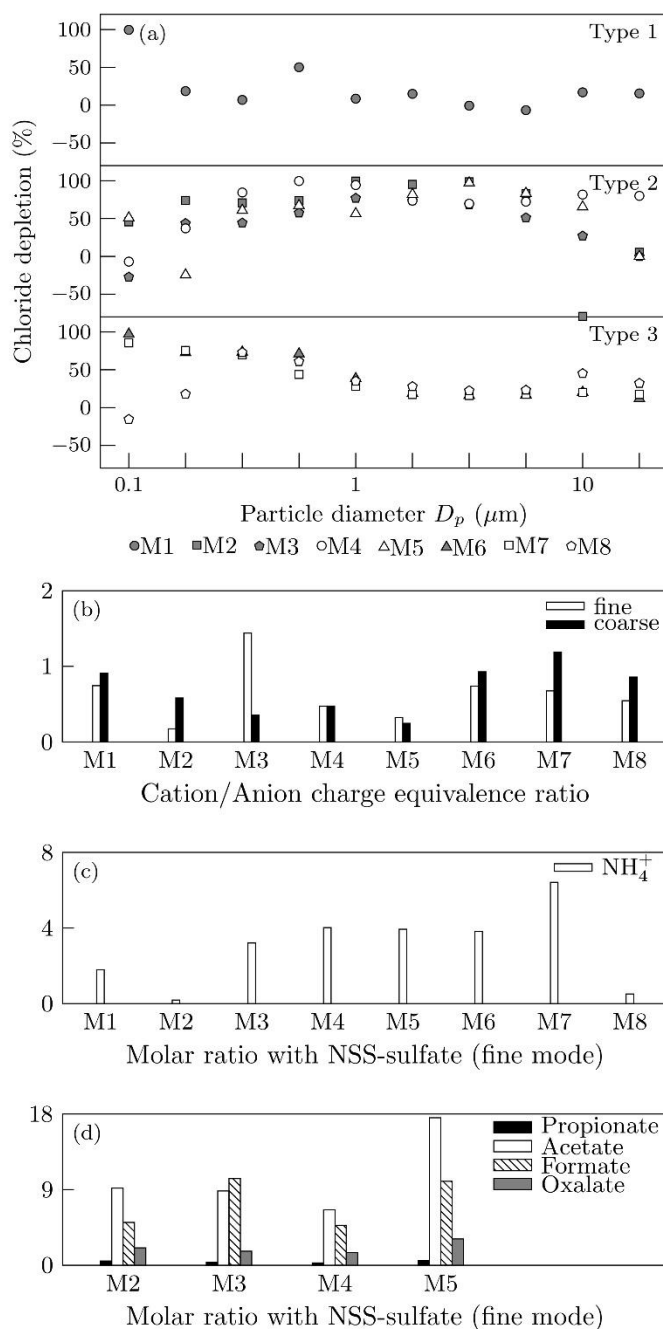


Figure 4.7 The general chemical characteristics of the Arctic aerosols: (a) The chloride depletion, (b) Cation/ Anion charge equivalence ratio, (c) Molar ratio of ammonium and NSS-sulfate in fine mode, (d) Molar ratio of the organics with NSS-sulfate in fine mode (specifically over the high Arctic Ocean).

5 Significant modification of sea-spray aerosols in the Arctic summer atmosphere

5.1 Abstract:

Significant calcium enrichment was observed in bulk and size segregated Arctic summer aerosols. The calcium enrichment was dominated in fine mode aerosols. Potassium was slightly enriched and showed the similar trend of fine mode preference in enrichment. No enrichment was observed for magnesium. Preferential binding with surface active organics and calcareous debris from marine organisms may have contributed to the excess calcium in the aerosol. In addition, a new mechanism of atmospheric processing and multiple evaporation condensation cycles of aerosols has been discussed as a possible source of fine mode calcium enrichment. With the application of ISORROPIA-II thermodynamic model, the modification in hygroscopic growth factor of calcium enriched aerosols has been calculated and the computation shows ~5% decrease in the HGF for the calcium enriched aerosols when compared to the corresponding pure sodium chloride aerosols.

5.2 Introduction.

Sea-spray aerosols (SSA) are the major components of natural aerosols in remote marine environments (Andreae & Rosenfeld, 2008). Surface wind driven whitecap formation and subsequent wave breaking is believed to be the predominant mechanism for SSA production; the massive energy supplied by surface winds results in breaking of waves and leads to production of SSA above the sea surface. The SSA mostly serve as background particles and are known to be able to scatter solar radiation. Because of their hygroscopic nature, these aerosols participate in cloud formation (Quinn et al., 2017) and influence climate's radiative property (Murphy et al., 1998; Bates et al., 2006; Srivastava & Satheesh, 2016). The SSA composition is complex and substantial seasonal and geospatial variations have been observed. The cations, sodium (Na), magnesium (Mg), calcium (Ca), potassium (K), and the anions, chloride (Cl) and sulfate (SO_4) are considered to be the major SSA components (Tang et al., 1997). In addition, organic compounds can also be present in significant amounts on the SSA (Vignati et al., 2010; Hansell & Carlson, 2014; Cochran et al., 2017).

Past studies on SSA composition at various locations had led the scientific community to believe that the ratio of the major soluble components remain unaltered in the aerosols from their bulk ratio in the sea-water (Savoie & Prospero, 1980; Keene et al., 1986), and helped researchers quantify the non sea-salt fraction of a certain component in marine aerosols. For instance, Na—being a stable component of sea-water usually present in substantial amounts—has routinely been used as a conservative tracer; its bulk sea-water ratio with other components is often applied to calculate their non-sea-salt fraction.

Growing evidence in the literature shows the presence of excess calcium in marine aerosols (Sievering et al., 2004; Leck & Svensson, 2015; Salter et al., 2016) and several mechanisms have been proposed. For instance, the contribution from “calcareous debris” of the marine organisms in the ocean and preferential binding of di-valent calcium with organic species are the leading hypothesis. In addition to these pure marine sources, anthropogenic and dust sources could also contribute to the non-sea-salt calcium on the aerosols. However, there is some disagreement in Duce and Hoffman (1976) who consider this observed calcium enrichment on SSA a result of poor experimental techniques, sea-salt fractionation, or incorrect assessment of non-sea-salt components of calcium.

To assess the impact of excess calcium on Arctic aerosols, it is necessary to understand the aerosol size distribution of calcium enrichment. Although many studies have shown the calcium enrichment on marine aerosols, few have presented its size-distribution pattern. Recently, Salter et al. (2016) and Leck and Svensson (2015) observed fine-mode accumulation of calcium enrichment over summer Arctic Ocean, but did not provide any detailed mechanism for such preference. Moreover, several of the studies on calcium enrichment (Cochran et al., 2016; Salter et al., 2016) were conducted in a laboratory setting using artificial sea-spray aerosols. Despite providing extensive information, these studies might fail to represent the real environment accurately.

The summer Arctic Ocean is isolated from the long-range transport of continental sources, thus providing a unique opportunity to investigate the calcium enrichment and its size distribution on the natural aerosols pre-dominantly of sea-spray origin. Since the marine biological activity play a crucial role in producing excess calcium on the sea-spray aerosols, we hypothesize that the recent warming induced modification in the biological

productivity of Arctic Ocean would also impact the calcium enrichment on the sea-spray aerosols. Moreover, in the summer Arctic, the aerosol concentrations—including the sea-salt components—are usually low (Mauritsen et al., 2011; Loewe et al., 2017) and this results in significantly less cloud condensation nuclei. Therefore, even a slight modification in the sea-spray aerosol composition would have a critical impact on its chemical, physical, and radiative processes.

With this goal, as a part of the US Arctic Geotraces program, we collected thirteen sets of bulk and eight sets of size-segregated aerosol samples from the Arctic Ocean in summer 2015. The major objectives are: 1) investigating the chemical modification in sea-spray aerosols from the bulk sea-water composition with respect to the major sea-water cations, 2) discussing the possible mechanisms contributing towards calcium enrichment, and 3) understanding its impact on the environment. We focused on the particle size dependence of the accumulation of excess calcium and attempted to provide a new mechanism to explain the fine mode preference of calcium enrichment. Finally, using the ISORROPIA-II thermodynamic model we investigated the modification of hygroscopic property of the calcium-enriched aerosols.

5.3 Methods.

Aerosol sampling was carried out on board the US Coast-Guard icebreaker, the USCGC Healy, from August 9, 2015 to October 10, 2015. The journey originated from and ended at Dutch Harbor, Alaska (53.9°N, 166.5°W). Eight sets of size segregated aerosol samples (M1–M8) were collected using a 11-stage MOUDI (Micro Orifice Uniform Deposit Impactor, MSP Corp.) and thirteen sets of bulk aerosol samples (C1–C15; C9 was blank, C3 was not used) using a low-volume air sampler Chemcomb (Thermo Scientific). The

cruise track, the sampling durations, and the meteorological conditions along the track have been shown in Figure 5.1.

NOAA HYSPLIT 4 back trajectory model has been used to compute 100 hour back-trajectories (in ensemble mode) from the moving ship's location every six hours. The blue background in Figure 5.1 shows the spatial frequency of these 100hr back trajectories, and indicates the sources of the air masses for our sampling locations and times. The details the back trajectory frequency calculation has been discussed in Mukherjee, Marsay, et al. (2018).

Ion chromatography (Dionex IC-2000) was applied to measure the concentrations of the water soluble cationic species (sodium, potassium, calcium, and magnesium) at the Rutgers University, Atmospheric Chemistry Laboratory; see Mukherjee, Marsay, et al. (2018) for detailed description of the laboratory procedures.

The enrichment factor for each species (EF_x) on aerosols (x= calcium, potassium, and magnesium) with respect to sodium was calculated using the following equation:

$$EF_x = \frac{(\text{concentration of species } x / \text{concentration of sodium})_{\text{aerosol}}}{(\text{concentration of species } x / \text{concentration of sodium})_{\text{sea-water}}}$$

The values for (conc. of x/conc. of sodium)_{sea-water} for each species was obtained from Savoie and Prospero (1980).

To investigate the modification in the hygroscopic growth factor for the calcium enriched aerosols and its size dependence, the HGF values were calculated using the ISORROPIA-II thermodynamic model (Fountoukis & Nenes, 2007) for the MOUDI samples.

The HGF at certain relative humidity (RH) was defined as (Lin et al., 2014),

$$\text{HGF} = \left(\frac{\text{Volume water(RH)} + \text{Volume of dry particle}}{\text{Volume of dry particle}} \right)^{1/3}$$

At a given RH, the volume of water and the volume of the total solid mass can be obtained from the ISORROPIA-II model (assuming the aerosols were internally mixed); these were added to calculate the total volume of the particle for the numerator at that RH. The total volume of the particle at 0% RH is used as the volume of the dry particle in the denominator.

A majority of models considers the chemical and physical properties of SSA are identical to sodium chloride solution to quantify the hygroscopic properties of SSA (Tang et al., 1997; Lewis & Schwartz, 2004; Zhang et al., 2009). In reality, this may be acceptable for the coarse particles but for fine particles this assumption may lead to different outcomes with respect to assessing the chemical and hygroscopic properties of SSA. Here we compared the HGF for the calcium enriched aerosols with the NaCl only system following the protocol described below.

The model was run in reverse mode and in meta-stable phase twice. In the first run, for the calcium-enriched aerosols, the concentrations of the water soluble species for each MOUDI stage were used as the input. In the second run, the NaCl-only system was considered, and only the concentrations of sodium and chloride in the aerosols were used as input. The HGF was computed for both systems at different RH values, varying from 40% to 90%.

5.4 Results.

Figure 5.2a shows the enrichment factor of the soluble cations (calcium, potassium, and magnesium) with respect to sodium in the Chemcomb bulk samples. The result shows

significant enrichment of calcium during the entire sampling period (average 7.7). Calcium enrichment was significantly high (average 11.3, $n=6$) near the Arctic polar region, which was almost entirely influenced by the polar air mass (Figure 5.1). Potassium was slightly enriched in all the deployments (average 1.7). No noticeable enrichment (except for C8) was observed for magnesium.

The calcium enrichment factor consistently decreases with increasing particle sizes in the fine mode (particle size $< 1.8\mu\text{m}$) with all the MOUDI deployments irrespective of the air mass source (Figure 5.2b). High calcium enrichment was observed in coarse particles in only two deployments, M3 and M6; these two sampling events were slightly influenced by the North American air masses and therefore, continental calcium sources might have impacted the enrichment. The mass-size distribution for potassium enrichment was entirely associated with fine particles. Similar to the bulk samples, no such enrichment was observed for magnesium.

5.5 Discussion.

In this section we discuss the possible sources of the calcium enrichment in the sea-spray aerosols; we conclude by proposing an alternative mechanism as well.

5.5.1 Sea-salt Fractionation.

Sea-salt fractionation and subsequent precipitation of mirabilite has been proposed by Hara et al. (2002) for Mg enrichment in aerosol over the Antarctic region. At low temperature, sea-salts can be fractionated during sea-ice formation and then gradually become enriched with other cations (such as Mg^{+2} , K^+ , and Ca^{+2}); the consequent sodium depletion would have resulted in a higher chloride/sodium ratio in the aerosols than their bulk sea-water ratio. However, the average chloride/sodium mass ratio for the bulk aerosol samples was

1.64, which is less than the chloride/sodium bulk sea-water ratio (1.81). Indeed, for each of the sampling events except one (C8), this ratio was less than the bulk sea-water ratio. (This observed lower chloride/sodium ratio or the absence of chloride in sea-salt samples is a common feature of marine aerosols reflecting chloride depletion.) For the exceptional event C8, the other cations, including Mg^{+2} , were substantially enriched suggesting the occurrence of sea-salt fractionation. But for the other sampling events, the observed low chloride/sodium mass ratio suggests that sea-salt fractionation might not have occurred and did not play a significant role in calcium enrichment. Furthermore, sea-salt fractionation occurs during sea-ice formation which requires extremely low sea-surface temperature, and therefore, happens mostly in the winter and early spring impacting only the winter aerosols (Richardson, 1976; Perovich & Richter-Menge, 1994; Jourdain & Legrand, 2002; Rhodes et al., 2017); hence the calcium enrichment in our summer Arctic aerosol samples cannot be entirely explained by this mechanism.

5.5.2 Dust.

Calcium containing aeolian dust and the anthropogenic combustion sources can be a possible source for the non-sea-salt fraction of calcium (Xhoffer et al., 1991). The bulk samples, which have shown the maximum enrichment in calcium, were influenced entirely by polar air (Figure 5.1 and 5.2), suggesting no direct influence of long-range air-sources for the observed calcium enrichment. Moreover, recent model studies show that the local dust sources at the Arctic peak during autumn and spring (Groot Zwaaftink et al., 2016), and not during our sampling period.

Nevertheless, aeolian dust sources can indirectly affect calcium enrichment via the following novel mechanism. Long range transport during winter can deposit and store high

calcium containing dust in the ice over the Arctic region. In the following summer, calcium enriched aerosols can be formed by the wind blowing over the melting ice. This hypothesis is supported by calcium enrichment observed in the three melt pond samples collected during the same expedition.

5.5.3 Preferential Binding.

In a laboratory setting, Cochran et al. (2016) observed the enhancement of both surface active organic compounds (linear carboxylates) and calcium in aerosols originating from bubble-bursting. Among the positively charged counter ions for the organic anionic species present in sea water, calcium shows the highest affinity towards such surface active carboxylate components (Verdugo, 2012; Adams & Allen, 2013; Shaloski et al., 2015); and this preferential binding of calcium might have caused the observed calcium enrichment in the Arctic aerosols. High abundance of mono- and di-carboxylates were detected near the polar region which partially support this hypothesis.

However, in a laboratory setting, Salter et al. (2016) did not observe any influence of organic materials on calcium enrichment in sea-spray aerosols originating from artificial and natural sea-water.

5.5.4 Coccoliths.

The excess calcium in aerosols can also originate from calcium-containing fragments continuously emitting from coccolithophore species in the ocean (Sievering et al., 2004). Coccolithophores are the single-celled phytoplanktons that produce calcium carbonate scales (coccoliths), which they discard during their growth and as a defense against predators. Laboratory studies have found that the coccolithophore *Emiliana huxleyi* was more sensitive towards sea-surface temperature alteration than ocean acidification (Winter

et al., 2013). Recent results found evidences of enhanced production of coccolithophores, especially *Emiliana huxleyi*, in the high Arctic and linked this phenomenon to sea-ice melting, intrusion of warm water in the polar ocean, ocean stratification due to global warming, and alteration in ocean acidification (Napp & Hunt, 2001; Hegseth & Sundfjord, 2008; Charalampopoulou et al., 2011). These suggest that the recent Arctic amplification might have a critical impact on the enhanced production of the coccolithophores and consequently on the excess calcium in Arctic aerosols. Indeed, this was the explanation proposed by Andreae et al. (1986) for the excess calcium observed on the coarse particles by Maenhaut et al. (1983).

Although we observed calcium enrichment predominantly in the fine mode, occasional coarse mode calcium enrichment was also observed (associated with M3 and M6). The CaCO_3 -containing planktonic debris emitted from the coccolithophores concentrate at the ocean surface microlayer and can be transmitted into the air both via large jet mode and small film mode bubble bursting (producing coarse particles and fine particles, respectively). However, in our expedition, sea-salt particles were highly concentrated in coarse mode, which suggests that large jet mode was the dominant form of bubble bursting. Therefore, coccolithophores are a possible explanation for the observed coarse mode calcium enrichment in our study.

5.5.5 Atmospheric Processing and Multiple Evaporation-Condensation Cycle.

Finally, in addition to the above mechanisms, we would like to propose the following new mechanism which explains the fine mode calcium enrichment observed in our study.

Due to its alkaline property, the calcium carbonate in the fresh sea-spray aerosols, originated from the solid calcite emitted by the planktonic organisms, reacts with the acidic

atmospheric gaseous components, such as SO₂, oxalic acid, etc. Many of the calcium-containing reaction end-products (such as calcium sulfate and calcium oxalate) remain insoluble in the aqueous layer of the aerosols (Mochida et al., 2003; Sullivan & Prather, 2007; Sullivan et al., 2009; Gierlus et al., 2012; Drozd et al., 2014). Typical aerosols undergo multiple evaporation-condensation cycles in their lifetime (Pruppacher & Jaenicke, 1995). The insoluble residue left after each such evaporation cycle therefore becomes increasingly enriched in calcium, and decreasingly favorable for further condensation, and eventually accumulates in fine mode (see Figure 5.3).

Our hypothesis is supported by the size distribution of calcium enrichment (Figure 5.2b) which shows higher enrichment in fine mode. To further test our hypothesis, we calculated the correlations of sulfate and oxalate concentrations with calcium concentrations and found significant correlation (0.65 and 0.69, respectively at 95% confidence level). Moreover, Hoornaert et al. (1996) observed large concentrations of calcium sulfate on the North Sea aerosols, suggesting a high possibility of interaction between gaseous SO₂ of calcium containing particles. However, our hypothesis—being based on limited amount of data over the Arctic—is somewhat speculative; we need significant further effort, both in laboratory and in field studies, to explore this mechanism in detail.

5.6 Environmental Significance.

Deviation from the bulk sea water ratio and aerosol enrichment of calcium have been observed in several studies over the Arctic Ocean. Therefore, the observed calcium enrichment in our study is not a one-time event, but rather is a part of a regular pattern. Given this consistent trend of calcium enrichment in Arctic aerosols—possibly a

consequence of amplified warming—it is of extreme importance to discuss its possible environmental impacts.

The alkaline CaCO_3 provides an ideal surface on the aerosols for the uptake of many atmospheric gases, such as nitric acid, hydrochloric acid, and the carboxylic acids, and their various chemical reactions (Mochida et al., 2003; Matsuki et al., 2005; Gierlus et al., 2012). Indeed, uptake of carboxylic acids by the calcium carbonate particles often acts as the major sink of these species.

The absorption of the atmospheric gases may result in modification of the hygroscopic nature of the original particles, and may change their cloud formation capacities. Climate models usually consider the sea-salt aerosols composed purely of sodium chloride. Since deliquescent properties of different calcium containing salts are different from those of pure NaCl, the underlying assumption in the climate models might fail to represent the accurate hygroscopicity of the calcium enriched aerosols.

Tang et al. (2015) reported that calcium, when combined with chloride, nitrate, and formate, had significantly higher hygroscopic parameter and CCN activity, compared to pure calcium carbonate; a smaller increment in CCN activity was reported for calcium sulfate and calcium acetate. On the other hand, using Raman spectroscopy, King et al. (2004) observed that calcium carbonate particles, after absorption of gaseous formic and acetic acid, did not deliquesce and therefore, may not participate in cloud formation. In a separate study, Mochida et al. (2003), proposed the formation of insoluble calcium oxalate as an explanation of oxalate enrichment observed in North Sea sea-salts; the formation of insoluble calcium oxalate can significantly enhance gaseous carboxylic acid uptake by calcium enriched aerosols, and subsequently decrease its hygroscopicity.

In our study, very little amount of nitrate was found, but significant amounts of chloride, sulfate, and oxalate were present. This suggests the possibility of the formation of hygroscopic calcium chloride and non-hygroscopic calcium mono oxalate and calcium sulfate on the Arctic aerosols. In either case, the large modification in HGF of the Arctic aerosols can be assumed; the precise modification in the overall hygroscopic property would depend on the abundance and the extent of interaction with the atmospheric acidic species.

Therefore, in order to quantify the deviation in hygroscopic growth by the excess calcium present in the Arctic aerosols, we calculated the hygroscopic growth factor as a function of aerosol particle diameter using the thermodynamic model ISORROPIA-II. The model was run in reverse mode and in metastable phase to reconstruct the aerosol concentrations; see Section 2 for details about the input variables. Except for a particle size of $0.1\mu\text{m}$, the HGF of calcium enriched aerosols was less than the corresponding NaCl-only system, by 3% for the coarse particles and 5% for the fine particles. However, at particle diameter $0.1\mu\text{m}$, the growth factor for the Arctic sea-salt aerosol increased by $\sim 3\%$ compared to NaCl only system (see Figure 5.4). This is possibly related to the low concentrations of soluble calcium and non-sea-salt sulfate at the corresponding particle sizes. Therefore for this particle size the effect of calcium on altering the hygroscopic property of sea-salt aerosols cannot be determined. These deviations from the NaCl system for the Arctic aerosols increases with increasing relative humidity. For instance, for the coarse particles, the HGF was essentially equal between the two systems at lower humidity (40%), however at higher humidity (90%), an average of 5% decrease in HGF was observed, compared to the NaCl only system.

The decreased HGF for calcium enriched aerosols might have resulted from precipitation of sparingly soluble CaSO_4 . These deviations, both in coarse mode and fine mode, are significant enough to be included in the future climate models. Computational studies using various thermodynamic models (E-AIM, ISORROPIA-II) show similar trend in HGF in calcium excess aerosols (Salter et al., 2016; Zieger et al., 2017). This is of increased importance in the Arctic summer when other sources of aerosols are limited and sea-salts constitute the major fraction of the total aerosols.

Unfortunately, we could not study the effect of organics on the hygroscopicity of the calcium-enriched sea-spray aerosols since ISORROPIA-II model does not incorporate organic components. However, several water soluble organics were found in abundance over the Arctic Ocean during this expedition. Therefore, the combined impact of these organics and the excess calcium in the aerosols should be thoroughly examined in future studies.

Acknowledgment. The authors would like to thank Christopher Marsay and William Landing for sample collection on the Arctic cruise, Shun Yu for advice during sample analysis, and X for comments on an early draft of this article. This research was supported by NSF grant 1435871.

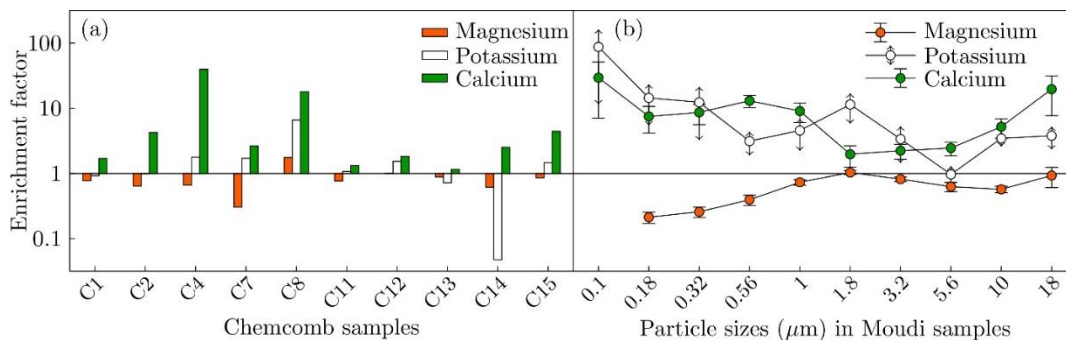


Figure 5.2 The enrichment factor of the major cations with respect of their bulk sea-water ratio with sodium: (a) bulk aerosol samples; (b) size-segregated aerosol samples.

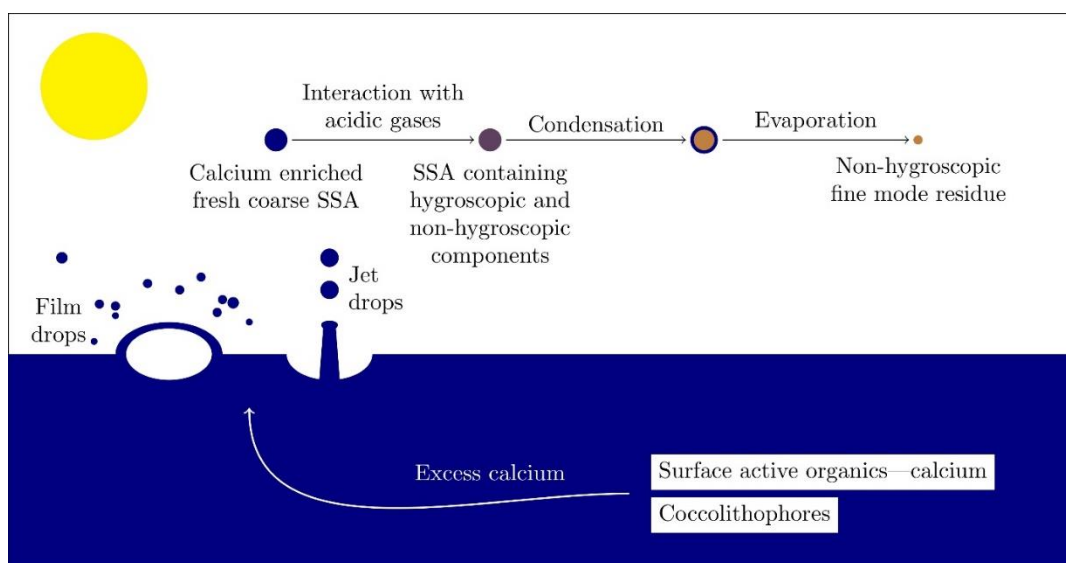


Figure 5.3 Schematic describing the effect on atmospheric processing and multiple evaporation-condensation cycle on calcium enriched aerosols to produce fine mode dominance of calcium enrichment.

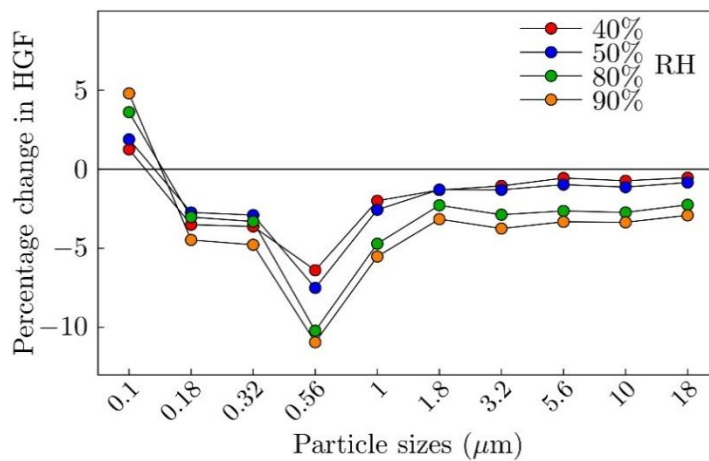


Figure 5.4 The percentage change in hygroscopic growth factor between calcium enriched aerosol system and the corresponding pure sodium chloride aerosol system at varying relative humidity.

6 Conclusion.

The major conclusions from this research, summarized from the individual chapters, are:

1. Laboratory experiments indicate that the dissolution of Fe from hematite under UV light depends significantly on the concentration of oxalate present. Overall, among the three organic ligands (formate, acetate, and oxalate) tested in the experiment, oxalate played the dominant role in accelerating Fe dissolution.

2. Long-term freezing of natural snow samples shows that the role of freeze-concentration effect on enhancing Fe solubility from natural snow is negligible. Due to freezing, the smear particles in snow compacted and clustered together and form particles with well-defined structures. This clustering process might be an effect of freeze-concentration but it failed to impose any significant impact on increasing Fe solubility.

3. Summer Arctic air is pristine and not impacted by the pollutant laden air-masses from the continental sources. For the total summer aerosol loading, the anthropogenic contribution was limited and natural sources dominated. Sea-salt was the major component by mass and distributed in the coarse mode. Non-sea-salt sulfate of mostly biogenic origin was enriched in fine particles. Among the organics measured in the study, oxalate concentration dominated and existed in both coarse and fine modes. Near the pole, both the fine and coarse mode aerosols were acidic, which suggests the formation of secondary organic aerosols via heterogeneous polymerization and hydration of several atmospheric precursors, such as isoprene, aldehydes, and carbonyls. Since the sea-salt aerosol concentration was low near the pole and the anthropogenic impact was significantly less, the water soluble organic components constituted a major fraction of Arctic aerosols at the

pole. The presence and the fine mode dominance of non-sea-salt sulfate and carboxylic acid aerosols underscore their importance in cloud formation in the Arctic region.

4. The Arctic sea-spray aerosols were significantly enriched in calcium and moderately enriched in potassium and depleted in magnesium with respect to their bulk sea-water ratios with sodium. Both the calcium and potassium enrichments were greatest in the fine particle mode. This chemical modification in SSA from the bulk sea-water chemical composition results in approximately 4–5% decrease (computed using ISORROPIA-II thermodynamic model) in the hygroscopic growth of calcium enriched aerosols compared to the corresponding pure sodium chloride aerosols; this is significant since the majority of chemical models assume aerosols to be composed of pure sodium chloride.

7 Further studies.

This research has produced many interesting new results, although several aspects needs more attention.

1. The laboratory experiment to investigate the role of organic ligands to promote Fe dissolution was conducted under 254nm UV light. Further studies need to be conducted under other UV wavelengths, such as within 315–400nm, which carries greater environmental relevance. Advanced experimental methods, such as XRD, scanning electron microscopy, FTIR techniques can be applied to gain more thorough insights on the complex formation processes. In addition, the experimental results can be compared with ambient samples. These results will significantly improve the current understanding of organic ligand induced Fe solubility.

2. The freezing experiment with natural snow to investigate the modification in Fe solubility did not produce consistent results among the six events. While the enhancement of Fe solubility could depend on the chemical characteristics of the snow, and thus vary from event to event, the small number (six) of observations was not adequate to arrive at a definitive conclusion on the occurrence of the freeze concentration effect in natural samples. In this research only two years of snow samples were collected and analyzed. We were able to perform STEM analysis on a limited number of snow and ice-melt samples. Since the concentration of Fe was low in the original snow samples, the modification of Fe due to freezing was measured in a few samples only. Detailed analysis with more such samples would significantly improve the understanding of freeze-induced Fe solubility. In addition, studying the freeze-induced modification in Fe solubility in snow samples on a temperature-controlled SEM stage would allow us to see the transformations of particle

morphology as the ice/snow melts. This approach will be applied in future studies to obtain improved knowledge of freeze-induced effect on particle morphology.

Moreover, events 1 and 2 contained ~70% of Fe in Fe_{fil} state. The reason for such high soluble Fe fraction is not completely known. Complexation of Fe with HULIS-like components could be a potential reason for such high Fe solubility. We attempted to detect the presence of HULIS-like components in snow samples and did not get any result. The method for identifying this component is still not well-developed and requires considerable effort. This is certainly an exciting project to pursue in the future.

3. The Arctic aerosols contained a significant fraction of water soluble organic components, especially near the pole. We were able to detect only a few of them. Detailed analysis to detect and quantify these organic species using gas chromatography (GCMS) would help understand the secondary organic aerosol formation mechanism. Secondary organic aerosol formation is sensitive to solar radiation. Multiple studies need to be conducted in the future to collect additional Arctic samples to specifically study the photochemical processes occurring at the onset of Arctic summer.

4. The modification in sea-spray aerosols in the form of calcium enrichment was detected in this research. Elemental analysis of individual aerosol particles could substantially help us to understand the precise composition of calcium enriched sea-spray aerosols. Potassium was slightly enriched and magnesium was depleted. The reasons for these two patterns were not understood completely.

8 References:

- Adams, E. M., & Allen, H. C. (2013). Palmitic acid on salt subphases and in mixed monolayers of cerebrosides: application to atmospheric aerosol chemistry. *Atmosphere*, *4*(4), 315-336.
- Adams, P. J., Seinfeld, J. H., & Koch, D. M. (1999). Global concentrations of tropospheric sulfate, nitrate, and ammonium aerosol simulated in a general circulation model. *Journal of Geophysical Research: Atmospheres*, *104*(D11), 13791-13823.
- Andreae, M., & Rosenfeld, D. (2008). Aerosol–cloud–precipitation interactions. Part 1. The nature and sources of cloud-active aerosols. *Earth-Science Reviews*, *89*(1), 13-41.
- Andreae, M., Talbot, R., Andreae, T., & Harriss, R. (1988). Formic and acetic acid over the central Amazon region, Brazil: 1. Dry season. *Journal of Geophysical Research: Atmospheres*, *93*(D2), 1616-1624.
- Andreae, M. O., Charlson, R. J., Bruynseels, F., Storms, H., Van Grieken, R., & Maenhaut, W. (1986). Internal mixture of sea salt, silicates, and excess sulfate in marine aerosols. *science*, *232*(4758), 1620-1623.
- Aristarain, A. J., Delmas, R. J., & Briat, M. (1982). Snow chemistry on James Ross Island (Antarctic Peninsula). *Journal of Geophysical Research: Oceans*, *87*(C13), 11004-11012.
- Atkinson, R. (1990). Gas-phase tropospheric chemistry of organic compounds: a review. *Atmospheric Environment. Part A. General Topics*, *24*(1), 1-41.
- Atkinson, R., & Carter, W. P. (1984). Kinetics and mechanisms of the gas-phase reactions of ozone with organic compounds under atmospheric conditions. *Chemical Reviews*, *84*(5), 437-470.
- Ayers, G., Gillett, R., & Gras, J. (1980). On the vapor pressure of sulfuric acid. *Geophysical research letters*, *7*(6), 433-436.
- Ayers, G., Ivey, J., & Gillett, R. (1991). Coherence between seasonal cycles of dimethyl sulphide, methanesulphonate and sulphate in marine air. *Nature*, *349*(6308), 404-406.
- Baboukas, E., Kanakidou, M., & Mihalopoulos, N. (2000). Carboxylic acids in gas and particulate phase above the Atlantic Ocean. *Journal of Geophysical Research: Atmospheres*, *105*(D11), 14459-14471.
- Banwart, S., Davies, S., & Stumm, W. (1989). The role of oxalate in accelerating the reductive dissolution of hematite (α -Fe₂O₃) by ascorbate. *Colloids and Surfaces*, *39*(2), 303-309.
- Barbaro, E., Padoan, S., Kirchgeorg, T., Zangrando, R., Toscano, G., Barbante, C., & Gambaro, A. (2017). Particle size distribution of inorganic and organic ions in coastal and inland Antarctic aerosol. *Environmental Science and Pollution Research*, *24*(3), 2724-2733.
- Barrie, L., Bottenheim, J., Schnell, R., Crutzen, P., & Rasmussen, R. (1988a). Ozone destruction and photochemical reactions at polar sunrise in the lower Arctic atmosphere. *Nature*, *334*(6178), 138-141.
- Barrie, L., Bottenheim, J., Schnell, R., Crutzen, P., & Rasmussen, R. (1988b). Ozone destruction and photochemical reactions at polar sunrise in the lower Arctic atmosphere. *Nature*, *334*(6178), 138.
- Barrie, L., & Hoff, R. (1985). Five years of air chemistry observations in the Canadian Arctic. *Atmospheric Environment (1967)*, *19*(12), 1995-2010.
- Bates, T., Anderson, T., Baynard, T., Bond, T., Boucher, O., Carmichael, G., Clarke, A., Erlick, C., Guo, H., & Horowitz, L. (2006). Aerosol direct radiative effects over the northwest Atlantic, northwest Pacific, and North Indian Oceans: estimates based on in-situ chemical and optical measurements and chemical transport modeling. *Atmospheric Chemistry and Physics*, *6*(6), 1657-1732.

- Bates, T. S., Calhoun, J. A., & Quinn, P. K. (1992). Variations in the methanesulfonate to sulfate molar ratio in submicrometer marine aerosol particles over the south Pacific Ocean. *Journal of Geophysical Research: Atmospheres*, *97*(D9), 9859-9865. doi:10.1029/92JD00411
- Bates, T. S., Quinn, P. K., Coffman, D. J., Johnson, J. E., Miller, T. L., Covert, D. S., Wiedensohler, A., Leinert, S., Nowak, A., & Neusüss, C. (2001). Regional physical and chemical properties of the marine boundary layer aerosol across the Atlantic during Aerosols99: An overview. *Journal of Geophysical Research: Atmospheres*, *106*(D18), 20767-20782.
- Behra, P., & Sigg, L. (1990). Evidence for redox cycling of iron in atmospheric water droplets. *Nature*, *344*(6265), 419-421.
- Betterton, E. A., & Anderson, D. J. (2001). Autoxidation of N (III), S (IV), and other species in frozen solution—A possible pathway for enhanced chemical transformation in freezing systems. *Journal of Atmospheric Chemistry*, *40*(2), 171-189.
- Bigg, E. K., & Leck, C. (2008). The composition of fragments of bubbles bursting at the ocean surface. *Journal of Geophysical Research: Atmospheres*, *113*(D11).
- Bigg, E. K., Leck, C., & Tranvik, L. (2004). Particulates of the surface microlayer of open water in the central Arctic Ocean in summer. *Marine Chemistry*, *91*(1), 131-141.
- Binran, K. (1984). The Chemical Society of Japan. *Maruzen, Tokyo*, 11-356.
- Bintanja, R., Van Oldenborgh, G., Drijfhout, S., Wouters, B., & Katsman, C. (2013). Important role for ocean warming and increased ice-shelf melt in Antarctic sea-ice expansion. *Nature Geoscience*, *6*(5), 376-379.
- Bonsang, B., Kanakidou, M., Lambert, G., & Monfray, P. (1988). The marine source of C 2-C 6 aliphatic hydrocarbons. *Journal of Atmospheric Chemistry*, *6*(1), 3-20.
- Bouwman, A., Lee, D., Asman, W., Dentener, F., Van Der Hoek, K., & Olivier, J. (1997). A global high-resolution emission inventory for ammonia. *Global Biogeochemical Cycles*, *11*(4), 561-587.
- Boyle, E. A., Bergquist, B. A., Kayser, R. A., & Mahowald, N. (2005). Iron, manganese, and lead at Hawaii Ocean Time-series station ALOHA: Temporal variability and an intermediate water hydrothermal plume. *Geochimica et Cosmochimica Acta*, *69*(4), 933-952.
- Breider, T. J., Mickley, L. J., Jacob, D. J., Ge, C., Wang, J., Payer Sulprizio, M., Croft, B., Ridley, D. A., McConnell, J. R., & Sharma, S. (2017). Multidecadal trends in aerosol radiative forcing over the Arctic: Contribution of changes in anthropogenic aerosol to Arctic warming since 1980. *Journal of Geophysical Research: Atmospheres*, *122*(6), 3573-3594.
- Bronshteyn, V. L., & Chernov, A. A. (1991). Freezing potentials arising on solidification of dilute aqueous solutions of electrolytes. *Journal of crystal growth*, *112*(1), 129-145.
- Buck, C. S., Landing, W. M., Resing, J. A., & Lebon, G. T. (2006). Aerosol iron and aluminum solubility in the northwest Pacific Ocean: Results from the 2002 IOC cruise. *Geochemistry, Geophysics, Geosystems*, *7*(4).
- Buck, C. S., Landing, W. M., Resing, J. A., & Measures, C. I. (2010). The solubility and deposition of aerosol Fe and other trace elements in the north atlantic ocean: observations from the A16N CLIVAR/CO 2 repeat hydrography section. *Marine Chemistry*, *120*(1), 57-70.
- Cadle, S. H., & Groblicki, P. J. (1982). An evaluation of methods for the determination of organic and elemental carbon in particulate samples *Particulate Carbon* (pp. 89-109): Springer.
- Chameides, W., & Davis, D. (1983). Aqueous-phase source of formic acid in clouds. *Nature*, *304*(5925), 427-429.
- Chameides, W., & Stelson, A. (1992). Aqueous-phase chemical processes in deliquescent sea-salt aerosols: A mechanism that couples the atmospheric cycles of S and sea salt. *Journal of Geophysical Research: Atmospheres*, *97*(D18), 20565-20580.

- Chang, R.-W., Leck, C., Graus, M., Müller, M., Paatero, J., Burkhart, J. F., Stohl, A., Orr, L., Hayden, K., & Li, S.-M. (2011). Aerosol composition and sources in the central Arctic Ocean during ASCOS.
- Charalampopoulou, A., Poulton, A. J., Tyrrell, T., & Lucas, M. I. (2011). Irradiance and pH affect coccolithophore community composition on a transect between the North Sea and the Arctic Ocean. *Marine Ecology Progress Series*, 431, 25-43.
- Chebji, A., & Carlier, P. (1996). Carboxylic acids in the troposphere, occurrence, sources, and sinks: A review. *Atmospheric Environment*, 30(24), 4233-4249.
- Chen, H., & Grassian, V. H. (2013). Iron dissolution of dust source materials during simulated acidic processing: the effect of sulfuric, acetic, and oxalic acids. *Environmental science & technology*, 47(18), 10312-10321.
- Chen, Y., & Siefert, R. L. (2004). Seasonal and spatial distributions and dry deposition fluxes of atmospheric total and labile iron over the tropical and subtropical North Atlantic Ocean. *Journal of Geophysical Research: Atmospheres*, 109(D9).
- Chen, Y., Tovar-Sanchez, A., Siefert, R. L., Sañudo-Wilhelmy, S. A., & Zhuang, G. (2011). Luxury uptake of aerosol iron by *Trichodesmium* in the western tropical North Atlantic. *Geophysical research letters*, 38(18).
- Christopher, S. A., Chou, J., Zhang, J., Li, X., Berendes, T., & Welch, R. M. (2000). Shortwave direct radiative forcing of biomass burning aerosols estimated using VIRS and CERES data. *Geophysical research letters*, 27(15), 2197-2200.
- Clarke, A. D., & Noone, K. J. (1985). Soot in the Arctic snowpack: A cause for perturbations in radiative transfer. *Atmospheric Environment (1967)*, 19(12), 2045-2053.
- Cochran, R. E., Jayarathne, T., Stone, E. A., & Grassian, V. H. (2016). Selectivity across the interface: A test of surface activity in the composition of organic-enriched aerosols from bubble bursting. *J. Phys. Chem. Lett*, 7(9), 1692-1696.
- Cochran, R. E., Laskina, O., Trueblood, J. V., Estillore, A. D., Morris, H. S., Jayarathne, T., Sultana, C. M., Lee, C., Lin, P., & Laskin, J. (2017). Molecular Diversity of Sea Spray Aerosol Particles: Impact of Ocean Biology on Particle Composition and Hygroscopicity. *Chem*, 2(5), 655-667.
- Colbeck, S. (1982). An overview of seasonal snow metamorphism. *Reviews of Geophysics*, 20(1), 45-61.
- Colbeck, S. (1983). Snow particle morphology in the seasonal snow cover. *Bulletin of the American Meteorological Society*, 64(6), 602-609.
- Crawford, I., Möhler, O., Schnaiter, M., Saathoff, H., Liu, D., McMeeking, G., Linke, C., Flynn, M., Bower, K., & Connolly, P. (2011). Studies of propane flame soot acting as heterogeneous ice nuclei in conjunction with single particle soot photometer measurements. *Atmospheric Chemistry and Physics*, 11(18), 9549-9561.
- Dasch, J. M., & Wolff, G. T. (1989). Trace inorganic species in precipitation and their potential use in source apportionment studies. *Water, Air, & Soil Pollution*, 43(3), 401-412.
- Dey, S., Goswami, S., & Ghosh, U. C. (2004). Hydrous ferric oxide (HFO)—a scavenger for fluoride from contaminated water. *Water, Air, and Soil Pollution*, 158(1), 311-323.
- Dodgen, H., & Rollefson, G. (1949). The complex ions formed by iron and thorium with fluoride in acid solution. *Journal of the American Chemical Society*, 71(8), 2600-2607.
- Domine, F., Taillandier, A., Houdier, S., Parrenin, F., Simpson, W. R., & Douglas, T. A. (2006). Interactions between snow metamorphism and climate: Physical and chemical aspects. *SPECIAL PUBLICATION-ROYAL SOCIETY OF CHEMISTRY*, 311, 27.

- Drozd, G., Woo, J., Häkkinen, S., Nenes, A., & McNeill, V. F. (2014). Inorganic salts interact with oxalic acid in submicron particles to form material with low hygroscopicity and volatility. *Atmospheric Chemistry and Physics*, 14(10), 5205-5215.
- Du, H., Kong, L., Cheng, T., Chen, J., Yang, X., Zhang, R., Han, Z., Yan, Z., & Ma, Y. (2010). Insights into ammonium particle-to-gas conversion: non-sulfate ammonium coupling with nitrate and chloride. *Aerosol Air Qual. Res*, 10(6), 589-595.
- Duce, R. A., & Hoffman, E. J. (1976). Chemical fractionation at the air/sea interface. *Annual Review of Earth and Planetary Sciences*, 4(1), 187-228.
- Duce, R. A., & Tindale, N. W. (1991). Atmospheric transport of iron and its deposition in the ocean. *Limnology and oceanography*, 36(8), 1715-1726.
- Duncan, J. L., Schindler, L. R., & Roberts, J. T. (1998). A new sulfate-mediated reaction: Conversion of acetone to trimethylbenzene in the presence of liquid sulfuric acid. *Geophysical research letters*, 25(5), 631-634.
- Edwards, R., & Sedwick, P. (2001). Iron in East Antarctic snow: Implications for atmospheric iron deposition and algal production in Antarctic waters. *Geophysical research letters*, 28(20), 3907-3910.
- Erel, Y., Pehkonen, S. O., & Hoffmann, M. R. (1993). Redox chemistry of iron in fog and stratus clouds. *Journal of Geophysical Research: Atmospheres*, 98(D10), 18423-18434.
- Falkowski, P. G. (1997). Evolution of the nitrogen cycle and its influence on the biological sequestration of CO₂ in the ocean. *Nature*, 387(6630), 272.
- Fenn, R. W., Gerber, H. E., & Wasshausen, D. (1963). Measurements of the sulphur and ammonium component of the arctic aerosol of the Greenland icecap. *Journal of the Atmospheric Sciences*, 20(5), 466-468.
- Ferek, R. J., Hobbs, P. V., Radke, L. F., Herring, J. A., Sturges, W. T., & Cota, G. F. (1995). Dimethyl sulfide in the arctic atmosphere. *Journal of Geophysical Research: Atmospheres*, 100(D12), 26093-26104.
- Ferrari, C. P., Padova, C., Fain, X., Gauchard, P.-A., Dommergue, A., Aspino, K., Berg, T., Cairns, W., Barbante, C., & Cescon, P. (2008). Atmospheric mercury depletion event study in Ny-Alesund (Svalbard) in spring 2005. Deposition and transformation of Hg in surface snow during springtime. *Science of the total Environment*, 397(1), 167-177.
- Finden, D., Tipping, E., Jaworski, G., & Reynolds, C. (1984). Light-induced reduction of natural iron (III) oxide and its relevance to phytoplankton. *Nature*, 309(5971), 783-784.
- Finlayson-Pitts, B. J., & Pitts Jr, J. N. (1999). *Chemistry of the upper and lower atmosphere: theory, experiments, and applications*: Academic press.
- Foster, K. L., Plastringe, R. A., Bottenheim, J. W., Shepson, P. B., Finlayson-Pitts, B. J., & Spicer, C. W. (2001). The role of Br₂ and BrCl in surface ozone destruction at polar sunrise. *science*, 291(5503), 471-474.
- Fountoukis, C., & Nenes, A. (2007). ISORROPIA II: a computationally efficient thermodynamic equilibrium model for K⁺-Ca²⁺-Mg²⁺-NH₄⁺-Na⁺-SO₄²⁻-NO₃⁻-Cl⁻-H₂O aerosols. *Atmospheric Chemistry and Physics*, 7(17), 4639-4659.
- Franz, T. P., & Eisenreich, S. J. (1998). Snow scavenging of polychlorinated biphenyls and polycyclic aromatic hydrocarbons in Minnesota. *Environmental science & technology*, 32(12), 1771-1778.
- Fridlind, A., & Jacobson, M. (2000). A study of gas-aerosol equilibrium and aerosol pH in the remote marine boundary layer during the First Aerosol Characterization Experiment (ACE 1). *Journal of Geophysical Research: Atmospheres*, 105(D13), 17325-17340.

- Fu, P., Kawamura, K., Chen, J., & Barrie, L. A. (2009). Isoprene, monoterpene, and sesquiterpene oxidation products in the high Arctic aerosols during late winter to early summer. *Environmental science & technology*, 43(11), 4022-4028.
- Fung, I. Y., Meyn, S. K., Tegen, I., Doney, S. C., John, J. G., & Bishop, J. K. (2000). Iron supply and demand in the upper ocean. *Global Biogeochemical Cycles*, 14(1), 281-295.
- Galloway, J. N., Likens, G. E., Keene, W. C., & Miller, J. M. (1982). The composition of precipitation in remote areas of the world. *Journal of Geophysical Research: Oceans*, 87(C11), 8771-8786.
- Galloway, J. N., Schlesinger, W. H., Levy, H., Michaels, A., & Schnoor, J. L. (1995). Nitrogen fixation: Anthropogenic enhancement-environmental response. *Global Biogeochemical Cycles*, 9(2), 235-252.
- Gao, Y., Kaufman, Y., Tanre, D., Kolber, D., & Falkowski, P. (2001). Seasonal distributions of aeolian iron fluxes to the global ocean. *Geophysical research letters*, 28(1), 29-32.
- Gao, Y., Xu, G., Zhan, J., Zhang, J., Li, W., Lin, Q., Chen, L., & Lin, H. (2013). Spatial and particle size distributions of atmospheric dissolvable iron in aerosols and its input to the Southern Ocean and coastal East Antarctica. *Journal of Geophysical Research: Atmospheres*, 118(22).
- Ghahremaninezhad, R., Norman, A.-L., Abbatt, J. P., Lévassieur, M., & Thomas, J. L. (2016). Biogenic, anthropogenic and sea salt sulfate size-segregated aerosols in the Arctic summer. *Atmospheric Chemistry and Physics*, 16(8), 5191-5202.
- Ghatak, D., & Miller, J. (2013). Implications for Arctic amplification of changes in the strength of the water vapor feedback. *Journal of Geophysical Research: Atmospheres*, 118(14), 7569-7578.
- Gierlus, K. M., Laskina, O., Abernathy, T. L., & Grassian, V. H. (2012). Laboratory study of the effect of oxalic acid on the cloud condensation nuclei activity of mineral dust aerosol. *Atmospheric Environment*, 46, 125-130.
- Gondwe, M., Krol, M., Gieskes, W., Klaassen, W., & De Baar, H. (2003). The contribution of ocean-leaving DMS to the global atmospheric burdens of DMS, MSA, SO₂, and NSS SO₄⁼. *Global Biogeochemical Cycles*, 17(2).
- Gondwe, M., Krol, M., Klaassen, W., Gieskes, W., & de Baar, H. (2004). Comparison of modeled versus measured MSA: nss SO₄⁼ ratios: A global analysis. *Global Biogeochemical Cycles*, 18(2).
- Gorbunov, B., Baklanov, A., Kakutkina, N., Windsor, H., & Toumi, R. (2001). Ice nucleation on soot particles. *Journal of Aerosol Science*, 32(2), 199-215.
- Graedel, T., Mandich, M., & Weschler, C. (1986). Kinetic model studies of atmospheric droplet chemistry: 2. Homogeneous transition metal chemistry in raindrops. *Journal of Geophysical Research: Atmospheres*, 91(D4), 5205-5221.
- Graedel, T., Weschler, C., & Mandich, M. (1985). Influence of transition metal complexes on atmospheric droplet acidity. *Nature*, 317(6034), 240-242.
- Grannas, A. M., Bausch, A. R., & Mahanna, K. M. (2007). Enhanced aqueous photochemical reaction rates after freezing. *The Journal of Physical Chemistry A*, 111(43), 11043-11049.
- Graversen, R. G. (2006). Do changes in the midlatitude circulation have any impact on the Arctic surface air temperature trend? *Journal of Climate*, 19(20), 5422-5438.
- Graversen, R. G., Mauritsen, T., Tjernström, M., Källén, E., & Svensson, G. (2008). Vertical structure of recent Arctic warming. *Nature*, 451(7174), 53.
- Graversen, R. G., & Wang, M. (2009). Polar amplification in a coupled climate model with locked albedo. *Climate Dynamics*, 33(5), 629-643.

- Groot Zwaaftink, C., Grythe, H., Skov, H., & Stohl, A. (2016). Substantial contribution of northern high-latitude sources to mineral dust in the Arctic. *Journal of Geophysical Research: Atmospheres*, *121*(22).
- Grotti, M., Soggia, F., Ianni, C., & Frache, R. (2005). Trace metals distributions in coastal sea ice of Terra Nova Bay, Ross Sea, Antarctica. *Antarctic Science*, *17*(2), 289-300.
- Gunz, D. W., & Hoffmann, M. R. (1990). Field investigations on the snow chemistry in central and southern California—I. Inorganic ions and hydrogen peroxide. *Atmospheric Environment. Part A. General Topics*, *24*(7), 1661-1671.
- Hallett, J. (1961). The growth of ice crystals on freshly cleaved covellite surfaces. *Philosophical Magazine*, *6*(69), 1073-1087.
- Hansell, D. A., & Carlson, C. A. (2014). *Biogeochemistry of marine dissolved organic matter*: Academic Press.
- Hara, K., Osada, K., Kido, M., Hayashi, M., Matsunaga, K., Iwasaka, Y., Yamanouchi, T., Hashida, G., & Fukatsu, T. (2004). Chemistry of sea-salt particles and inorganic halogen species in Antarctic regions: Compositional differences between coastal and inland stations. *Journal of Geophysical Research: Atmospheres*, *109*(D20).
- Hara, K., Osada, K., Matsunaga, K., Sakai, T., Iwasaka, Y., & Furuya, K. (2002). Concentration trends and mixing states of particulate oxalate in Arctic boundary layer in winter/spring. *Journal of Geophysical Research: Atmospheres*, *107*(D19).
- Hara, K., Osada, K., Yabuki, M., & Yamanouchi, T. (2012). Seasonal variation of fractionated sea-salt particles on the Antarctic coast. *Geophysical research letters*, *39*(18).
- Hawkings, J. R., Wadham, J. L., Tranter, M., Raiswell, R., Benning, L. G., Statham, P. J., Tedstone, A., Nienow, P., Lee, K., & Telling, J. (2014). Ice sheets as a significant source of highly reactive nanoparticulate iron to the oceans. *Nature Communications*, *5*.
- Heaton, R. W., Rahn, K. A., & Lowenthal, D. H. (1990). Determination of trace elements, including regional tracers, in Rhode Island precipitation. *Atmospheric Environment. Part A. General Topics*, *24*(1), 147-153.
- Hegseth, E. N., & Sundfjord, A. (2008). Intrusion and blooming of Atlantic phytoplankton species in the high Arctic. *Journal of Marine Systems*, *74*(1), 108-119.
- Heimbürger, A., Losno, R., & Triquet, S. (2013). Solubility of iron and other trace elements over the Southern Indian Ocean. *Biogeosciences Discussions*, *10*(3).
- Heintzenberg, J., & Leck, C. (1994). Seasonal variation of the atmospheric aerosol near the top of the marine boundary layer over Spitsbergen related to the Arctic sulphur cycle. *Tellus B: Chemical and Physical Meteorology*, *46*(1), 52-67.
- Heist, R. H., Colling, K. M., & DuPuis, C. S. (1976). Homogeneous nucleation in associated vapors. I. Acetic acid. *The Journal of Chemical Physics*, *65*(12), 5147-5154.
- Helmets, E., & Schrems, O. (1995). Wet deposition of metals to the tropical North and the South Atlantic Ocean. *Atmospheric Environment*, *29*(18), 2475-2484.
- Herman, F., & Gorham, E. (1957). Total mineral material, acidity, sulphur and nitrogen in rain and snow at Kentville, Nova Scotia. *Tellus*, *9*(2), 180-183.
- Hillamo, R., Kerminen, V. M., Aurela, M., Mäkelä, T., Maenhaut, W., & Leek, C. (2001). Modal structure of chemical mass size distribution in the high Arctic aerosol. *Journal of Geophysical Research: Atmospheres*, *106*(D21), 27555-27571.
- Hobbs, P. (1968). SNOW: METAMORPHISM OF DEPOSITED SNOWS: metamorphism of deposited snow *Geomorphology* (pp. 1025-1028): Springer.
- Hofmann, H., Hoffmann, P., & Lieser, K. (1991). Transition metals in atmospheric aqueous samples, analytical determination and speciation. *Fresenius' journal of analytical chemistry*, *340*(9), 591-597.

- Hoornaert, S., Van Malderen, H., & Van Grieken, R. (1996). Gypsum and other calcium-rich aerosol particles above the North Sea. *Environmental science & technology*, 30(5), 1515-1520.
- Hoppel, W. (1987). Nucleation in the MSA-water vapor system. *Atmospheric Environment (1967)*, 21(12), 2703-2709.
- Hoque, M., Kawamura, K., Seki, O., & Hoshi, N. (2015). Spatial distributions of dicarboxylic acids, ω -oxoacids, pyruvic acid and α -dicarbonyls in the remote marine aerosols over the North Pacific. *Marine Chemistry*, 172, 1-11.
- Hsu, S. C., Liu, S. C., Kao, S. J., Jeng, W. L., Huang, Y. T., Tseng, C. M., Tsai, F., Tu, J. Y., & Yang, Y. (2007). Water-soluble species in the marine aerosol from the northern South China Sea: High chloride depletion related to air pollution. *Journal of Geophysical Research: Atmospheres*, 112(D19).
- Hu, Q.-H., Xie, Z.-Q., Wang, X.-M., Kang, H., He, Q.-F., & Zhang, P. (2013). Secondary organic aerosols over oceans via oxidation of isoprene and monoterpenes from Arctic to Antarctic. *Scientific Reports*, 3.
- Inoue, J., Liu, J., Pinto, J. O., & Curry, J. A. (2006). Intercomparison of Arctic regional climate models: Modeling clouds and radiation for SHEBA in May 1998. *Journal of Climate*, 19(17), 4167-4178.
- Jaffrezo, J. L., Davidson, C., Kuhns, H., Bergin, M., Hillamo, R., Maenhaut, W., Kahl, J., & Harris, J. (1998). Biomass burning signatures in the atmosphere of central Greenland. *Journal of Geophysical Research: Atmospheres*, 103(D23), 31067-31078.
- Jang, M., Czoschke, N. M., Lee, S., & Kamens, R. M. (2002). Heterogeneous atmospheric aerosol production by acid-catalyzed particle-phase reactions. *science*, 298(5594), 814-817.
- Jang, M., & Kamens, R. M. (2001). Characterization of secondary aerosol from the photooxidation of toluene in the presence of NO_x and 1-propene. *Environmental science & technology*, 35(18), 3626-3639.
- Jeong, D., Kim, K., & Choi, W. (2012). Accelerated dissolution of iron oxides in ice. *Atmospheric Chemistry and Physics*, 12(22), 11125-11133.
- Jickells, T., An, Z., Andersen, K. K., Baker, A., Bergametti, G., Brooks, N., Cao, J., Boyd, P., Duce, R., & Hunter, K. (2005). Global iron connections between desert dust, ocean biogeochemistry, and climate. *science*, 308(5718), 67-71.
- Johansen, A. M., Siefert, R. L., & Hoffmann, M. R. (2000). Chemical composition of aerosols collected over the tropical North Atlantic Ocean. *Journal of Geophysical Research: Atmospheres*, 105(D12), 15277-15312.
- Johnson, K. S., Coale, K. H., Elrod, V. A., & Tindale, N. W. (1994). Iron photochemistry in seawater from the equatorial Pacific. *Marine Chemistry*, 46(4), 319-334.
- Johnson, K. S., Gordon, R. M., & Coale, K. H. (1997). What controls dissolved iron concentrations in the world ocean? *Marine Chemistry*, 57(3-4), 137-161.
- Jones, P., Trenberth, K., Ambenje, P., Bojariu, R., Easterling, D., Klein, T., Parker, D., Renwick, J., Rusticucci, M., & Soden, B. (2007). Observations: surface and atmospheric climate change. *Climate change*, 235-336.
- Jourdain, B., & Legrand, M. (2002). Year-round records of bulk and size-segregated aerosol composition and HCl and HNO₃ levels in the Dumont d'Urville (coastal Antarctica) atmosphere: Implications for sea-salt aerosol fractionation in the winter and summer. *Journal of Geophysical Research: Atmospheres*, 107(D22).
- Journet, E., Desboeufs, K. V., Caquineau, S., & Colin, J. L. (2008). Mineralogy as a critical factor of dust iron solubility. *Geophysical research letters*, 35(7).
- Kawamura, K., & Ikushima, K. (1993). Seasonal changes in the distribution of dicarboxylic acids in the urban atmosphere. *Environmental science & technology*, 27(10), 2227-2235.

- Kawamura, K., & Kaplan, I. R. (1983). Organic compounds in the rainwater of Los Angeles. *Environmental science & technology*, 17(8), 497-501.
- Kawamura, K., & Kaplan, I. R. (1987). Motor exhaust emissions as a primary source for dicarboxylic acids in Los Angeles ambient air. *Environmental science & technology*, 21(1), 105-110.
- Kawamura, K., Kasukabe, H., & Barrie, L. A. (1996). Source and reaction pathways of dicarboxylic acids, ketoacids and dicarbonyls in arctic aerosols: One year of observations. *Atmospheric Environment*, 30(10), 1709-1722.
- Kawamura, K., Kasukabe, H., & Barrie, L. A. (2010). Secondary formation of water-soluble organic acids and α -dicarbonyls and their contributions to total carbon and water-soluble organic carbon: Photochemical aging of organic aerosols in the Arctic spring. *Journal of Geophysical Research: Atmospheres*, 115(D21).
- Kawamura, K., Kasukabe, H., Yasui, O., & Barrie, L. A. (1995). Production of dicarboxylic acids in the arctic atmosphere at polar sunrise. *Geophysical research letters*, 22(10), 1253-1256.
- Kawamura, K., Ng, L. L., & Kaplan, I. R. (1985). Determination of organic acids (C1-C10) in the atmosphere, motor exhausts, and engine oils. *Environmental science & technology*, 19(11), 1082-1086.
- Kawamura, K., Ono, K., Tachibana, E., Charrière, B., & Sempéré, R. (2012). Distributions of low molecular weight dicarboxylic acids, ketoacids and [alpha]-dicarbonyls in the marine aerosols collected over the Arctic Ocean during late summer. *Biogeosciences*, 9(11), 4725.
- Kawamura, K., & Sakaguchi, F. (1999). Molecular distributions of water soluble dicarboxylic acids in marine aerosols over the Pacific Ocean including tropics. *Journal of Geophysical Research: Atmospheres*, 104(D3), 3501-3509.
- Kawamura, K., Seméré, R., Imai, Y., Fujii, Y., & Hayashi, M. (1996). Water soluble dicarboxylic acids and related compounds in Antarctic aerosols. *Journal of Geophysical Research: Atmospheres*, 101(D13), 18721-18728.
- Kawamura, K., & Usukura, K. (1993). Distributions of low molecular weight dicarboxylic acids in the North Pacific aerosol samples. *Journal of Oceanography*, 49(3), 271-283.
- Kay, J. E., L'Ecuyer, T., Chepfer, H., Loeb, N., Morrison, A., & Cesana, G. (2016). Recent advances in Arctic cloud and climate research. *Current Climate Change Reports*, 2(4), 159-169.
- Keene, W. C., & Galloway, J. N. (1988). The biogeochemical cycling of formic and acetic acids through the troposphere: An overview of current understanding. *Tellus B*, 40(5), 322-334.
- Keene, W. C., Pszenny, A. A., Galloway, J. N., & Hawley, M. E. (1986). Sea-salt corrections and interpretation of constituent ratios in marine precipitation. *Journal of Geophysical Research: Atmospheres*, 91(D6), 6647-6658.
- Kelly, T. J., Daum, P. H., & Schwartz, S. E. (1985). Measurements of peroxides in cloudwater and rain. *Journal of Geophysical Research: Atmospheres*, 90(D5), 7861-7871.
- Kerminen, V.-M., Aurela, M., Hillamo, R. E., & Virkkula, A. (1997). Formation of particulate MSA: deductions from size distribution measurements in the Finnish Arctic. *Tellus B: Chemical and Physical Meteorology*, 49(2), 159-171.
- Kerminen, V.-M., Hillamo, R., Teinilä, K., Pakkanen, T., Allegrini, I., & Sparapani, R. (2001). Ion balances of size-resolved tropospheric aerosol samples: implications for the acidity and atmospheric processing of aerosols. *Atmospheric Environment*, 35(31), 5255-5265.
- Kerminen, V.-M., Teinilä, K., & Hillamo, R. (2000). Chemistry of sea-salt particles in the summer Antarctic atmosphere. *Atmospheric Environment*, 34(17), 2817-2825.
- Kerminen, V.-M., Teinilä, K., Hillamo, R., & Mäkelä, T. (1999). Size-segregated chemistry of particulate dicarboxylic acids in the Arctic atmosphere. *Atmospheric Environment*, 33(13), 2089-2100.

- Kerminen, V.-M., Teinilä, K., Hillamo, R., & Pakkanen, T. (1998). Substitution of chloride in sea-salt particles by inorganic and organic anions. *Journal of Aerosol Science*, 29(8), 929-942.
- Kerminen, V. M., & Leck, C. (2001). Sulfur chemistry over the central Arctic Ocean during the summer: Gas-to-particle transformation. *Journal of Geophysical Research: Atmospheres*, 106(D23), 32087-32099.
- Kieber, R. J., Skrabal, S. A., Smith, B., & Willey, J. D. (2005). Organic complexation of Fe (II) and its impact on the redox cycling of iron in rain. *Environmental science & technology*, 39(6), 1576-1583.
- Kieber, R. J., Willey, J. D., & Avery, G. B. (2003). Temporal variability of rainwater iron speciation at the Bermuda Atlantic Time Series Station. *Journal of Geophysical Research: Oceans*, 108(C8), n/a-n/a. doi:10.1029/2001JC001031
- Kieber, R. J., Williams, K., Willey, J. D., Skrabal, S., & Avery, G. B. (2001). Iron speciation in coastal rainwater: concentration and deposition to seawater. *Marine Chemistry*, 73(2), 83-95.
- Kim, K., Choi, W., Hoffmann, M. R., Yoon, H.-I., & Park, B.-K. (2010). Photoreductive dissolution of iron oxides trapped in ice and its environmental implications. *Environmental science & technology*, 44(11), 4142-4148.
- King, M., Fisher, F., Thompson, K., & Ward, A. (2004). Reactions on atmospheric mineral aerosol. *Central Laser Facility, CCLRC Rutherford Appleton Laboratory: Chilton, UK, 2005*, 135.
- Kirk, J. (1994). Optics of UVB radiation in natural waters. *Ergebnisse Limnol*, 43, 16.
- Kulmala, M., Pirjola, L., Mäkelä, J., & O'Dowd, C. (2000). *Stable sulfate clusters as a source of new atmospheric particles*. Paper presented at the AIP Conference Proceedings.
- Kumai, M. (1985). Acidity of snow and its reduction by alkaline aerosols. *Annals of Glaciology*, 6(1), 92-94.
- Künzli, N., Jerrett, M., Mack, W. J., Beckerman, B., LaBree, L., Gilliland, F., Thomas, D., Peters, J., & Hodis, H. N. (2005). Ambient air pollution and atherosclerosis in Los Angeles. *Environmental health perspectives*, 113(2), 201.
- Kuroiwa, D. (1974). *Metamorphism of snow and ice sintering observed by time lapse cinephotomicrography*. Paper presented at the Snow Mechanics Symposium.
- Lalonde, J. D., Poulain, A. J., & Amyot, M. (2002). The role of mercury redox reactions in snow on snow-to-air mercury transfer. *Environmental science & technology*, 36(2), 174-178.
- Lannuzel, D., Schoemann, V., De Jong, J., Chou, L., Delille, B., Becquevort, S., & Tison, J.-L. (2008). Iron study during a time series in the western Weddell pack ice. *Marine Chemistry*, 108(1), 85-95.
- Laurila, T., & Hakola, H. (1996). Seasonal cycle of C₂ - C₅ hydrocarbons over the Baltic Sea and Northern Finland. *Atmospheric Environment*, 30(10), 1597-1607.
- Leck, C., & Bigg, E. K. (2010). New particle formation of marine biological origin. *Aerosol Science and Technology*, 44(7), 570-577.
- Leck, C., Norman, M., Bigg, E. K., & Hillamo, R. (2002). Chemical composition and sources of the high Arctic aerosol relevant for cloud formation. *Journal of Geophysical Research: Atmospheres*, 107(D12).
- Leck, C., & Persson, C. (1996). The central Arctic Ocean as a source of dimethyl sulfide Seasonal variability in relation to biological activity. *Tellus B: Chemical and Physical Meteorology*, 48(2), 156-177.
- Leck, C., & Svensson, E. (2015). Importance of aerosol composition and mixing state for cloud droplet activation over the Arctic pack ice in summer. *Atmospheric Chemistry and Physics*, 15(5), 2545-2568.
- Levasseur, M., Gosselin, M., & Michaud, S. (1994). A new source of dimethylsulfide (DMS) for the arctic atmosphere: ice diatoms. *Marine Biology*, 121(2), 381-387.

- Lewis, E. R., & Schwartz, S. E. (2004). *Sea salt aerosol production: mechanisms, methods, measurements, and models-A critical review* (Vol. 152): American Geophysical Union.
- Li, S.-M., Barrie, L., Talbot, R., Harriss, R., Davidson, C., & Jaffrezo, J.-L. (1993). Seasonal and geographic variations of methanesulfonic acid in the Arctic troposphere. *Atmospheric Environment. Part A. General Topics*, 27(17-18), 3011-3024.
- Li, S. M., & Barrie, L. A. (1993). Biogenic sulfur aerosol in the Arctic troposphere: 1. Contributions to total sulfate. *Journal of Geophysical Research: Atmospheres*, 98(D11), 20613-20622.
- Li, S. M., Barrie, L. A., & Sirois, A. (1993). Biogenic sulfur aerosol in the Arctic troposphere: 2. Trends and seasonal variations. *Journal of Geophysical Research: Atmospheres*, 98(D11), 20623-20631.
- Li, S. M., & Winchester, J. W. (1993). Water soluble organic constituents in Arctic aerosols and snow pack. *Geophysical research letters*, 20(1), 45-48.
- Lightfoot, P. D., Cox, R., Crowley, J., Destriau, M., Hayman, G., Jenkin, M., Moortgat, G., & Zabel, F. (1992). Organic peroxy radicals: kinetics, spectroscopy and tropospheric chemistry. *Atmospheric Environment. Part A. General Topics*, 26(10), 1805-1961.
- Limbeck, A., Kulmala, M., & Puxbaum, H. (2003). Secondary organic aerosol formation in the atmosphere via heterogeneous reaction of gaseous isoprene on acidic particles. *Geophysical research letters*, 30(19).
- Lin, Z., Zhang, Z., Zhang, L., Tao, J., Zhang, R., Cao, J., Fan, S., & Zhang, Y. (2014). An alternative method for estimating hygroscopic growth factor of aerosol light-scattering coefficient: a case study in an urban area of Guangzhou, South China. *Atmospheric Chemistry and Physics*, 14(14), 7631-7644.
- Liss, P. S., Hatton, A. D., Malin, G., Nightingale, P. D., & Turner, S. M. (1997). Marine sulphur emissions. *Philosophical Transactions of the Royal Society of London B: Biological Sciences*, 352(1350), 159-169.
- Liu, J., Chen, Z., Francis, J., Song, M., Mote, T., & Hu, Y. (2016). Has Arctic sea ice loss contributed to increased surface melting of the Greenland ice sheet? *Journal of Climate*, 29(9), 3373-3386.
- Liu, L., Kong, S., Zhang, Y., Wang, Y., Xu, L., Yan, Q., Lingaswamy, A., Shi, Z., Lv, S., & Niu, H. (2017). Morphology, composition, and mixing state of primary particles from combustion sources—crop residue, wood, and solid waste. *Scientific Reports*, 7.
- Liu, X., & Millero, F. J. (2002). The solubility of iron in seawater. *Marine Chemistry*, 77(1), 43-54.
- Loewe, K., Ekman, A. M., Paukert, M., Sedlar, J., Tjernström, M., & Hoose, C. (2017). Modelling micro-and macrophysical contributors to the dissipation of an Arctic mixed-phase cloud during the Arctic Summer Cloud Ocean Study (ASCOS). *Atmospheric Chemistry and Physics*, 17(11), 6693-6704.
- Lu, J., & Cai, M. (2009). Seasonality of polar surface warming amplification in climate simulations. *Geophysical research letters*, 36(16).
- Luo, C., & Gao, Y. (2010). Aeolian iron mobilisation by dust–acid interactions and their implications for soluble iron deposition to the ocean: a test involving potential anthropogenic organic acidic species. *Environmental Chemistry*, 7(2), 153-161.
- Maenhaut, W., Raemdonck, H., Selen, A., Van Grieken, R., & Winchester, J. W. (1983). Characterization of the atmospheric aerosol over the eastern equatorial Pacific. *Journal of Geophysical Research: Oceans*, 88(C9), 5353-5364.
- Marti, J. J., Jefferson, A., Cai, X. P., Richert, C., McMurry, P. H., & Eisele, F. (1997). H₂SO₄ vapor pressure of sulfuric acid and ammonium sulfate solutions. *Journal of Geophysical Research: Atmospheres*, 102(D3), 3725-3735.

- Martin, J. H. (1990). Glacial-interglacial CO₂ change: The iron hypothesis. *Paleoceanography*, 5(1), 1-13.
- Martin, J. H., & Fitzwater, S. E. (1988). Iron deficiency limits phytoplankton growth in the north-east Pacific subarctic. *Nature*, 331(6154), 341.
- Matsuki, A., Iwasaka, Y., Shi, G., Zhang, D., Trochkin, D., Yamada, M., Kim, Y. S., Chen, B., Nagatani, T., & Miyazawa, T. (2005). Morphological and chemical modification of mineral dust: Observational insight into the heterogeneous uptake of acidic gases. *Geophysical research letters*, 32(22).
- Matsumoto, K., Nagao, I., Tanaka, H., Miyaji, H., Iida, T., & Ikebe, Y. (1998). Seasonal characteristics of organic and inorganic species and their size distributions in atmospheric aerosols over the northwest Pacific Ocean. *Atmospheric Environment*, 32(11), 1931-1946.
- Matsumoto, K., Tanaka, H., Nagao, I., & Ishizaka, Y. (1997). Contribution of particulate sulfate and organic carbon to cloud condensation nuclei in the marine atmosphere. *Geophysical research letters*, 24(6), 655-658.
- Mauritsen, T., Sedlar, J., Tjernström, M., Leck, C., Martin, M., Shupe, M., Sjogren, S., Sierau, B., Persson, P., & Brooks, I. (2011). An Arctic CCN-limited cloud-aerosol regime. *Atmospheric Chemistry and Physics*, 11(1), 165-173.
- McMinn, A., & Hegseth, E. (2004). Quantum yield and photosynthetic parameters of marine microalgae from the southern Arctic Ocean, Svalbard. *Journal of the Marine Biological Association of the United Kingdom*, 84(5), 865-871.
- Meier, W. N., Stroeve, J., & Fetterer, F. (2007). Whither Arctic sea ice? A clear signal of decline regionally, seasonally and extending beyond the satellite record. *Annals of Glaciology*, 46(1), 428-434.
- Millero, F., & Sohn, M. (1992). Minor elements of seawater. *Chemical Oceanography*. CRC, 115-156.
- Mochida, M., Umemoto, N., Kawamura, K., & Uematsu, M. (2003). Bimodal size distribution of C₂-C₄ dicarboxylic acids in the marine aerosols. *Geophysical research letters*, 30(13).
- Mukherjee, P., & Gao, Y. (2016). Efficiency of organic ligands in adsorptive dissolution and photoreductive dissolution of hematite. *International journal of environmental science and technology*, 13(5), 1195-1206.
- Mukherjee, P., Glamoclija, M., & Gao, Y. (2018). Insignificant impact of freezing and compaction on iron solubility in natural snow. *Journal of Atmospheric Chemistry*, 1-24.
- Mukherjee, P., Marsay, C., Yu, S., Fan, S., Buck, C., Landing, W. M., & Gao, Y. (2018). *Characterization of the water-soluble inorganic and organic species on aerosols over the Arctic Ocean*. In preparation.
- Mungall, E. L., Abbatt, J. P., Wentzell, J. J., Lee, A. K., Thomas, J. L., Blais, M., Gosselin, M., Miller, L. A., Papakyriakou, T., & Willis, M. D. (2017). Microlayer source of oxygenated volatile organic compounds in the summertime marine Arctic boundary layer. *Proceedings of the National Academy of Sciences*, 114(24), 6203-6208.
- Murphy, D., Anderson, J., Quinn, P., McInnes, L., Brechtel, F., Kreidenweis, S., Middlebrook, A., Pósfai, M., Thomson, D., & Buseck, P. (1998). Influence of sea-salt on aerosol radiative properties in the Southern Ocean marine boundary layer. *Nature*, 392(6671), 62-65.
- Naito, K., Matsui, M., & Imai, I. (2005). Ability of marine eukaryotic red tide microalgae to utilize insoluble iron. *Harmful Algae*, 4(6), 1021-1032.
- Napp, J. M., & Hunt, G. L. (2001). Anomalous conditions in the south-eastern Bering Sea 1997: linkages among climate, weather, ocean, and Biology. *Fisheries Oceanography*, 10(1), 61-68.

- Narukawa, M., Kawamura, K., Anlauf, K., & Barrie, L. (2003). Fine and coarse modes of dicarboxylic acids in the Arctic aerosols collected during the Polar Sunrise Experiment 1997. *Journal of Geophysical Research: Atmospheres*, *108*(D18).
- Nilsson, E., Rannik, Ü., Swietlicki, E., Leck, C., Aalto, P. P., Zhou, J., & Norman, M. (2001). Turbulent aerosol fluxes over the Arctic Ocean: 2. Wind-driven sources from the sea. *Journal of Geophysical Research: Atmospheres*, *106*(D23), 32139-32154.
- Norman, A., Barrie, L., Toom-Sauntry, D., Sirois, A., Krouse, H., Li, S., & Sharma, S. (1999). Sources of aerosol sulphate at Alert: Apportionment using stable isotopes. *Journal of Geophysical Research: Atmospheres*, *104*(D9), 11619-11631.
- Novakov, T., & Penner, J. (1993). Large contribution of organic aerosols to cloud-condensation-nuclei concentrations. *Nature*, *365*(6449), 823-826.
- O'Dowd, C. D., Smith, M. H., Consterdine, I. E., & Lowe, J. A. (1997). Marine aerosol, sea-salt, and the marine sulphur cycle: A short review. *Atmospheric Environment*, *31*(1), 73-80.
- Özsoy, T., & Saydam, A. C. (2001). Iron speciation in precipitation in the North-Eastern Mediterranean and its relationship with Sahara dust. *Journal of Atmospheric Chemistry*, *40*(1), 41-76.
- Paramonov, M., Grönholm, T., & Virkkula, A. (2011). Below-cloud scavenging of aerosol particles by snow at an urban site in Finland. *Boreal Environ. Res*, *16*, 304-320.
- Paris, R., & Desboeufs, K. (2013). Effect of atmospheric organic complexation on iron-bearing dust solubility. *Atmospheric Chemistry and Physics*, *13*(9), 4895-4905.
- Paris, R., Desboeufs, K., & Journet, E. (2011). Variability of dust iron solubility in atmospheric waters: Investigation of the role of oxalate organic complexation. *Atmospheric Environment*, *45*(36), 6510-6517.
- Park, K.-T., Jang, S., Lee, K., Yoon, Y. J., Kim, M.-S., Park, K., Cho, H.-J., Kang, J.-H., Udisti, R., & Lee, B.-Y. (2017). Observational evidence for the formation of DMS-derived aerosols during Arctic phytoplankton blooms. *Atmospheric Chemistry and Physics*, *17*(15), 9665-9675.
- Pehkonen, S. O., Siefert, R., Erel, Y., Webb, S., & Hoffmann, M. R. (1993). Photoreduction of iron oxyhydroxides in the presence of important atmospheric organic compounds. *Environmental science & technology*, *27*(10), 2056-2062.
- Pehkonen, S. O., Siefert, R. L., & Hoffmann, M. R. (1995). Photoreduction of iron oxyhydroxides and the photooxidation of halogenated acetic acids. *Environmental science & technology*, *29*(5), 1215-1222.
- Peltzer, E. T., & Bada, J. L. (1981). Low molecular weight α -hydroxy carboxylic and dicarboxylic acids in reducing marine sediments. *Geochimica et Cosmochimica Acta*, *45*(10), 1847-1854.
- Perovich, D. K., & Richter-Menge, J. A. (1994). Surface characteristics of lead ice. *Journal of Geophysical Research: Oceans*, *99*(C8), 16341-16350.
- Pike, S., & Moran, S. (2001). Trace elements in aerosol and precipitation at New Castle, NH, USA. *Atmospheric Environment*, *35*(19), 3361-3366.
- Pistone, K., Eisenman, I., & Ramanathan, V. (2014). Observational determination of albedo decrease caused by vanishing Arctic sea ice. *Proceedings of the National Academy of Sciences*, *111*(9), 3322-3326.
- Polyakov, I. V., Timokhov, L. A., Alexeev, V. A., Bacon, S., Dmitrenko, I. A., Fortier, L., Frolov, I. E., Gascard, J.-C., Hansen, E., & Ivanov, V. V. (2010). Arctic Ocean warming contributes to reduced polar ice cap. *Journal of Physical Oceanography*, *40*(12), 2743-2756.
- Prospero, J., & Savoie, D. (1991). Impact of oceanic sources of biogenic sulphur on sulphate aerosol concentrations at Mawson, Antarctica. *Nature*, *350*(6315), 221.

- Prospero, J., Savoie, D., Nees, R., Duce, R., & Merrill, J. (1985). Particulate sulfate and nitrate in the boundary layer over the North Pacific Ocean. *Journal of Geophysical Research: Atmospheres*, *90*(D6), 10586-10596.
- Pruppacher, H., & Jaenicke, R. (1995). The processing of water vapor and aerosols by atmospheric clouds, a global estimate. *Atmospheric Research*, *38*(1-4), 283-295.
- Quinn, P., Bates, T., Schulz, K., & Shaw, G. (2009). Decadal trends in aerosol chemical composition at Barrow, Alaska: 1976–2008. *Atmospheric Chemistry and Physics*, *9*(22), 8883-8888.
- Quinn, P., Coffman, D., Johnson, J., Upchurch, L., & Bates, T. (2017). Small fraction of marine cloud condensation nuclei made up of sea spray aerosol. *Nature Geoscience*, *10*(9), 674.
- Quinn, P., Miller, T., Bates, T., Ogren, J., Andrews, E., & Shaw, G. (2002). A 3-year record of simultaneously measured aerosol chemical and optical properties at Barrow, Alaska. *Journal of Geophysical Research: Atmospheres*, *107*(D11).
- Quinn, P., Shaw, G., Andrews, E., Dutton, E., Ruoho-Airola, T., & Gong, S. (2007). Arctic haze: current trends and knowledge gaps. *Tellus B*, *59*(1), 99-114.
- Quinn, P. K., Bates, T. S., Johnson, J. E., Covert, D. S., & Charlson, R. J. (1990). Interactions between the sulfur and reduced nitrogen cycles over the central Pacific Ocean. *Journal of Geophysical Research: Atmospheres*, *95*(D10), 16405-16416.
- Quinn, P. K., Charlson, R. J., & Bates, T. S. (1988). Simultaneous observations of ammonia in the atmosphere and ocean. *Nature*, *335*(6188), 336-338.
- Quinn, P. K., Charlson, R. J., & Zoller, W. H. (1987). Ammonia, the dominant base in the remote marine troposphere: a review. *Tellus B*, *39*(5), 413-425.
- Rhodes, R. H., Yang, X., Wolff, E. W., McConnell, J. R., & Frey, M. M. (2017). Sea ice as a source of sea salt aerosol to Greenland ice cores: a model-based study. *Atmospheric Chemistry and Physics*, *17*(15), 9417-9433.
- Ricard, V., Jaffrezo, J. L., Kerminen, V. M., Hillamo, R., Teinilä, K., & Maenhaut, W. (2002). Size distributions and modal parameters of aerosol constituents in northern Finland during the European Arctic Aerosol Study. *Journal of Geophysical Research: Atmospheres*, *107*(D14).
- Richardson, C. (1976). Phase relationships in sea ice as a function of temperature. *Journal of Glaciology*, *17*(77), 507-519.
- Rijkenberg, M. J., Gerringa, L. J., Velzeboer, I., Timmermans, K. R., Buma, A. G., & de Baar, H. J. (2006). Iron-binding ligands in Dutch estuaries are not affected by UV induced photochemical degradation. *Marine Chemistry*, *100*(1-2), 11-23.
- Rolph, G., Stein, A., & Stunder, B. (2017). Real-time environmental applications and display system: Ready. *Environmental Modelling & Software*, *95*, 210-228.
- Russell, Y. G., & Heist, R. H. (1978). Homogeneous nucleation in associated vapors. II. Formic and propanoic acids. *The Journal of Chemical Physics*, *69*(8), 3723-3728.
- Salter, M. E., Hamacher-Barth, E., Leck, C., Werner, J., Johnson, C. M., Riipinen, I., Nilsson, E. D., & Zieger, P. (2016). Calcium enrichment in sea spray aerosol particles. *Geophysical research letters*, *43*(15), 8277-8285.
- Sattler, B., Puxbaum, H., & Psenner, R. (2001). Bacterial growth in supercooled cloud droplets. *Geophysical research letters*, *28*(2), 239-242.
- Savoie, D., & Prospero, J. (1980). Water-soluble potassium, calcium, and magnesium in the aerosols over the tropical North Atlantic. *Journal of Geophysical Research: Oceans*, *85*(C1), 385-392.
- Savoie, D. L., & Prospero, J. M. (1989). Comparison of oceanic and continental sources of non-sea-salt sulphate over the Pacific Ocean. *Nature*, *339*(6227), 685.

- Screen, J. A., & Simmonds, I. (2010). The central role of diminishing sea ice in recent Arctic temperature amplification. *Nature*, *464*(7293), 1334-1337.
- Sedwick, P. N., & DiTullio, G. R. (1997). Regulation of algal blooms in Antarctic shelf waters by the release of iron from melting sea ice. *Geophysical research letters*, *24*(20), 2515-2518.
- Sedwick, P. N., DiTullio, G. R., & Mackey, D. J. (2000). Iron and manganese in the Ross Sea, Antarctica: seasonal iron limitation in Antarctic shelf waters. *Journal of Geophysical Research: Oceans*, *105*(C5), 11321-11336.
- Sedwick, P. N., Sholkovitz, E. R., & Church, T. M. (2007). Impact of anthropogenic combustion emissions on the fractional solubility of aerosol iron: Evidence from the Sargasso Sea. *Geochemistry, Geophysics, Geosystems*, *8*(10).
- Sempère, R., & Kawamura, K. (1994). Comparative distributions of dicarboxylic acids and related polar compounds in snow, rain and aerosols from urban atmosphere. *Atmospheric Environment*, *28*(3), 449-459.
- Serreze, M. C., & Barry, R. G. (2011). Processes and impacts of Arctic amplification: A research synthesis. *Global and Planetary Change*, *77*(1), 85-96.
- Shaked, Y., Kustka, A. B., & Morel, F. M. (2005). A general kinetic model for iron acquisition by eukaryotic phytoplankton. *Limnology and oceanography*, *50*(3), 872-882.
- Shaloski, M. A., Sobyra, T. B., & Nathanson, G. M. (2015). DCI Transport through Dodecyl Sulfate Films on Salty Glycerol: Effects of Seawater Ions on Gas Entry. *The Journal of Physical Chemistry A*, *119*(50), 12357-12366.
- Shao-Meng, L., & Winchester, J. W. (1989). Geochemistry of organic and inorganic ions of late winter Arctic aerosols. *Atmospheric Environment (1967)*, *23*(11), 2401-2415.
- Sharma, S., Chan, E., Ishizawa, M., Toom-Sauntry, D., Gong, S., Li, S., Tarasick, D., Leitch, W., Norman, A., & Quinn, P. (2012). Influence of transport and ocean ice extent on biogenic aerosol sulfur in the Arctic atmosphere. *Journal of Geophysical Research: Atmospheres*, *117*(D12).
- Shelley, R. U., Morton, P. L., & Landing, W. M. (2015). Elemental ratios and enrichment factors in aerosols from the US-GEOTRACES North Atlantic transects. *Deep Sea Research Part II: Topical Studies in Oceanography*, *116*, 262-272.
- Sholkovitz, E. R., Sedwick, P. N., Church, T. M., Baker, A. R., & Powell, C. F. (2012). Fractional solubility of aerosol iron: Synthesis of a global-scale data set. *Geochimica et Cosmochimica Acta*, *89*, 173-189.
- Siefert, R. L., Johansen, A. M., & Hoffmann, M. R. (1999). Chemical characterization of ambient aerosol collected during the southwest monsoon and intermonsoon seasons over the Arabian Sea: Labile-Fe (II) and other trace metals. *Journal of Geophysical Research: Atmospheres*, *104*(D3), 3511-3526.
- Siefert, R. L., Pehkonen, S. O., Erel, Y., & Hoffmann, M. R. (1994). Iron photochemistry of aqueous suspensions of ambient aerosol with added organic acids. *Geochimica et Cosmochimica Acta*, *58*(15), 3271-3279.
- Sievering, H., Caine, J., Harvey, M., McGregor, J., Nichol, S., & Quinn, P. (2004). Aerosol non-sea-salt sulfate in the remote marine boundary layer under clear-sky and normal cloudiness conditions: Ocean-derived biogenic alkalinity enhances sea-salt sulfate production by ozone oxidation. *Journal of Geophysical Research: Atmospheres*, *109*(D19).
- Siefert, C., & Sulzberger, B. (1991). Light-induced dissolution of hematite in the presence of oxalate. A case study. *Langmuir*, *7*(8), 1627-1634.
- Simpson, W., Carlson, D., Hönninger, G., Douglas, T., Sturm, M., Perovich, D., & Platt, U. (2007). First-year sea-ice contact predicts bromine monoxide (BrO) levels at Barrow, Alaska

- better than potential frost flower contact. *Atmospheric Chemistry and Physics*, 7(3), 621-627.
- Soli, A. L., & Byrne, R. H. (1996). The hydrolysis and fluoride complexation behavior of Fe (III) at 25 C and 0.68 molal ionic strength. *Journal of solution chemistry*, 25(8), 773-785.
- Song, C. H., & Carmichael, G. R. (2001). A three-dimensional modeling investigation of the evolution processes of dust and sea-salt particles in east Asia. *Journal of Geophysical Research: Atmospheres*, 106(D16), 18131-18154.
- Song, F., & Gao, Y. (2009). Chemical characteristics of precipitation at metropolitan Newark in the US East Coast. *Atmospheric Environment*, 43(32), 4903-4913.
- Srivastava, N., & Satheesh, S. (2016). Modulation in Direct Radiative Forcing Caused by Wind Generated Sea-Salt Aerosols. *Aerosol and Air Quality Research*, 16, 2869-2883.
- Stein, A., Draxler, R. R., Rolph, G. D., Stunder, B. J., Cohen, M., & Ngan, F. (2015). NOAA's HYSPLIT atmospheric transport and dispersion modeling system. *Bulletin of the American Meteorological Society*, 96(12), 2059-2077.
- Steinberg, S. M., & Bada, J. L. (1984). Oxalic, glyoxalic and pyruvic acids in eastern Pacific Ocean waters. *Journal of Marine Research*, 42(3), 697-708.
- Stookey, L. L. (1970). Ferrozine---a new spectrophotometric reagent for iron. *Analytical chemistry*, 42(7), 779-781.
- Stumm, W., & Wollast, R. (1990). Coordination chemistry of weathering: Kinetics of the surface-controlled dissolution of oxide minerals. *Reviews of Geophysics*, 28(1), 53-69.
- Sullivan, R., Moore, M., Petters, M., Kreidenweis, S., Roberts, G., & Prather, K. (2009). Effect of chemical mixing state on the hygroscopicity and cloud nucleation properties of calcium mineral dust particles. *Atmospheric Chemistry and Physics*, 9(10), 3303-3316.
- Sullivan, R. C., & Prather, K. A. (2007). Investigations of the diurnal cycle and mixing state of oxalic acid in individual particles in Asian aerosol outflow. *Environmental Science Technology*, 41(23), 8062-8069.
- Sulzberger, B., Suter, D., Siffert, C., Banwart, S., & Stumm, W. (1989). Dissolution of Fe (III)(hydr) oxides in natural waters; laboratory assessment on the kinetics controlled by surface coordination. *Marine Chemistry*, 28(1-3), 127-144.
- Sun, J., & Ariya, P. A. (2006). Atmospheric organic and bio-aerosols as cloud condensation nuclei (CCN): A review. *Atmospheric Environment*, 40(5), 795-820.
- Sunda, W. (2001). Bioavailability and Bioaccumulation of Iron in the Sea, in "The Biogeochemistry of Iron in Seawater", edited by DR Turner, K. Hunter: Wiley, Chichester, UK.
- Sunda, W. G., & Huntsman, S. A. (1997). Interrelated influence of iron, light and cell size on marine phytoplankton growth. *Nature*, 390(6658), 389.
- Sung, W., & Morgan, J. J. (1980). Kinetics and product of ferrous iron oxygenation in aqueous systems. *Environmental science & technology*, 14(5), 561-568.
- Suzuki, K., KAWAMURA, K., KASUKABE, H., YANASE, A., & BARRIE, L. A. (1995). *Concentration changes of MSA and major ions in Arctic aerosols during polar sunrise*. Paper presented at the Proceedings of the NIPR Symposium on Polar Meteorology and Glaciology.
- Swanson, A. L., Blake, N. J., Dibb, J. E., Albert, M. R., Blake, D. R., & Rowland, F. S. (2002). Photochemically induced production of CH₃Br, CH₃I, C₂H₅I, ethene, and propene within surface snow at Summit, Greenland. *Atmospheric Environment*, 36(15), 2671-2682.
- Tagliabue, A., Bowie, A. R., Boyd, P. W., Buck, K. N., Johnson, K. S., & Saito, M. A. (2017). The integral role of iron in ocean biogeochemistry. *Nature*, 543(7643), 51.
- Takenaka, N., Daimon, T., Ueda, A., Sato, K., Kitano, M., Bandow, H., & Maeda, Y. (1998). Fast oxidation reaction of nitrite by dissolved oxygen in the freezing process in the tropospheric aqueous phase. *Journal of Atmospheric Chemistry*, 29(2), 135-150.

- Takenaka, N., Ueda, A., Daimon, T., Bandow, H., Dohmaru, T., & Maeda, Y. (1996). Acceleration mechanism of chemical reaction by freezing: The reaction of nitrous acid with dissolved oxygen. *The Journal of Physical Chemistry*, *100*(32), 13874-13884.
- Talbot, R., Andreae, M., Berresheim, H., Jacob, D. J., & Beecher, K. (1990). Sources and sinks of formic, acetic, and pyruvic acids over Central Amazonia: 2. Wet season. *Journal of Geophysical Research: Atmospheres*, *95*(D10), 16799-16811.
- Talbot, R., Beecher, K., Harriss, R., & Cofer, W. (1988). Atmospheric geochemistry of formic and acetic acids at a mid-latitude temperate site. *Journal of Geophysical Research: Atmospheres*, *93*(D2), 1638-1652.
- Talbot, R., Vijgen, A., & Harriss, R. (1992). Soluble species in the Arctic summer troposphere: Acidic gases, aerosols, and precipitation. *Journal of Geophysical Research: Atmospheres*, *97*(D15), 16531-16543.
- Tang, I. N., Tridico, A., & Fung, K. (1997). Thermodynamic and optical properties of sea salt aerosols. *Journal of Geophysical Research: Atmospheres*, *102*(D19), 23269-23275.
- Tang, M., Whitehead, J., Davidson, N., Pope, F., Alfarra, M., McFiggans, G., & Kalberer, M. (2015). Cloud condensation nucleation activities of calcium carbonate and its atmospheric ageing products. *Physical Chemistry Chemical Physics*, *17*(48), 32194-32203.
- Toom-Sauntry, D., & Barrie, L. A. (2002). Chemical composition of snowfall in the high Arctic: 1990–1994. *Atmospheric Environment*, *36*(15), 2683-2693.
- Turekian, V. C., Macko, S. A., & Keene, W. C. (2003). Concentrations, isotopic compositions, and sources of size-resolved, particulate organic carbon and oxalate in near-surface marine air at Bermuda during spring. *Journal of Geophysical Research: Atmospheres*, *108*(D5).
- Turpin, B. J., Huntzicker, J. J., & Hering, S. V. (1994). Investigation of organic aerosol sampling artifacts in the Los Angeles Basin. *Atmospheric Environment*, *28*(19), 3061-3071.
- Vavrus, S. (2004). The impact of cloud feedbacks on Arctic climate under greenhouse forcing. *Journal of Climate*, *17*(3), 603-615.
- Verdugo, P. (2012). Marine microgels. *Annual Review of Marine Science*, *4*, 375-400.
- Vignati, E., Facchini, M., Rinaldi, M., Scannell, C., Ceburnis, D., Sciare, J., Kanakidou, M., Myriokefalitakis, S., Dentener, F., & O'Dowd, C. (2010). Global scale emission and distribution of sea-spray aerosol: Sea-salt and organic enrichment. *Atmospheric Environment*, *44*(5), 670-677.
- Viollier, E., Inglett, P., Hunter, K., Roychoudhury, A., & Van Cappellen, P. (2000). The ferrozine method revisited: Fe (II)/Fe (III) determination in natural waters. *Applied geochemistry*, *15*(6), 785-790.
- Virkkula, A., Mäkinen, M., Hillamo, R., & Stohl, A. (1995). Atmospheric aerosol in the Finnish Arctic: particle number concentrations, chemical characteristics, and source analysis. *Water, Air, and Soil Pollution*, *85*(4), 1997-2002.
- Voelker, B. M., & Sulzberger, B. (1996). Effects of fulvic acid on Fe (II) oxidation by hydrogen peroxide. *Environmental science & technology*, *30*(4), 1106-1114.
- Vogt, M., & Liss, P. (2009). Dimethylsulfide and climate. *Surface Ocean-Lower Atmosphere Processes*, 197-232.
- Vong, R. J., Hansson, H. C., Ross, H. B., Covert, D. S., & Charlson, R. J. (1988). Northeastern Pacific submicrometer aerosol and rainwater composition: A multivariate analysis. *Journal of Geophysical Research: Atmospheres*, *93*(D2), 1625-1637.
- Wagenbach, D., Ducroz, F., Mulvaney, R., Keck, L., Minikin, A., Legrand, M., Hall, J., & Wolff, E. (1998). Sea-salt aerosol in coastal Antarctic regions. *Journal of Geophysical Research: Atmospheres*, *103*(D9), 10961-10974.

- Walna, B., Kurzyca, I., Bednorz, E., & Kolendowicz, L. (2013). Fluoride pollution of atmospheric precipitation and its relationship with air circulation and weather patterns (Wielkopolski National Park, Poland). *Environmental monitoring and assessment*, 185(7), 5497-5514.
- Walsh, J. E., Chapman, W. L., & Portis, D. H. (2009). Arctic cloud fraction and radiative fluxes in atmospheric reanalyses. *Journal of Climate*, 22(9), 2316-2334.
- Walsh, J. E., Vavrus, S. J., & Chapman, W. L. (2005). Workshop on modeling of the Arctic atmosphere. *Bulletin of the American Meteorological Society*, 86(6), 845-852.
- Wang, Y., & Reardon, E. J. (2001). Activation and regeneration of a soil sorbent for defluoridation of drinking water. *Applied geochemistry*, 16(5), 531-539.
- Weber, R. J., Guo, H., Russell, A. G., & Nenes, A. (2016). High aerosol acidity despite declining atmospheric sulfate concentrations over the past 15 years. *Nature Geoscience*, 9(4), 282.
- Wells, M. L., Price, N. M., & Bruland, K. W. (1995). Iron chemistry in seawater and its relationship to phytoplankton: a workshop report. *Marine Chemistry*, 48(2), 157-182.
- Wentworth, G. R., Murphy, J. G., Croft, B., Martin, R. V., Pierce, J. R., Côté, J.-S., Courchesne, I., Tremblay, J.-É., Gagnon, J., & Thomas, J. L. (2016). Ammonia in the summertime Arctic marine boundary layer: sources, sinks, and implications. *Atmospheric Chemistry and Physics*, 16(4), 1937-1953.
- Wieland, E., Wehrli, B., & Stumm, W. (1988). The coordination chemistry of weathering: III. A generalization on the dissolution rates of minerals. *Geochimica et Cosmochimica Acta*, 52(8), 1969-1981.
- Willey, J. D., Kieber, R. J., Williams, K. H., Crozier, J. S., Skrabal, S. A., & Avery, G. B. (2000). Temporal variability of iron speciation in coastal rainwater. *Journal of Atmospheric Chemistry*, 37(2), 185-205.
- Winkler, P. (1986). Relations between aerosol acidity and ion balance *Chemistry of multiphase atmospheric systems* (pp. 269-298): Springer.
- Winter, A., Henderiks, J., Beaufort, L., Rickaby, R. E., & Brown, C. W. (2013). Poleward expansion of the coccolithophore *Emiliania huxleyi*. *Journal of Plankton Research*, 36(2), 316-325.
- Wu, J., Boyle, E., Sunda, W., & Wen, L.-S. (2001). Soluble and colloidal iron in the oligotrophic North Atlantic and North Pacific. *science*, 293(5531), 847-849.
- Xhoffer, C., Bernard, P., Van Grieken, R., & Van der Auwera, L. (1991). Chemical characterization and source apportionment of individual aerosol particles over the North Sea and the English Channel using multivariate techniques. *Environmental science & technology*, 25(8), 1470-1478.
- Xia, L., & Gao, Y. (2010). Chemical composition and size distributions of coastal aerosols observed on the US East Coast. *Marine Chemistry*, 119(1-4), 77-90.
- Xia, L., & Gao, Y. (2011). Characterization of trace elements in PM_{2.5} aerosols in the vicinity of highways in northeast New Jersey in the US east coast. *Atmospheric Pollution Research*, 2(1), 34-44.
- Xiu, G., Zhang, D., Chen, J., Huang, X., Chen, Z., Guo, H., & Pan, J. (2004). Characterization of major water-soluble inorganic ions in size-fractionated particulate matters in Shanghai campus ambient air. *Atmospheric Environment*, 38(2), 227-236.
- Xu, G., Gao, Y., Lin, Q., Li, W., & Chen, L. (2013). Characteristics of water-soluble inorganic and organic ions in aerosols over the Southern Ocean and coastal East Antarctica during austral summer. *Journal of Geophysical Research: Atmospheres*, 118(23).
- Xu, N., & Gao, Y. (2008). Characterization of hematite dissolution affected by oxalate coating, kinetics and pH. *Applied geochemistry*, 23(4), 783-793.

- Yan, Y., Fu, P., Jing, B., Peng, C., Boreddy, S., Yang, F., Wei, L., Sun, Y., Wang, Z., & Ge, M. (2017). Hygroscopic behavior of water-soluble matter in marine aerosols over the East China Sea. *Science of the total Environment*, 578, 307-316.
- Yao, X., Fang, M., & Chan, C. K. (2003). The size dependence of chloride depletion in fine and coarse sea-salt particles. *Atmospheric Environment*, 37(6), 743-751.
- Ye, P., Xie, Z., Yu, J., & Kang, H. (2015). Spatial distribution of methanesulphonic acid in the Arctic aerosol collected during the Chinese Arctic Research Expedition. *Atmosphere*, 6(5), 699-712.
- Yeatman, S., Spokes, L., & Jickells, T. (2001). Comparisons of coarse-mode aerosol nitrate and ammonium at two polluted coastal sites. *Atmospheric Environment*, 35(7), 1321-1335.
- Yin, F., Grosjean, D., & Seinfeld, J. H. (1990). Photooxidation of dimethyl sulfide and dimethyl disulfide. I: Mechanism development. *Journal of Atmospheric Chemistry*, 11(4), 309-364.
- Yu, S. (2000). Role of organic acids (formic, acetic, pyruvic and oxalic) in the formation of cloud condensation nuclei (CCN): a review. *Atmospheric Research*, 53(4), 185-217.
- Zappoli, S., Andracchio, A., Fuzzi, S., Facchini, M., Gelencser, A., Kiss, G., Krivacsy, Z., Molnar, A., Meszaros, E., & Hansson, H.-C. (1999). Inorganic, organic and macromolecular components of fine aerosol in different areas of Europe in relation to their water solubility. *Atmospheric Environment*, 33(17), 2733-2743.
- Zepp, R. G., Faust, B. C., & Hoigne, J. (1992). Hydroxyl radical formation in aqueous reactions (pH 3-8) of iron (II) with hydrogen peroxide: the photo-Fenton reaction. *Environmental science & technology*, 26(2), 313-319.
- Zhan, J., Gao, Y., Li, W., Chen, L., Lin, H., & Lin, Q. (2014). Effects of ship emissions on summertime aerosols at Ny-Alesund in the Arctic. *Atmospheric Pollution Research*, 5(3), 500-510.
- Zhang, R., Wooldridge, P. J., Abbatt, J. P., & Molina, M. J. (1993). Physical chemistry of the sulfuric acid/water binary system at low temperatures: stratospheric implications. *The Journal of Physical Chemistry*, 97(28), 7351-7358.
- Zhang, X., Hu, L., Twardowski, M. S., & Sullivan, J. M. (2009). Scattering by solutions of major sea salts. *Optics express*, 17(22), 19580-19585.
- Zhao, Y., & Gao, Y. (2008). Acidic species and chloride depletion in coarse aerosol particles in the US east coast. *Science of the total Environment*, 407(1), 541-547.
- Zhiyuan, C., Shichang, K., & Dahe, Q. (2009). Seasonal features of aerosol particles recorded in snow from Mt. Qomolangma (Everest) and their environmental implications. *Journal of Environmental Sciences*, 21(7), 914-919.
- Zhou, X., Beine, H. J., Honrath, R. E., Fuentes, J. D., Simpson, W., Shepson, P. B., & Bottenheim, J. W. (2001). Snowpack photochemical production of HONO: a major source of OH in the Arctic boundary layer in springtime. *Geophysical research letters*, 28(21), 4087-4090.
- Zhu, X., Prospero, J., & Millero, F. (1997). Diel variability of soluble Fe (II) and soluble total Fe in North African dust in the trade winds at Barbados. *Journal of Geophysical Research: Atmospheres*, 102(D17), 21297-21305.
- Zhu, X., Prospero, J. M., Savoie, D. L., Millero, F. J., Zika, R. G., & Saltzman, E. S. (1993). Photoreduction of iron (III) in marine mineral aerosol solutions. *Journal of Geophysical Research: Atmospheres*, 98(D5), 9039-9046.
- Zhuang, G., Duce, R. A., & Kester, D. R. (1990). The dissolution of atmospheric iron in surface seawater of the open ocean. *Journal of Geophysical Research: Oceans*, 95(C9), 16207-16216.
- Zhuang, G., Yi, Z., & Wallace, G. T. (1995). Iron (II) in rainwater, snow, and surface seawater from a coastal environment. *Marine Chemistry*, 50(1-4), 41-50.

- Zieger, P., Väisänen, O., Corbin, J., Partridge, D. G., Bastelberger, S., Mousavi-Fard, M., Rosati, B., Gysel, M., Krieger, U., & Leck, C. (2017). Revising the hygroscopicity of inorganic sea salt particles. *Nature Communications*, *8*, 15883.
- Ziemba, L. D., Dibb, J. E., Griffin, R. J., Huey, L. G., & Beckman, P. (2010). Observations of particle growth at a remote, Arctic site. *Atmospheric Environment*, *44*(13), 1649-1657.
- Zinder, B., Furrer, G., & Stumm, W. (1986). The coordination chemistry of weathering: II. Dissolution of Fe (III) oxides. *Geochimica et Cosmochimica Acta*, *50*(9), 1861-1869.
- Zobrist, B., Marcolli, C., Koop, T., Luo, B., Murphy, D., Lohmann, U., Zardini, A., Krieger, U., Corti, T., & Cziczo, D. (2006). Oxalic acid as a heterogeneous ice nucleus in the upper troposphere and its indirect aerosol effect. *Atmospheric Chemistry and Physics*, *6*(10), 3115-3129.
- Zuo, Y., & Hoigne, J. (1992). Formation of hydrogen peroxide and depletion of oxalic acid in atmospheric water by photolysis of iron (III)-oxalato complexes. *Environmental science & technology*, *26*(5), 1014-1022.